

論文 / 著書情報
Article / Book Information

題目(和文)	電気化学マイクロリアクターを使用した有機電解合成に関する研究
Title(English)	Study on electroorganic synthesis using an electrochemical microreactor
著者(和文)	雨宮史尋
Author(English)	Fumihiko Amemiya
出典(和文)	学位:博士(工学), 学位授与機関:東京工業大学, 報告番号:甲第8374号, 授与年月日:2011年3月26日, 学位の種別:課程博士, 審査員:跡部 真人, 瀧上 壽雄
Citation(English)	Degree:Doctor (Engineering), Conferring organization: Tokyo Institute of Technology, Report number:甲第8374号, Conferred date:2011/3/26, Degree Type:Course doctor, Examiner:.
学位種別(和文)	博士論文
Type(English)	Doctoral Thesis

Study on Electroorganic Synthesis Using an Electrochemical Microreactor

(電気化学マイクロリアクターを使用した有機電解合成に関する研究)

by

Fumihito Amemiya

A Doctoral Thesis Submitted to
the Department of Electronic Chemistry,
Interdisciplinary Graduate School of Science and Engineering,
Tokyo Institute of Technology

Yokohama, Japan

December 2010

Contents

Chapter 1	General Introduction	1
1-1	Introduction and Overview of Microreactor Technology	2
1-2	Outline of This Thesis	9
1-3	References	11
Chapter 2	Self-supported Paired Electrosynthesis Using a Microreactor Without Intentionally Added Supporting Electrolyte	14
2-1	Introduction	15
2-2	Experimental Section	26
2-3	Results and Discussion	31
2-3-1	Selection of electrode materials	31
2-3-2	Preparative experiment of the self-supported paired electrosynthetic system	36
2-3-3	Effect of electrode distance	38
2-3-4	Effect of flow rate	41
2-3-5	Effect of current density	43
2-3-6	Effect of flow mode	45
2-3-7	Generality of the self-supported paired electro-synthetic system	47
2-4	Conclusion	50
2-5	References	51
Chapter 3	Electrochemical Conversion of Primary Amine to Secondary Amine Using a Microreactor: Analogous System of Photocatalytic Redox Combined Synthesis	54

3-1	Introduction	55
3-2	Experimental Section	63
3-3	Results and Discussion	66
3-3-1	Linear sweep voltammetry	66
3-3-2	Preparative electrolysis for the conversion of benzylamine to dibenzylamine using a microreactor	68
3-3-3	Comparison with a conventional batch type reactor	72
3-3-4	Effect of electrode distance	73
3-3-5	Effect of flow rate	74
3-3-6	Effect of current density	75
3-3-7	Improvement of the microreactor: Suppression of the over-oxidation of product amine 3 to intermediate imine 2	76
3-4	Conclusion	81
3-5	References	82
Chapter 4	Product Selectivity Control by Using a Liquid-liquid Parallel Laminar Flow in a Microreactor	86
4-1	Introduction	87
4-2	Experimental Section	99
4-3	Results and Discussion	106
4-3-1	Cyclic voltammetry in the microreactor	106
4-3-2	Reduction potentials of substrates	107
4-3-3	Preparative experiments of the cathodic cross-coupling reaction	109
4-3-4	Estimation of diffusion coefficient for 2a and CFD	

simulations of the liquid-liquid parallel laminar flow in the microreactor	111
4-3-5 Necessity of the liquid-liquid parallel laminar flow mode for the product selectivity control	130
4-3-6 Versatility of this system	131
4-4 Conclusion	135
4-5 References	136
Chapter 5 Summary	140
List of Publications	143
Acknowledgements	145

Chapter 1

General Introduction

This thesis describes the development of electroorganic synthetic systems using electrochemical microreactors. The aim of this chapter is to introduce microreactor technology, reviewing their potential advantages and practical applications, and finally to outline this thesis.

1-1 Introduction and Overview of Microreactor Technology

Microreactor is usually defined as a miniaturized chemical reaction device composed of specially fabricated channel(s).^[1] The characteristic dimensions of the structure of such channels typically range from sub-micrometer to sub-millimeter range. These channels are often made on or in metal, glass, silicon wafers, or polydimethylsiloxane (PDMS). Microreactor system always employs flow system with gas(es), liquid(s), or gas-liquid combined media, composed of some parts such as microreactor main unit(s), pump(s), micromixer(s), microseparator(s), (micro) heat exchanger(s), reaction media collection unit(s), and media transfer tubes.

Although one microreactor unit can produce only a small amount of desired compound, microreactor system with multiplying unit cells, which is so-called “numbering-up” system, enables simultaneous productions of a large amount of target product. In addition, microreactor technology offers quite a lot of attractive advantages that have been widely proved. Hence, microreactor technology has received much attention in the synthetic organic chemistry community over the past two decades, following demonstration of the utility of such systems for micro total analysis (μ -TAS).^[2] Fundamental advantages and potential benefits of microreactor technology are summarized below with some empirical applications.

1-1-1 Extremely large surface-to-volume ratio

One of the most typical characteristic feature of microreactor is extremely large surface-to-volume ratio compared to a classical batch type reactor. As an example, when 1 mL of liquid is in a cubic tube having 1 cm width, the contact area of the liquid toward the channel walls become 4 cm^2 . If the tube has $100 \text{ }\mu\text{m}$ width, the length should be 100 m, and accordingly the contact area should be 400 cm^2 (100 times larger than that of cubic tube). This feature, which is called as scale effect^[3], is regarded as the prime advantage of microreactor.

Hence, microreactor provides ideal circumstances for heterogeneous reactions such as heterogeneous catalytic reaction. For instance, Kobayashi and co-workers successfully demonstrated the gas-liquid-solid triphase hydrogenation reaction using a microreactor (Figure 1-1).^[4] By using their system, the hydrogenation reactions proceeded smoothly to afford the desired products quantitatively within 2 minutes for a variety of alkenes and alkynes. It is noteworthy that microreactor is favorable not only for these heterogeneous catalytic reactions but also for electrode reactions because electrode reactions are typical solid-liquid phase boundary reactions.

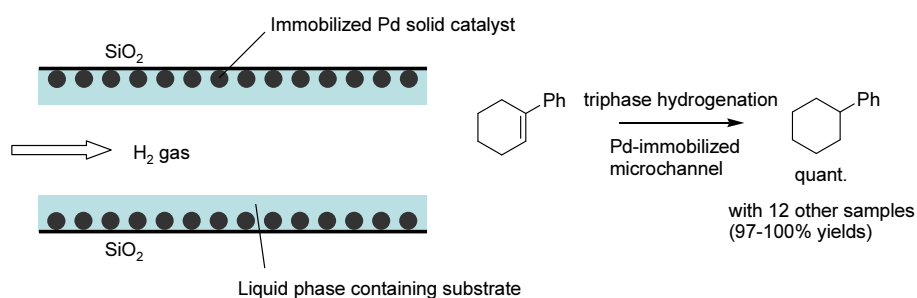


Figure 1-1. Schematic illustrations of triphase hydrogenation reaction using the Pd-immobilized microchannel.

1-1-2 Precise temperature control & Precise residence time control

Since reactions using highly reactive reagents are usually quite exothermic, heat removal is an important factor in controlling the yield and selectivity of such reactions. In microreactor, significantly rapid heat transfer can be achieved by virtue of a large surface area per unit volume, making precise temperature control possible. In addition, the residence time can be greatly reduced in microreactor, and this feature is also quite effective in controlling reactions with short lived species.

Yoshida's group has continued the research about flash chemistry by using microreactors. They control fast reactions which are generally difficult to handle precisely in a conventional batch type reactor. For example, recently, they reported that the switch between kinetic and thermodynamic control in the reaction with nitro-substituted aryl lithium compounds was achieved by using a microreactor (Figure 1-2).^[5] This reaction provided two isomeric products whose the ratio depended on the

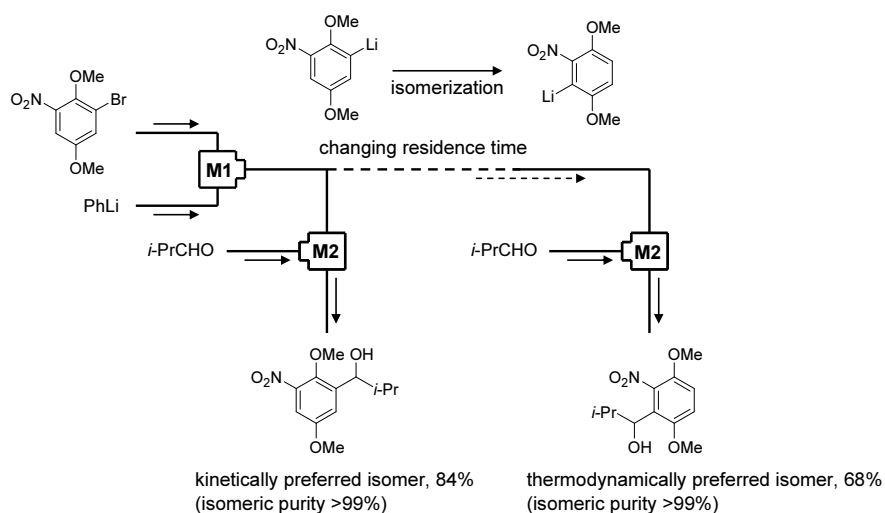


Figure 1-2. Switch between kinetic and thermodynamic control by changing the residence time in the reaction with nitro-substituted aryl lithium compound in the microreactor. **M1** and **M2** signify T-shaped micromixers. The microreactor channels and micromixers were set in a cooling bath to control the reaction temperature.

residence time of aryl lithium compounds in the microreactor channel. By adjusting the suitable residence time, the kinetically preferred isomer or thermodynamically preferred isomer was obtained selectively. Constant temperatures were certainly maintained during such exothermic reactions with highly reactive intermediates in the microreactor.

1-1-3 Strict laminar flow control

Reynolds number (Re) characterizes the flow regimes in channels, such as laminar or turbulent flow. Re is the ratio of inertial forces to viscous forces, and consequently, the value quantifies the relative importance of these two types of forces for given flow conditions as a dimensionless number. The Reynolds equation is given as:

$$\text{Re} = \frac{\rho v_s L}{\mu} \quad \text{Equation 1-1}$$

where ρ is the density of fluid (kg m^{-3}), v_s is the mean fluid velocity (m s^{-1}), L is a characteristic linear dimension (m), and μ is the dynamic viscosity of the fluid (Pa s or $\text{kg m}^{-1} \text{s}^{-1}$). In rectangular channels, L is replaced by the hydraulic diameter (D_h) which defined as:

$$L = D_h = \frac{4S}{l_p} \quad \text{Equation 1-2}$$

where S is the cross-sectional area of the channel (m^2), and l_p is the wetted perimeter (m). The l_p for a channel is the total perimeter of all channel walls that are in contact with the flow. When Re of a flow is less than 2000, the flow becomes laminar flow, where viscous forces are dominant. In contrast, turbulent flow occurs when Re is over 4000 and the flow is dominated by inertial forces.

In microreactor channels, generally, Re is significantly small ($\ll 2000$), so that the

flow is strict laminar flow control. This is mainly due to the extremely small value of L . Therefore, a stable liquid-liquid parallel laminar flow could be also obtained in a microreactor channel by using Y-shaped (or T-shaped) junction with two input streams. In fact, Hibara and co-workers demonstrated a multilayer flow system integrated on microchips.^[6] They showed that interfacial tension had a much larger effect on the interface in the microchannel than gravity, enabling the formation of quite stable liquid-liquid interface. Although the analysis model should be extended to dynamic interfaces to consider the contributions of viscosity and viscoelasticity, they also demonstrated the solvent extraction of Co complex as a typical application of the multilayer flow system.

1-1-5 Extremely fast molecular diffusion

Generally, the molecular diffusion is expressed by following equation:

$$\text{molecular diffusion} = -S \cdot D \cdot \Delta C \quad \text{Equation 1-3}$$

where S is the superficial area, D is the molecular diffusion coefficient, and ΔC is the concentration gradient. When the scale of the fluid changes to ε^{-1} , the scale factor of molecular diffusion becomes ε^{-2} according to the Equation 1-3. Briefly, the molecular diffusion is inversely proportional to the square value of the scale. At the same time, the volume of the fluid becomes ε^{-3} . This means that the ratio of the molecular diffusion to the volume becomes ε , so that the decrease of the scale increases the molecular diffusion efficiency. Hence, the molecular diffusion in a microreactor channel is significantly fast compared to the macro-scale batch type reactor.

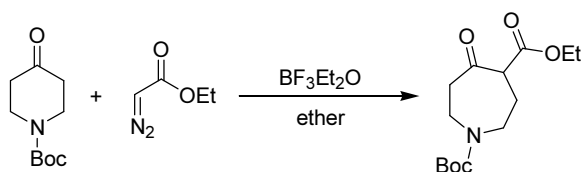
Actually, in our previous work, we have successfully demonstrated the electrochemical methoxylation of furan by using a electrochemical microreactor.^[7] The fast diffusion of anodically generated protons toward the cathode played an important

role in this system (for more details, see: 2-1 Introduction in chapter 2).

1-1-6 Improvement of reaction process safety

From the viewpoint of safe operation of hazardous reactions, microreactor systems are more preferable processes than traditional batch or flow systems. The highly efficient heat transfer and small reaction volumes of microreactor systems allow safer handling of exothermic reactions, reactions involving explosive and toxic materials, and other hazardous reactions that are normally difficult to scale up.

Researchers of Johnson & Johnson group have proved the safety enhancement of hazardous ring-expansion reaction by using a microreactor system (Scheme 1-1).^[8] This reaction uses ether (as solvent) and potentially hazardous diazo compound. This reaction is very exothermic, which the heat release rate is not feed-control. In addition, this very sluggish reaction needs an initiation period. Furthermore, evolution of large amounts of nitrogen gas could result in over-pressurization of the reaction vessel. Hence, from these problematic features of the reaction, scaling up to kilogram scales using conventional batch type reactor could not be recommended. However, the microreactor system enabled to carry out this reaction smoothly and safely with precise control. Applying the conditions established on the 70 mg scale reaction in batch mode, the reaction proceeded to give the desired product in 89% yield (91 g per hour) without any further optimization in the microreactor.



Scheme 1-1

1-1-7 Other advantages

Adding above advantages, following advantages would be also obtained:

- Faster transfer of research results into production
- Fast and cost-saving reaction screening
- Smaller plant size for distributed production
- Mass production flexibility by numbering-up technique
- Higher reproducibility with simplified and precise process operations

1-2 Outline of This Thesis

Microreactor technology for organic synthesis has been significantly investigated for the past two decades, however, the integrated use of microreactor technology with electroorganic synthesis has been quite limited so far.^[9] Only a few examples containing our previous works have been reported. As introduced in the previous section, microreactor has a lot of advantages, which should be more purposely applied for a wide range of organic synthesis and organic mass production processes. Electron transfer is one of the most typical driving factors for organic reaction, and electroorganic synthesis serves as a straightforward and powerful method for organic electron transfer processes (advantages of electroorganic synthesis, see: 2-1 Introduction of Chapter 2).^[10] Therefore, the integrated use of microreactor technology with electroorganic synthesis would offer one of the most sophisticated processes in organic chemistry.

With these backgrounds in mind, this thesis focuses on practical applications of an electrochemical microreactor to electroorganic synthesis. The electrochemical microreactor used in this thesis, which was developed in our previous work, had a geometry with the anode plate and cathode plate directly facing each other. A spacer with several tens μm of thickness was used to leave a rectangular channel exposed, and the two electrode plates were simply sandwiched together. This simple cell structure instantly provides micro-scale effects in the reaction field, and therefore, enables electrochemistry in a microreactor with large electrode surface area. The large electrode surface area is significantly profitable for synthetic applications even in laboratory scale mass production.

In addition, this thesis aims to propose novel systems which are realized only by using the electrochemical microreactor. In other words, research demonstrations in this

thesis purposely utilize specific advantages of the electrochemical microreactor to develop novel systems. Therefore, similar reaction results would be never obtained by using a conventional batch type reactor.

Finally, outlines of each chapter are described below.

In Chapter 1 (current chapter), microreactor technology with their potential advantages and practical applications, and the outline of this thesis are introduced.

In Chapter 2, a self-supported paired electrosynthetic microreactor system using acetonitrile is developed. This system enables paired electrochemical reactions composed of organic chloride reduction/alcohol oxidation combination to proceed without intentionally added supporting electrolyte. The successful demonstration of this system provides a practical methodology for constructing a self-supported electrosynthetic microreactor system using aprotic solvent.

In Chapter 3, a $[S/\pm e^-/I/\mp e^-/P]$ type electrochemical conversion of benzylamine to dibenzylamine using a microreactor is investigated as an analogue of photocatalytic redox combined reaction. By comparison with a conventional batch type reactor, a clear advantage of this electrochemical microreactor system is demonstrated.

In Chapter 4, a new method for product selectivity control by using a liquid-liquid parallel laminar flow in a microreactor is demonstrated. The combined use of suitable flow mode and corresponding cathode material enables chemoselective cathodic reduction to control the product regioselectivity. The formation of liquid-liquid parallel laminar flow in the microreactor channel is supported by CFD simulations.

In Chapter 5, the summary and further aspects of the present works are described.

1-3 References

- [1] For selected books and reviews on microreactor technology, see: a) *Microreaction Technology* (Ed. W. Ehrfeld), Springer, Berlin, **1998**; b) S.J. Haswell, P.D.I. Fletcher, G.M. Greenway, V. Skelton, P. Styring, D.O. Morgan, S.Y.F. Wong, B.H. Warrington, in *Automated Synthetic Methods for Speciality Chemicals* (Ed. W. Hoyle), Royal Society of Chemistry, Cambridge, **1999**, p. 26; c) *Microsystem Technology in Chemistry and Life Sciences* (Eds. A. Manz, H. Becker), Springer, Berlin, **1999**; d) *Microreactors* (Eds. W. Ehrfeld, V. Hessel, H. Löwe), Wiley-VCH, Weinheim, **2000**; e) K.F. Jensen, *Chem. Eng. Sci.* **2001**, *56*, 293; f) S.J. Haswell, R.J. Middleton, B. O'Sullivan, V. Skelton, P. Watts, P. Styring, *Chem. Commun.* **2001**, 391; g) P.D.I. Fletcher, S.J. Haswell, E. Pombo-Villar, B.H. Warrington, P. Watts, S.Y.F. Wong, X. Zhang, *Tetrahed.* **2002**, *58*, 4735; h) K. Jähnisch, V. Hessel, H. Löwe, *Angew. Chem. Int. Ed.* **2004**, *43*, 406; i) K. Geyer, J.D.C. Codée, P.H. Seeberger, *Chem. Eur. J.* **2006**, *12*, 8434. j) A.J. deMello, *Nature* **2006**, *442*, 394; k) B.P. Mason, K.E. Price, J.L. Steinbacher, A.R. Bogdan, D.T. McQuade, *Chem. Rev.* **2007**, *107*, 2300; l) J. Yoshida, S. Suga, *Electrochemistry* **2007**, *75*, 58; m) J. Yoshida, A. Nagaki, T. Yamada, *Chem. Eur. J.* **2008**, *14*, 7450; n) T. Fukuyama, Md. T. Rahman, M. Sato, I. Ryu, *Synlett* **2008**, *2*, 151; o) F.E. Valera, M. Quaranta, A. Moran, J. Blacker, A. Armstrong, J.T. Cabral, D.G. Blackmond, *Angew. Chem. Int. Ed.* **2010**, *49*, 2478.
- [2] For example: A. Manz, N. Graber, H.M. Widmer, *Sen. Actuators B* **1990**, *1*, 244.
- [3] In micrometer region, the effects of parameters related to the volume such as mass and inertial forces are relatively decreased. In contrast, the parameters related to the surfaces or interfaces such as diffusion, heat transfer, viscosity, and

surface tension remarkably contribute to the system. This tendency related to micro-fluids is called as scale effects.

- [4] J. Kobayashi, Y. Mori, K. Okamoto, R. Akiyama, M. Ueno, T. Kitamori, S. Kobayashi, *Science* **2004**, *304*, 1305.
- [5] A. Nagaki, H. Kim, J. Yoshida, *Angew. Chem. Int. Ed.* **2009**, *48*, 8063.
- [6] A. Hibara, M. Tokeshi, K. Uchiyama, H. Hisamoto, T. Kitamori, *Anal. Sci.* **2001**, *17*, 89.
- [7] a) D. Horii, M. Atobe, T. Fuchigami, F. Marken, *Electrochem. Commun.* **2005**, *7*, 35; b) D. Horii, M. Atobe, T. Fuchigami, F. Marken, *J. Electrochem. Soc.* **2005**, *153*, D143.
- [8] X. Zhang, S. Stefanick, F.J. Villani, *Org. Process Res. Dev.* **2004**, *8*, 455.
- [9] a) M. Kupper, V. Hessel, H. Löwe, W. Stark, J. Kinkel, M. Michel, H. Schmidt-Traub, *Electrochim. Acta* **2003**, *48*, 2889; b) C.A. Paddon, M. Atobe, T. Fuchigami, P. He, P. Watts, S.J. Haswell, G.J. Pritchard, S.D. Bull, F. Marken, *J. Appl. Electrochem.* **2006**, *36*, 617; c) K. Bouzek, V. Jiříčný, R. Kodým, J. Křišťál, T. Bystron, *Electrochim. Acta* **2010**, *55*, 8172.
- [10] For principal reviews and the book on electroorganic synthesis, see: a) S. Wawzonek, *Science* **1967**, *155*, 39; b) T. Shono, *Tetrahed.* **1984**, *40*, 811; c) M.M. Baizer, *Pure & Appl. Chem.* **1986**, *58*, 889; d) E. Steckhan, T. Arns, W.R. Heineman, G. Hilt, D. Hoormann, J. Jorissen, L. Kroner, B. Lewall, H. Pütter, *Chemosphere* **2001**, *43*, 63; e) *Organic Electrochemistry*, fourth ed. (Eds. H. Lund, O. Hammerich), Marcel Dekker, New York, **2001**; f) G. Hilt, *Angew. Chem. Int. Ed.* **2002**, *41*, 3586; g) T. Fuchigami, T. Tajima, *Electrochemistry* **2006**, *74*, 585;

h) J. Yoshida, K. Kataoka, R. Horcajada, A. Nagaki, *Chem. Rev.* **2008**, *108*, 2265;

i) H. Tanaka, M. Kuroboshi, K. Mitsudo, *Electrochemistry* **2009**, *86*, 1129.

Chapter 2

Self-supported Paired Electrosynthesis Using a Microreactor without Intentionally Added Supporting Electrolyte

A self-supported paired electrosynthetic microreactor system using acetonitrile has been developed. This system enables paired electrochemical reactions composed of organic chloride reduction/alcohol oxidation combination to progress without intentionally added supporting electrolyte. A simultaneous supply of the reduction and oxidation products was conducted in good to moderate yields in a single pass of substrate solutions by the use of parallel laminar flow mode. More importantly, the successful demonstration of this system can provide a practical methodology for constructing a microreactor system which enables an electroorganic process to progress without added supporting electrolytes even in aprotic solvents.

2-1 Introduction

2-1-1 Background

Environmental consciousness in almost all industrial fields has become a large movement in recent history. Synthetic chemistry have been strongly influenced by such movement and especially, the field of chemistry toward environmental consciousness has come to be known as “green/sustainable chemistry”.^[1]

Green/sustainable chemistry intends to design and develop alternative processes which minimize the use and generation of environmentally hazardous chemicals during the production of desired compounds. P.T. Anastas and J.C. Warner propounded 12 principles of green chemistry which definite the philosophy and provide practical guidelines when researchers works on this field.^[2]

The 12 principles are:

1. **Prevention**

It is better to prevent waste than to treat or clean up waste after it is formed.

2. **Atom Economy**

Synthetic methods should be designed to maximize the incorporation of all materials used in the process into the final product.

3. **Less Hazardous Chemical Syntheses**

Wherever practicable, synthetic methods should be designed to use and generate substances that possess little or no toxicity to human health and the environment.

4. **Designing Safer Chemicals**

Chemical products should be designed to effect their desired function while minimizing their toxicity.

5. **Safer Solvents and Auxiliaries**

The use of auxiliary substances (*e.g.*, solvents, separation agents, *etc.*) should be made unnecessary wherever possible and innocuous when used.

6. **Design for Energy Efficiency**

Energy requirements of chemical processes should be recognized for their environmental and economic impacts and should be minimized. If possible, synthetic methods should be conducted at ambient temperature and pressure.

7. **Use of Renewable Feedstocks**

A raw material or feedstock should be renewable rather than depleting whenever technically and economically practicable.

8. **Reduce Derivatives**

Unnecessary derivatization (use of blocking groups, protection/ deprotection, temporary modification of physical/chemical processes) should be minimized or avoided if possible, because such steps require additional reagents and can generate waste.

9. **Catalysis**

Catalytic reagents (as selective as possible) are superior to stoichiometric reagents.

10. **Design for Degradation**

Chemical products should be designed so that at the end of their function they break down into innocuous degradation products and do not persist in the environment.

11. **Real-time Analysis for Pollution Prevention**

Analytical methodologies need to be further developed to allow for real-time, in-process monitoring and control prior to the formation of hazardous substances.

12. Inherently Safer Chemistry for Accident Prevention

Substances and the form of a substance used in a chemical process should be chosen to minimize the potential for chemical accidents, including releases, explosions, and fires.

Among many methodologies which are fitted and introduced in the above principles, it has been regarded that electroorganic synthesis has a potentiality for a green/sustainable process because it has some original features along with these principles.

As stated briefly in Chapter 1, electroorganic synthesis has been established as a powerful tool for molecular transformation over the past century. Instead of the use of hazardous chemical oxidant and reductant, electrooxidation and electroreduction can be achieved by electron transfer between substrate molecules and electrodes. By this simple and straightforward method, highly reactive species such as radical cations and radical anions can be generated and then, various types of reactions such as carbon-carbon bond formations and functional group transformations are accomplished. In addition, such electrochemical transformations are usually operated under mild and benign conditions. Since these reactions can be strictly controlled by closing or opening of the circuit of electric current source, electrochemical transformations are carried out in safety without running out of control.

From these point of views, electroorganic synthesis can serve as green/sustainable procedures, and hence it has received significant research interest from both academia and industry.^[3]

However, although enormous contributions have been made, electroorganic synthesis is still in development to fulfill their potential as environmentally friendly processes. The need of adding supporting electrolyte to solvent causes one of the most

critical problems regarding electroorganic synthesis. In conventional processes, a large amount of supporting electrolyte is required in order to provide sufficient electrical conductivity to solvent for electrolysis, but the presence of the supporting electrolyte might cause separation and industrial waste problems. The problem of adding supporting electrolyte is a conspicuous drawback of electroorganic synthesis.

Recently, to solve supporting electrolyte separation problem, electrosynthetic systems using ion exchange membranes as solid polymer electrolytes^[4] and thermomorphic biphasic organic solutions^[5] have been developed. Although these methods are one of the smart solutions about the separation problem of electrolyte, the waste problem of electrolyte still remains.

On the other hand, a capillary gap cell has also been developed especially for commercial use.^[6] The narrow electrode distance reduces cell voltage and the cell allows minimizing electrolyte addition in electrosynthetic processes.

In 2002, Marken and his research group have successfully demonstrated that by using a micro-meter gap flow cell (thin layer flow cell), the two electron/two proton reduction of tetraethyl ethylenetetra-carboxylate in ethanol was realized without intentionally added supporting electrolyte (Figure 2-1).^[7] Tetraethyl ethanetetra-carboxylate was obtained in good yield simply after solvent evaporation. The thin layer flow cell employed in this work had a geometry with working and auxiliary electrodes directly facing each other. The distance between anode and cathode was 50 μm so that the two diffusion layers of working and auxiliary electrode could overlap or become “coupled”. This overlapping diffusion layer enabled that ions electrogenerated locally and *in situ* between electrodes played the role of supporting electrolyte, and consequently, the “self-supported” bulk electrolysis was carried out without intentionally added supporting electrolyte.

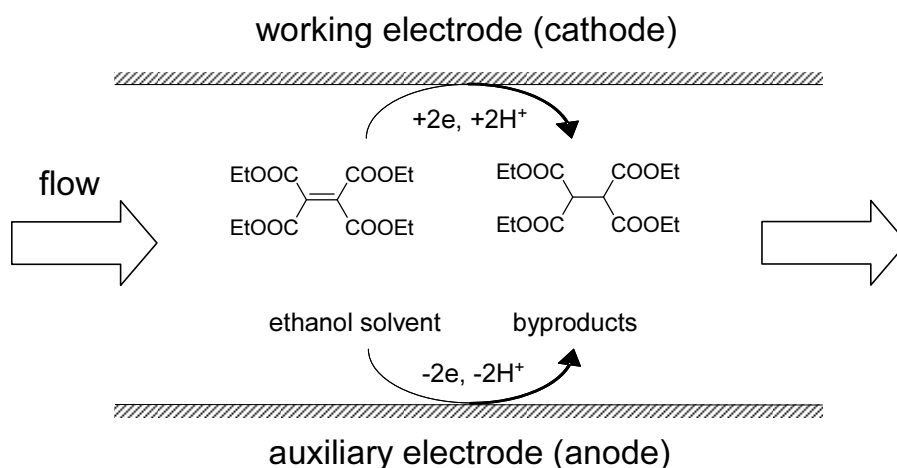


Figure 2-1. Schematic representation of the hydrogenation of activated olefin in ethanol using a thin layer flow cell in the absence of supporting electrolyte.

On the basis of this preliminary study of the self-supported electrolysis system, some practical systems have been reported. Yoshida's group reported a flow-through porous thin-gap electrode microreactor permitting operation without supporting electrolyte.^[8] In their system, two porous electrodes were facing each other and separated (at a distance of micrometer size) by a porous spacer, and the electric flow and the liquid flow were parallel. Our research group has also developed electrolyte-free electrochemical system for electrochemical methoxylation of furan using an electrochemical microreactor (Figure 2-2).^[9] The microreactor employed in this work is similar to the Marken's thin layer flow cell. It has a simple geometry with working and counter electrodes directly facing each other. The distance between these electrodes is sufficiently small enough to ensure that the electrogenerated ions derived from substrate and solvent can play the role of electrolyte. Consequently, the process becomes to be self-supported.

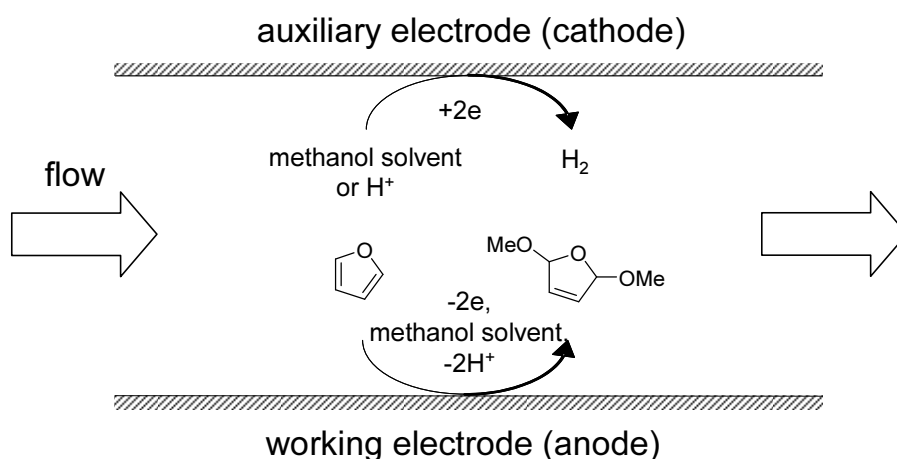


Figure 2-2. Schematic representation of the anodic methoxylation of furan in methanol using a microreactor in the absence of supporting electrolyte.

These examples of the electrochemical system without intentionally added supporting electrolyte show the capability of microreactor as an environmentally friendly organic electrochemical tool. The self-supported system is one of the straightforward solutions for the supporting electrolyte problem in electroorganic synthesis, and therefore, it can be stated that further extensive study of the self-supported microreactor system is highly desirable. Particularly, a practical methodology for designing of self-supported system has still not been established. It is important to establish how to design the system which becomes to be self-supported.

2-1-2 Mechanism of self-supported system

Although self-supported microreactor systems reported previously were well designed, the solvents of these systems were limited to protic solvents such as methanol and ethanol in all cases. Other solvents such as acetonitrile cannot be used for their systems due to the extremely high cell voltages.

Such a difference between protic and aprotic solvents can be explained on the basis of mechanism in each solvent as stated below.

In the case of protic solvent

Firstly, protic solvents such as methanol and ethanol are easily oxidized at the anode to give protons. These electrogenerated protons are smoothly migrated to the cathode *via* hydrogen bond network by proton jump mechanism (Grotthuss mechanism).^[10] Then, migrated protons and/or solvent are readily reduced at the cathode. Each process is proceeded simultaneously and harmonized, and consequently, the system can be carried out with low cell voltage. For synthetic systems, either anodic oxidation of solvent or cathodic reduction of proton and/or solvent is replaced by the desired electrochemical reaction of a substrate. Actually the previous examples were constructed by this mechanism.

In the case of aprotic solvent

Self-supported systems using aprotic solvents often require extremely high cell voltages. This situation would be caused by the following reasons in their mechanism. First, aprotic solvent like acetonitrile is hardly oxidized at the anode, so that an adequate amount of proton for carrying electric charge cannot be produced at the anode. Second, the proton transfer between electrodes is slower than that in protic solvent. Third, the cathodic reduction of acetonitrile cannot proceeded smoothly because acetonitrile has a high reduction potential. Consequently, additional large electric energy would be required in order to proceed these problematic steps in the aprotic solvent system.

In the previous reports, the electrogenerated proton derived from solvent or substrate worked as a main charge carrier of the system. However, if the other stable ionic species are generated *in situ* from substrate, they would also work as charge

carriers instead of proton. In order to realize the self-supported system using aprotic solvent, such alternative ionic species derived from substrates should be employed as charge carriers.

Recently, Haswell and his coworkers reported that an electrochemical cross-coupling reaction of dimethyl fumarate with benzyl bromide was successfully carried out by using a microreactor without intentionally added supporting electrolyte in DMF solvent (Figure 2-3).^[11] Bromide ions were released *in situ* from benzyl bromide by progress of the reaction, and then, they worked as electric charge carriers in this system. Additionally, dimethyl fumarate reduction at the cathode and DMF decomposition at the anode are easily occurred at low reduction and oxidation potentials, respectively. These reasonable reaction designs enable the system to be self-supported even in aprotic solvent.

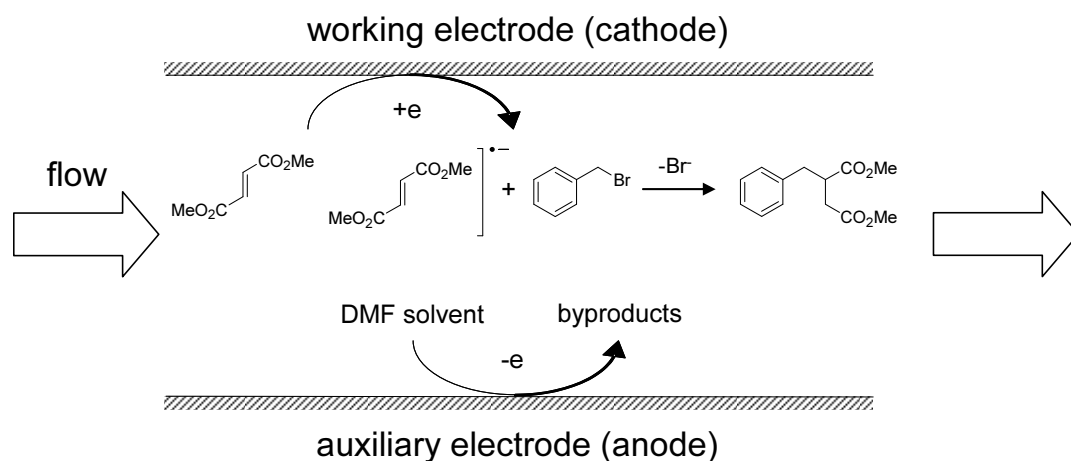


Figure 2-3. Schematic representation of the reductive C-C coupling reaction of dimethyl fumarate with benzyl bromide in DMF using a microreactor in the absence of supporting electrolyte. (It is not clear whether the final coupling step proceeds through a second- electron transfer process or not.)

2-1-3 *Objective and strategy of this chapter*

As already mentioned, the extensive study of self-supported microreactor system is quite attractive subject. Although one example of the self-supported system in aprotic solvent has already been reported, further practical examples will provide the methodology for designing of self-supported system. Moreover, the overcome of solvent limitation will expand the versatility of self-supported system. With this in mind, the purpose of this chapter is to demonstrate a novel self-supported paired electrochemical process in acetonitrile as solvent using a microreactor.

Meanwhile, acetonitrile is a conventional solvent in organic synthesis especially in electrochemical synthesis. Its high dielectric constant allows smooth electric charge transfer between electrodes in the presence of adequate amounts of supporting electrolyte. Wide variety of organic and inorganic compounds can be dissolved in it, and more importantly, acetonitrile has a very wide potential window. High stability of acetonitrile toward anodic oxidation and cathodic reduction enables to electrolyze many kinds of organic compounds. However, in a self-supported system, anodic or cathodic decomposition reaction of acetonitrile cannot be employed as an auxiliary reaction because of its high stability. In order to employ acetonitrile as a solvent for self-supported system, paired electrode reactions of substrate(s), which stable ionic species can be generated, should be applied to the system.

Paired electrode reactions (or paired electrosynthesis) mean the simultaneously synchronous utilization of anodic and cathodic reactions for efficient synthesis of desired products.^[12] In conventional electrode processes, often attention is focused on only one of the reactions in a divided cell arrangement or the accompanying reaction at the counter electrode (*e.g.*, sacrificial electrode) is chosen to be innocuous, not to interfere with starting materials, intermediates, or products. The auxiliary reaction at

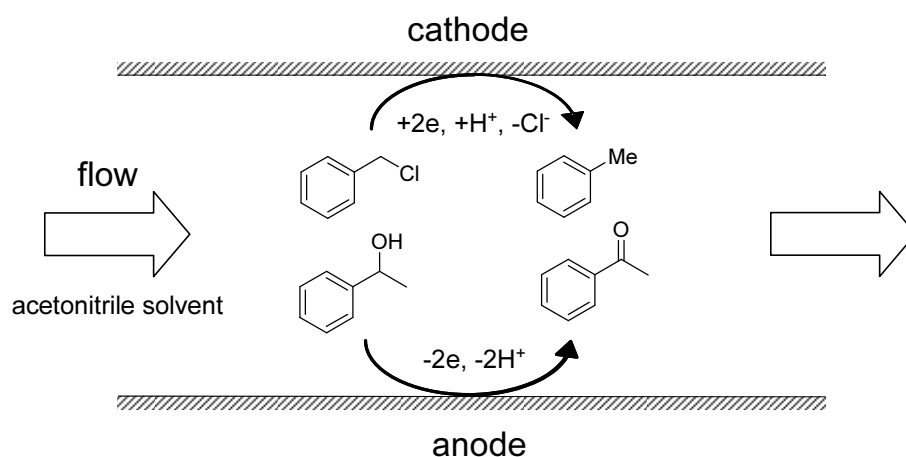


Figure 2-4. Schematic representation of the paired electrode reactions of benzyl chloride and 1-phenylethanol in acetonitrile using a microreactor in the absence of supporting electrolyte.

the counter electrode would be deserted. In paired electrode reactions both the anodic and cathodic reactions can be matched and contribute to the formation of the final product(s). Consequently, paired electrode reactions should be very preferable from a practical aspect and significant number of studies concerning about the paired electrosynthetic process has been reported since 1976.^[13] In the present work, both cathodic and anodic reactions in a paired electrosynthesis should be purposely used for the construction of self-supported system using acetonitrile as solvent.

To demonstrate the practicability of the self-supported paired electrosynthetic system using acetonitrile, two substrates such as benzyl chloride and 1-phenylethanol were employed (Figure 2-4). In this starting substrate combination, benzyl chloride would be reduced at the cathode and 1-phenylethanol would be oxidized at the anode to give the corresponding two products (toluene and acetophenone, respectively). These substrates would also release ionic species such as chloride ion and proton following the respective electrode reactions, and these released ionic species would act as the main carrier of electric charge. Thus, the whole system would become to be self-supported without the need for the solvent (acetonitrile) decomposition.

Chapter 2 Self-supported Paired Electrosynthesis Using a Microreactor without Intentionally Added Supporting Electrolyte

The demonstration of the above concept, reaction conditions, application of liquid-liquid parallel laminar flow mode, and versatility of this system were investigated in this chapter.

2-2 Experimental Section

2-2-1 Microreactor

The microreactor had a geometry with Ag cathode (3 cm width, 3 cm length, Nilaco) and indium tin oxide (ITO) anode (3cm width, 3cm length, Geomatec) directly facing each other. A spacer (adhesive tape, 80 μm thickness, Nitto Denko) was used to leave a rectangular channel exposed, and the two electrodes were simply sandwiched together (area of the electrode channel was 3 cm^2). After connecting Teflon tubing to inlet and outlet, the reactor was sealed with epoxy resin (Figure 2-5).

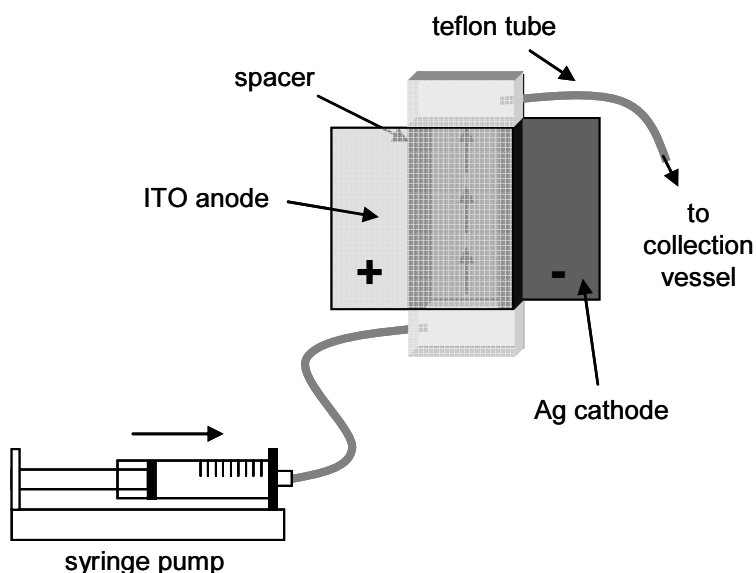


Figure 2-5. Schematic illustration of the microreactor.

2-2-2 Two inlet microreactor

The two inlet microreactor consisted of two plates. Each plate was glued to the electrode plate (Ag cathode plate or ITO anode plate, 3 cm width, 3 cm length) and glass plate (2.6 cm width, 3 cm length) together. A slit was provided on the anode side for introducing alcohol solutions into the reactor. A spacer (adhesive tape, 80 μm

thickness, Nitto Denko) was used to leave a rectangular channel exposed, and the two plates were simply sandwiched together. After connecting Teflon tubing to inlets and outlet, the reactor was sealed with epoxy resin. The dimensions of the channel were 1 cm width, 80 μm height and 6 cm in total length. The area of the electrode channel was 3 cm^2 (Figure 2-6).

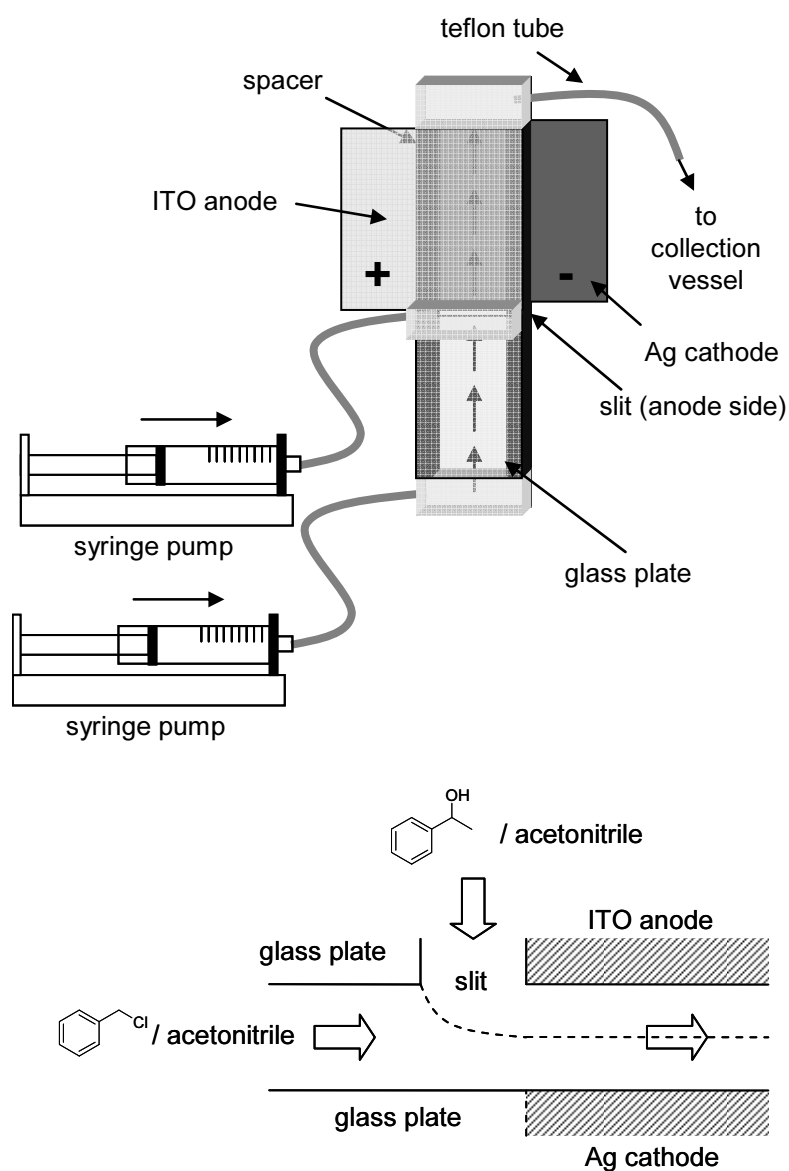


Figure 2-6. Schematic illustrations of the two inlet microreactor.

2-2-3 Materials

Dehydrated acetonitrile was purchased from Wako Pure Chemical Industries. Benzyl chloride, 1-phenylethanol, toluene, acetophenone, tetra-*n*-butylammonium tetrafluoroborate (*n*-Bu₄NBF₄), α -chloro-*p*-xylene, 4-cyanobenzyl chloride, benzyl bromide and 1-(*p*-tolyl)ethanol were purchased from Tokyo Kasei Kogyo. All purchased chemicals were used as received.

4-(1-hydroxyethyl)benzointrile was prepared according to the literature procedure.^[14] Specifically, NaBH₄ was added to a solution of the 4'-cyanoacetophenone in EtOH at 0 °C. After the addition was completed, the reaction mixture was stirred at room temperature until TLC showed no starting material was left. After evaporation of the solvent, the residue was dissolved in AcOEt and H₂O and extracted three times with AcOEt. The combined organic layer was dried over Na₂SO₄, filtered, and evaporated. The residue was purified by silica gel column chromatography to give the desired product as pale yellow oil in 65 % yield. ¹H-NMR (CDCl₃, 270 MHz) δ : 7.64 (d, 2H, *J* = 8.2 Hz), 7.49 (d, 2H, *J* = 8.2 Hz), 4.97 (q, 1H, *J* = 6.5 Hz), 2.01 (br s, 1H), 1.50 (d, 3H, *J* = 6.5 Hz)

2-2-4 Linear sweep voltammetry

Linear sweep voltammetry was performed by using a ALS/CHI Electrochemical Analyzer (630C, CH Instruments). Linear sweep voltammograms were recorded using an undivided cell equipped with a working disk electrode (3 mm diameter), an auxiliary electrode (Pt plate, 6 cm²), and a saturated calomel reference electrode.

2-2-5 *General procedure for paired electrosynthesis*

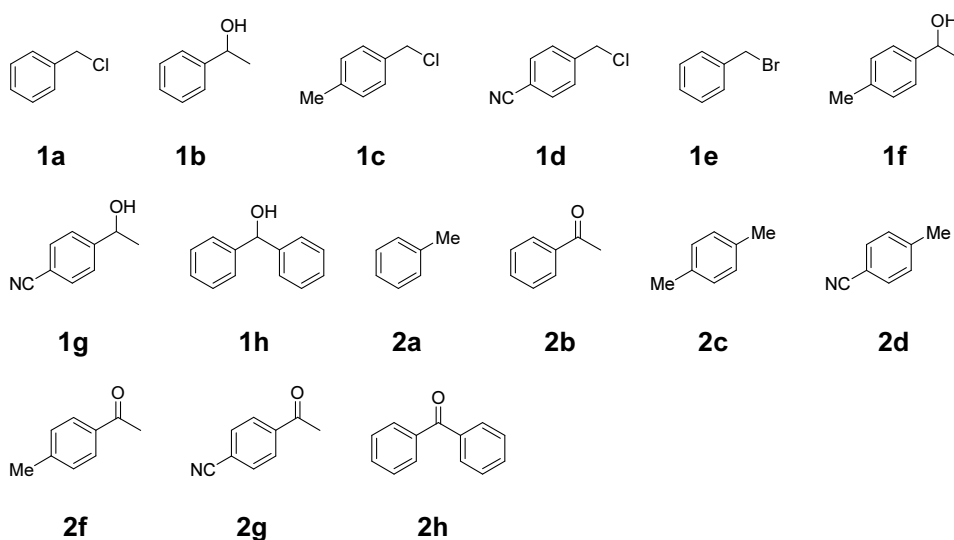
Bulk electrolysis was conducted with a constant current by using a PGSTAT (HA-501, Hokuto Denko) in a beaker cell. For the electrolysis using the microreactor, an acetonitrile solution containing organic halide (30 mM) and alcohol (30 mM) was introduced through the inlet of the reactor (Figure 2-5). For the electrolysis using the two inlet microreactor, an acetonitrile solution containing organic halide (30 mM) was introduced through cathode side inlet and an acetonitrile solution containing alcohol (30 mM) was introduced through anode side inlet, respectively (Figure 2-6). The flow rate of the reaction solutions was controlled by syringe pump (KDS100, KD Scientific). 0.5 mL of electrolyzed solutions were collected and analyzed by high performance liquid chromatography (HPLC) to determine substrate conversions and product yields. The HPLC analysis was performed by an external standard method with Shimadzu LC-6A liquid chromatograph equipped with a UV detector (SPD-6A, Shimadzu) and a Develosil[®] ODS-5 column (Nomura Chemical). Conditions of the HPLC analysis of each compound were shown in Table 2-1.

Table 2-1. HPLC conditions utilized for the determination of conversions and yields.^a

Compound	acetonitrile/water (v/v)	Retention time (min)
1a	55/45	10.7
1b	55/45	4.0
1c	30/70	15.6
1d	50/50	33.1
1e	50/50	15.4
1f	50/50	5.4
1g	55/45	3.3
1h	50/50	6.4
2a	55/45	12.9
2b	55/45	5.4
2c	55/45	19.8
2d	30/70	28.6
2f	50/50	7.9
2g	55.45	4.2
2h	50/50	10.8

^aFlow rate was 1.0 mL min⁻¹. Compounds were detected at 254 nm.

For the structure of compounds, see below.

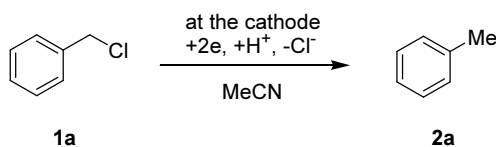


2-3 Results and Discussion

2-3-1 Selection of electrode materials

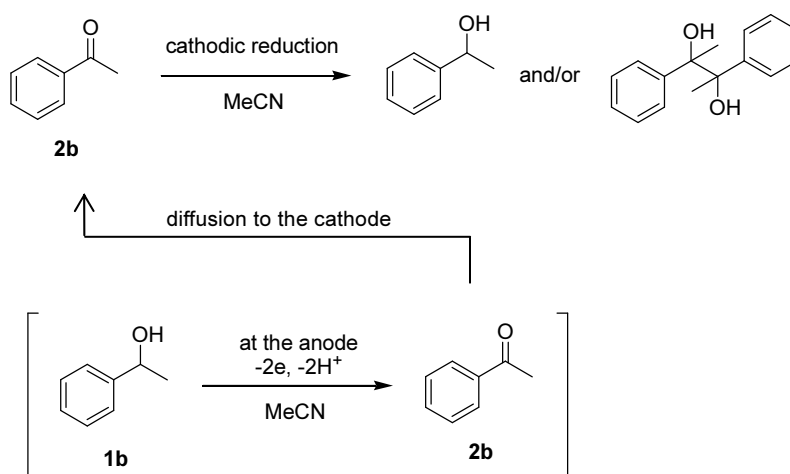
The electrode material is an important factor in selecting the course of an electrode reaction and in controlling the efficiency of the reaction.^[15] Especially in the desired system, as acetonitrile solvent doesn't participate in the electrode reactions, the smooth cathodic reduction and anodic oxidation of substrates are extremely important. In order to select suitable electrode materials for the system, linear sweep voltammograms for the reduction of benzyl chloride (**1a**) and the oxidation of 1-phenylethanol (**1b**) using several electrodes were measured.

Cathode material



Linear sweep voltammograms for the reduction of benzyl chloride were recorded in the presence of 0.1 M *n*-Bu₄NBF₄ supporting electrolyte in acetonitrile solution at a platinum (Pt), grassy carbon (GC), and silver (Ag) disk electrodes, respectively (Scheme 2-1, Figure 2-7). As shown in Figure 2-7 (a), the reduction current for benzyl chloride at the Ag disk electrode was observed at much more positive potential than that recorded at Pt and GC electrodes. It is well known that the Ag electrode has a catalytic activity toward the reduction of organic halides.^[16] Our result also follows these previous reports. Furthermore, it should be noted that the anodic product (acetophenone) derived from 1-phenylethanol can easily access the cathode surface and its reduction may occur because the distance between the anode and cathode is

very small (Scheme 2-2). In this regard, as shown in Figure 2-7 (b), the reduction of acetophenone at the Ag electrode occurred at a much more negative potential than that of benzyl chloride, and hence, the benzyl chloride reduction would progress smoothly without interference from acetophenone reduction. Therefore, it can be stated that the Ag electrode is the better cathode material in this system.



Scheme 2-2

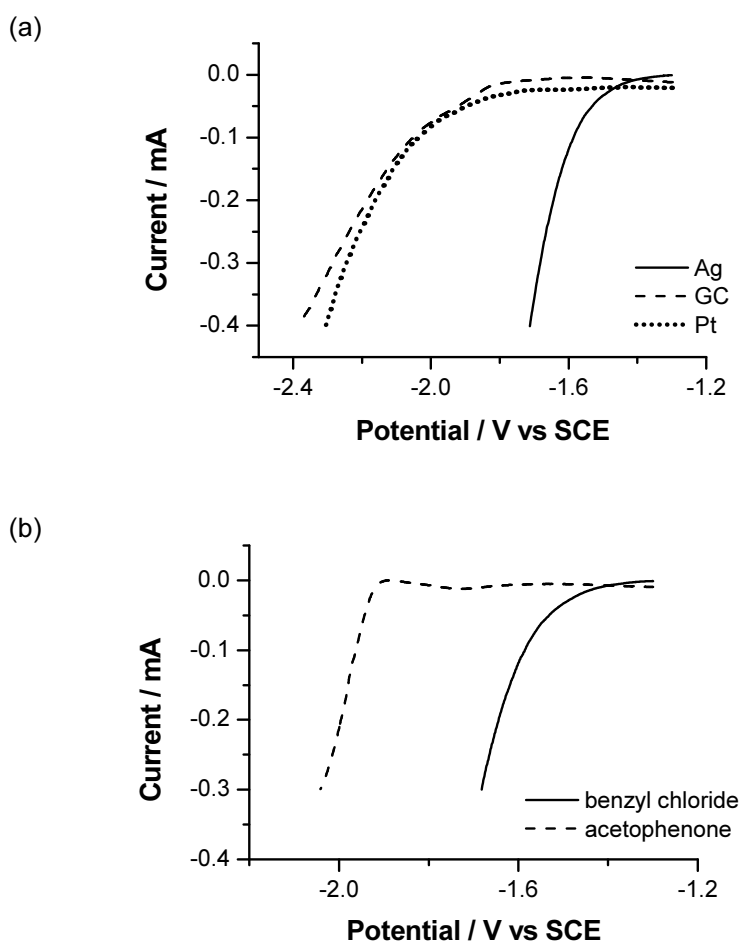
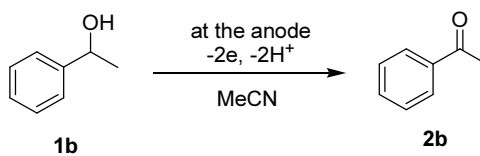


Figure 2-7. Linear sweep voltammograms of (a) 30 mM benzyl chloride/acetonitrile solution recorded at various disk electrodes (diameter: 3 mm) and (b) 30 mM acetophenone/acetonitrile solution and 30 mM benzyl chloride/acetonitrile solution recorded at a Ag disk electrode (diameter: 3 mm). The scan rate was 20 mV s^{-1} .

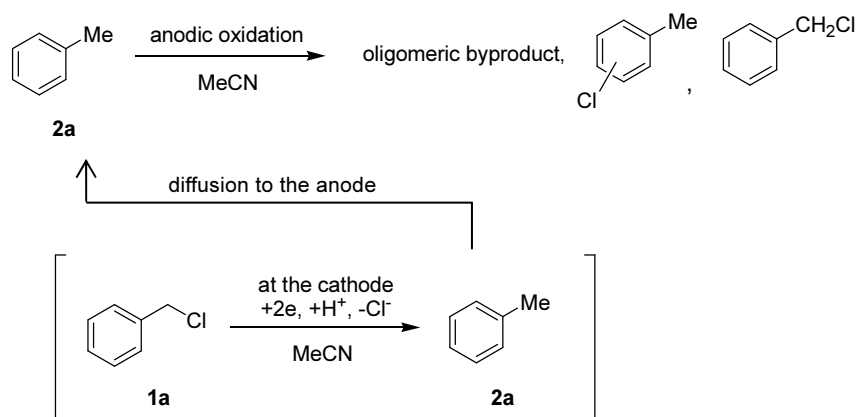
Anode material



Scheme 2-3

Scheme 2-3 shows the desired anodic reaction of this system and Figure 2-8 shows linear sweep voltammograms for the oxidation of 1-phenylethanol and toluene in the

presence of 0.1 M *n*-Bu₄NBF₄ supporting electrolyte in acetonitrile solution at a Pt, GC, and indium tin oxide (ITO) disk electrodes. Since toluene is a cathodic product, its anodic oxidation should be also paid attention (Scheme 2-4). When the Pt disk electrode was used as the anode material, the observed current for toluene oxidation was higher than that of 1-phenylethanol oxidation (Figure 2-8 (a)). At the GC disk electrode, the current for toluene oxidation was nearly equal to that of 1-phenylethanol oxidation (Figure 2-8(b)). Hence, if these electrodes are used as the anode material for the system, the toluene oxidation would interfere with the desired alcohol oxidation. After the testing of several anode materials, it was clarified that the oxidation of toluene was significantly suppressed by using the ITO disk electrode although the desired alcohol oxidation occurred smoothly (Figure 2-8 (c)). From these results, the ITO electrode is the suitable anode material for the system.



Scheme 2-4

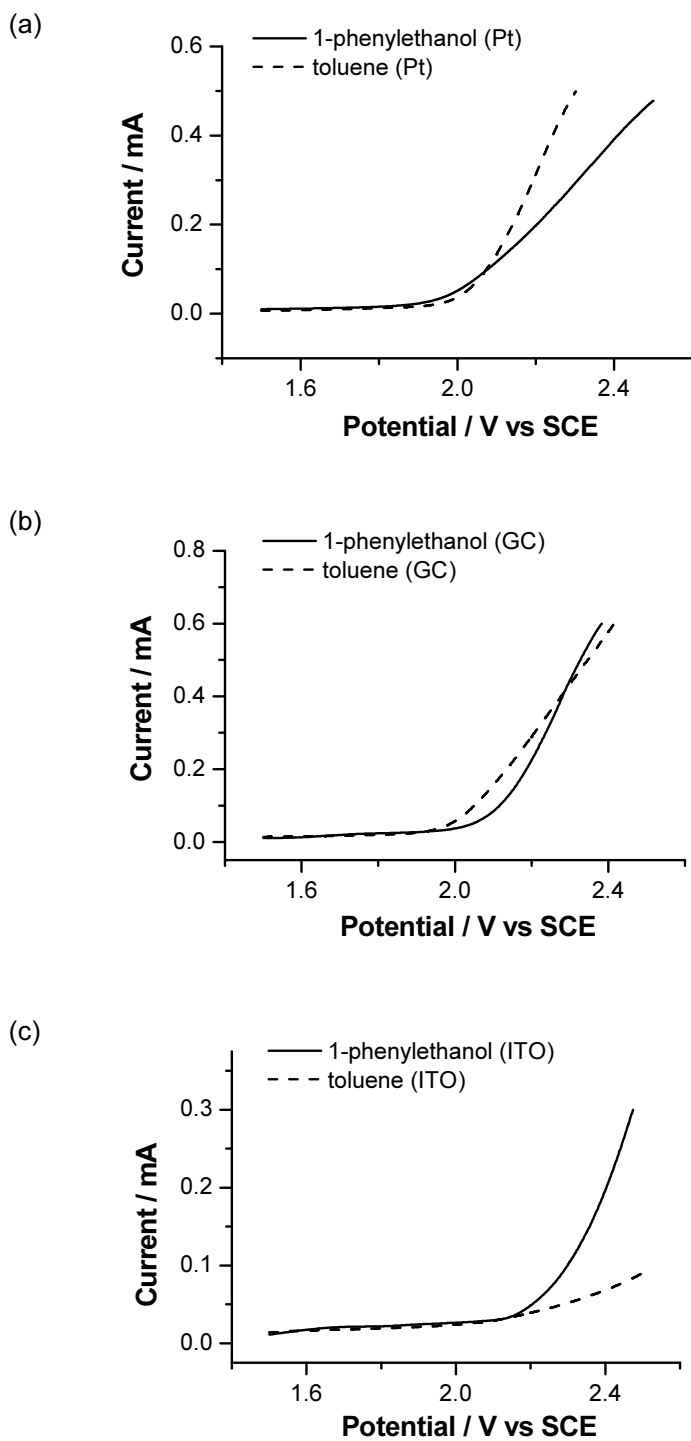


Figure 2-8. Linear sweep voltammograms of 30 mM 1-phenylethanol/acetonitrile solution and 30 mM toluene/acetonitrile solution recorded at (a) Pt, (b) GC, and (c) ITO disk electrodes (diameter: 3 mm). The scan rate was 20 mV s⁻¹.

2-3-2 *Preparative experiment of the self-supported paired electrosynthetic system*

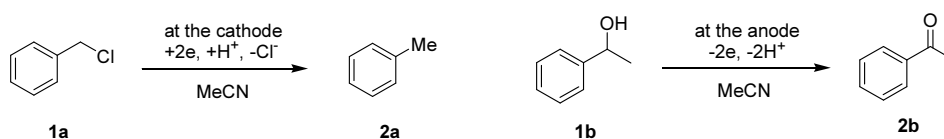
Next, preparative experiments of the self-supported paired electrosynthesis using acetonitrile as solvent were carried out. Experiments were conducted in a microreactor composed of Ag cathode/ITO anode combination, and results are shown in Table 2-2.

In entry 1, the electrolysis was conducted in the presence of Bu₄NBF₄ as a supporting electrolyte. Conversions of benzyl chloride (**1a**) and 1-phenylethanol (**1b**) were fairly good in this condition, and corresponding products (toluene (**2a**) and acetophenone (**2b**)) were obtained in moderate yields. Chloro toluenes were detected by GC-MS and HPLC as byproducts in low yields. These byproducts would be generated by anodic oxidation of toluene and following nucleophilic attack by chloride ions. Other byproducts such as 2,3-diphenylbutane-2,3-diol and 1-chlorophenyl ethanols were also detected by GC-MS.

When **1a** was only used as a substrate and any supporting electrolytes were not added, the electrolysis proceeded smoothly with high conversion of **1a** but the yield of **2a** was significantly low (entry 2). Anodic oxidation of toluene was considerably occurred to give some byproducts and no cathodic product other than **2a** was obtained. Hence, in this case, the self-supported paired reaction system was constructed by cathodic reduction of **1a** and anodic oxidation of **2a**. Cathodically generated chloride ions and anodically generated protons would act as charge carriers and the cell voltage during the electrolysis was kept at 7 to 8 V.

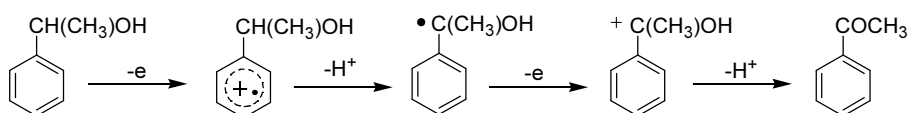
On the other hand, the electrolysis hardly proceeded when the substrate was only **1b** (entry 3). The cell voltage was too high to continue the electrolysis (over 40 V). This result would be explained as follows. The amount of proton at the cathode surface was not enough and substrate **1b** and acetonitrile solvent were hardly reduced.

Table 2-2. Preparative experiment of the self-supported paired electrosynthesis using a microreactor and acetonitrile as solvent.^a



Entry	Solute(s)	Conversion (%)		Yield (%)	
		1a	1b	2a	2b
1	1a (30 mM) 1b (30 mM) Bu ₄ NBF ₄ (100 mM)	76	75	43	55
2	1a (30 mM)	>99	-	17	-
3 ^b	1b (30 mM)	-	-	-	-
4	1a (30 mM) 1b (30 mM)	88	61	40	16

^aExperiments were carried out under the following conditions. Electrode distance: 80 μm , flow rate: 10 $\mu\text{L min}^{-1}$, current density: 1.0 mA cm^{-2} . Conversions and yields were determined by HPLC analysis. ^bThe cell voltage was too high to conduct the electrolysis.



Scheme 2-5

In entry 4, the paired electrosynthesis in the acetonitrile solution containing both **1a** and **1b** was proceeded very smoothly with a lower cell voltage (*ca.* 6 V), although the yields for both products were relatively low. This low yield would be ascribed to measurable side reactions of substrates and products at each counter electrode. Actually, 25% yields of chloro toluene species were obtained as byproducts. In

addition, the electrode surface was partially covered with tar film after the several time electrolyses.^[17] However, it is not clear why a difference in the result between entry 1 and entry 4 is induced. In particular, **2b** was obtained in significantly low yield in entry 4. One plausible explanation can be given as follows. Generally, direct anodic oxidation of **1b** in acetonitrile gives **2b** via an ECEC mechanism (Scheme 2-5).^[18] The initially formed radical cation loses a proton to give the α -hydroxybenzyl radical, which undergoes subsequent oxidation and proton loss. The rate determining step of this reaction is the first proton loss step, so that the initially formed radical cations have some lifetime and the lifetime of this intermediate would affect the yield of final product.^[19] When the reaction is carried out without intentionally added supporting electrolyte, these radical cations would be unstable since no counter ion exist in this case. Therefore, either decomposition of the intermediate or attacking by some kinds of nucleophile would be occurred as side reactions.

Regardless of the low yields of desired products, it can be stated that the self-supported paired electrochemical system using acetonitrile as solvent was successfully demonstrated.

2-3-3 Effect of electrode distance

In the operation of electrochemical microreactor systems, there are many parameters such as electrode distance, linear fluid speed, volumetric flow rate, amount of charge passed, current density, *etc.* Therefore, controlling parameters for the self-supported paired electrochemical synthesis are quite important to optimize the system.

Firstly, the effect of electrode distance on the self-supported system was investigated. The cell dimension and other parameters were fixed to the values which were used in the previous section, and results are shown in Figure 2-9. It is expected that narrower

electric double layers are formed by narrower electrode distance because electrogenerated ionic species would promptly diffuse to the counter electrodes in the narrower electrode distance. Consequently, the cell voltage would be lowered and the reaction efficiencies would be improved.

However, remarkable changes in the reaction results were not observed between the electrode distance from 20 μm to 80 μm . The formations of electric double layers were not affected by the electrode distance in this range. On the other hand, yields of chloro-toluenes were decreased with increasing the electrode distance. Chloro-toluenes as byproducts were formed *via* anodic oxidation of toluene (**2a**) as a cathodic product. When the cell had wide electrode distance, **2a** would be ejected from the cell before reaching the anode. Consequently, extremely narrow electrode distance should be avoided to suppress the generation of byproducts.

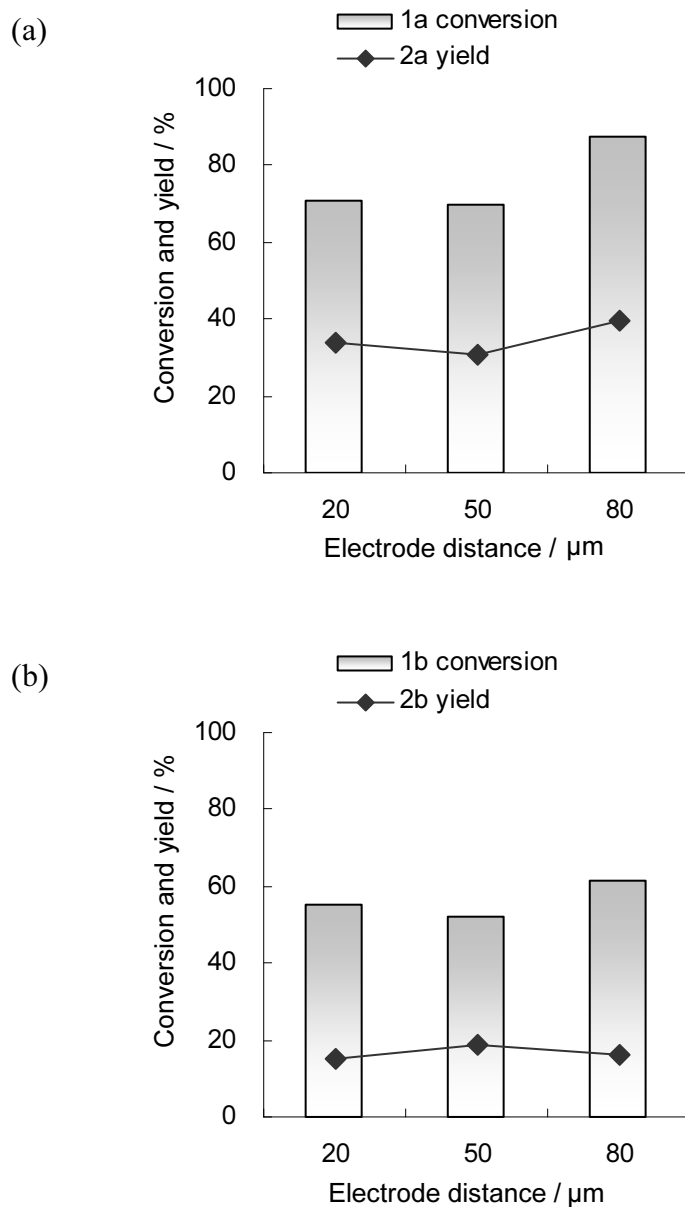
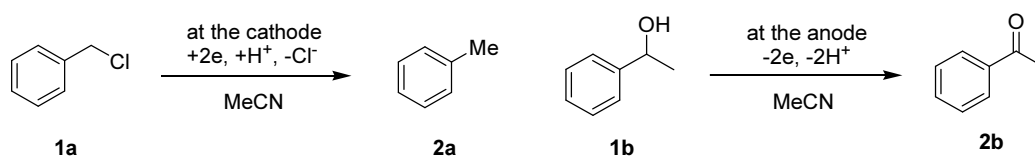


Figure 2-9. The effect of the electrode distance on the conversion of (a) benzyl chloride (**1a**) and (b) 1-phenylethanol (**1b**) and the yield of (a) toluene (**2a**) and (b) acetophenone (**2b**). Experiments were carried out under the following conditions. Flow rate: $10 \mu\text{L min}^{-1}$, current density: 1.0 mA cm^{-2} . Conversions and yields were determined by HPLC analysis.

2-3-4 *Effect of flow rate*

Subsequently, the effect of flow rate on the self-supported system was investigated. As Figure 2-10 (a) illustrates, a highest conversion of **1a** was obtained at a flow rate of 10 $\mu\text{L min}^{-1}$, and this was decreased with increasing the flow rate. Similar tendency was observed in **2a** yields. On the other hand, **2b** yield was increased with increasing the flow rate up to 20 $\mu\text{L min}^{-1}$ while **1b** conversion was decreased, as shown in Figure 2-10 (b). This flow rate effect can be explained as follows. Product **2b** was ejected from the reactor before reaching the counter electrode (cathode) when the flow rate was relatively fast. Therefore, re-reduction of product **2b** at the counter electrode was inhibited and consequently product selectivity was improved.

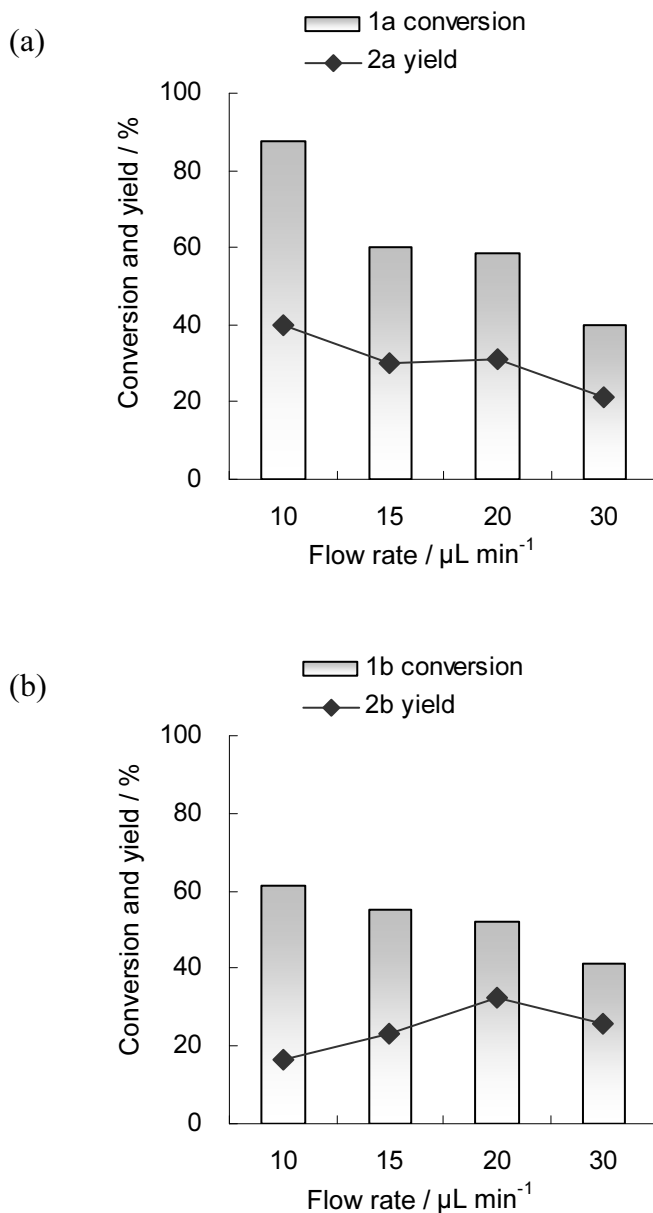
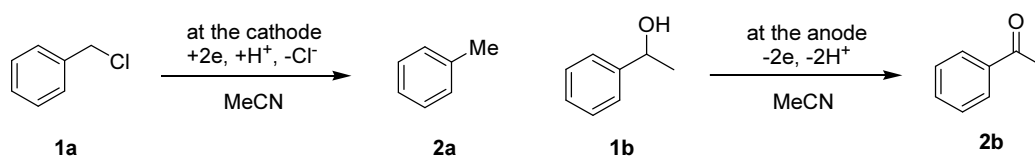


Figure 2-10. The effect of the flow rate on the conversion of (a) benzyl chloride (**1a**) and (b) 1-phenylethanol (**1b**) and the yield of (a) toluene (**2a**) and (b) acetophenone (**2b**). Experiments were carried out under the following conditions. Electrode distance: 80 μm , current density: 1.0 mA cm^{-2} . Conversions and yields were determined by HPLC analysis.

2-3-5 *Effect of current density*

Next, the effect of current density on the self-supported system was investigated. It is expected that higher current density results in higher conversion of substrate whereas product selectivity is generally decreased. Actually, as shown in Figure 2-11, conversions of **1a** and **1b** were increased with an increasing the current density. On the other hand, the reaction selectivity was decreased with an increasing the current density. High conversion of **1b** and low yield of **2b** were obtained at 1.3 mA cm^{-2} . In this condition, many kinds of side reaction products derived from **1b** and/or **2b** were detected. Therefore, the current density should be kept lower to maintain higher product selectivity.

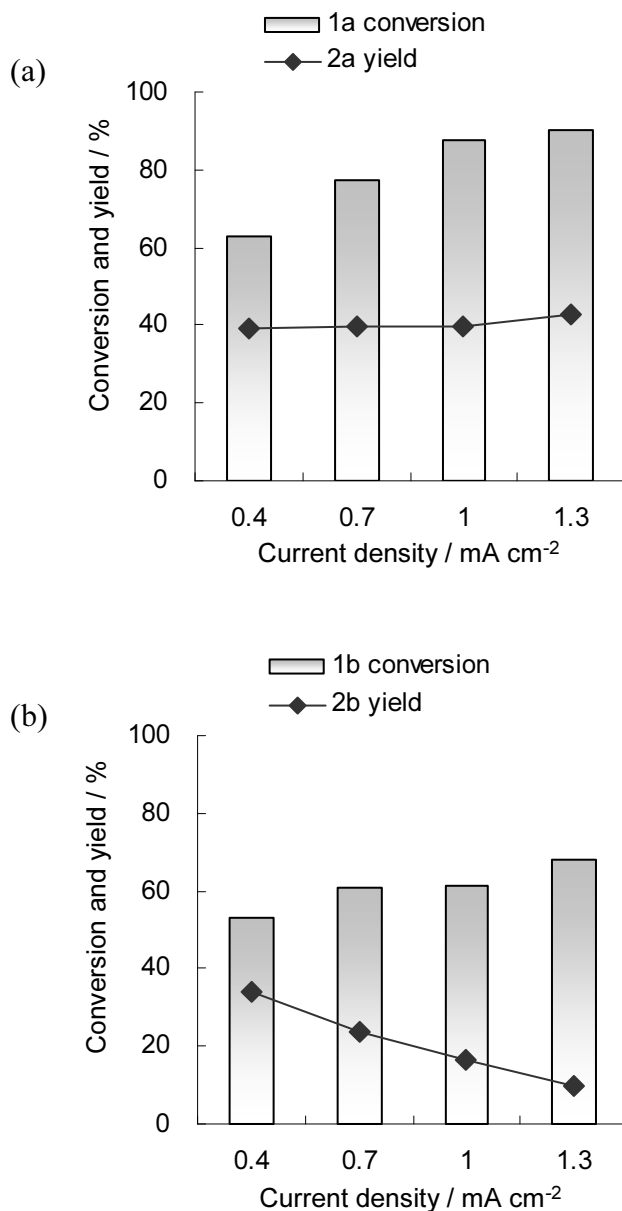
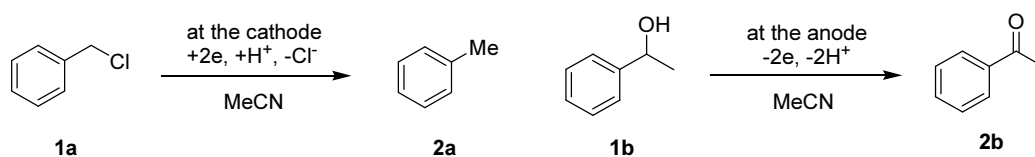


Figure 2-11. The effect of the current density on the conversion of (a) benzyl chloride (**1a**) and (b) 1-phenylethanol (**1b**) and the yield of (a) toluene (**2a**) and (b) acetophenone (**2b**). Experiments were carried out under the following conditions. Electrode distance: 80 μm , flow rate: 10 $\mu\text{L min}^{-1}$. Conversions and yields were determined by HPLC analysis.

2-3-6 *Effect of flow mode*

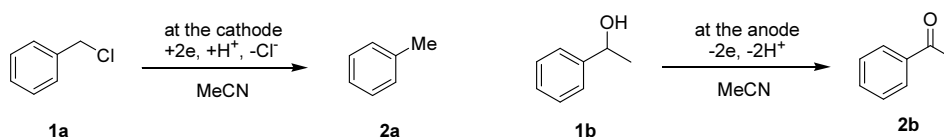
Although effects of some parameters were investigated in the above sections, conversions and yields of the self-supported paired electrochemical system are still insufficient. Actually, the conversions and yields were influenced by the parameters tested and their effects were often complicated. This situation would not be overcome by simple optimization of such parameters.

The yields of products would be mainly suppressed by the electrochemical reactions of substrates and products at each counter electrode. Thus, to avoid this problem, a parallel laminar flow mode by two inlet microreactor (two inlet flow mode) was employed for this system (see. Figure 2-6 in the experimental section). The channel of the microreactor is very small enough to insure that the flow is stable and laminar. In fact, in our previous work, the existence of the parallel laminar flow in the similar microreactor was confirmed by voltammetric experiments.^[20] When benzyl chloride (**1a**) and 1-phenylethanol (**1b**) solutions are introduced through the cathode side inlet and anode side inlet respectively, a stable liquid-liquid parallel laminar flow would be formed in the channel, and hence, the desired cathodic and anodic reactions would proceed effectively without interference from each other.

Table 2-3 shows experimental results of the electrochemical reaction using two types of flow modes. In entry 2, it was observed that product selectivity of anodic reaction was improved by using two inlet flow mode compared to the original flow mode (entry 1), as expected. However, it is not clear why the yield of cathodic product **2a** was decreased in this condition. The product selectivity was improved at lower current density (entry 3). Moreover, at lower flow rate conversions and yields were increased presumably (entry 5). From these results, it was demonstrated that a liquid-liquid parallel laminar flow mode (two inlet flow mode) enables to improve

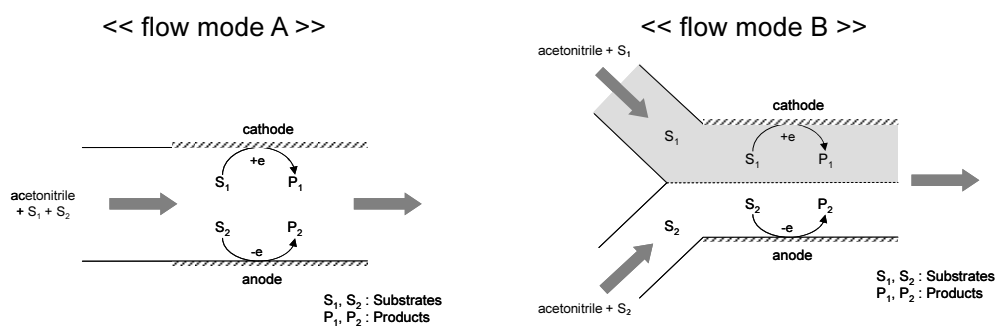
conversions and yields in this system and this flow mode can be an effective method to construct the self-supported paired electrochemical system.

Table 2-3. Experimental results of the electrochemical reaction using two types of flow modes.^a



Entry	Flow mode ^b	Flow rate ($\mu\text{L min}^{-1}$)	Current density (mA cm^{-2})	Conversion (%)		Yield (%)	
				1a	1b	2a	2b
1	A	10	1.0	88	61	40	16
2	B	10	1.0	78	75	25	44
3	B	10	0.4	52	52	22	50
4	A	5	0.4	55	30	27	7
5	B	5	0.4	89	75	35	70

^aExperiments were carried out under the following conditions. Electrode distance: 80 μm . At the flow mode A, both substrates (**1a** and **1b**) were dissolved in acetonitrile and introduced into the reactor at the indicated flow rate. At the flow mode B, acetonitrile solutions of **1a** and **1b** were introduced into the reactor at the indicated flow rate, respectively. Conversions and yields were determined by HPLC analysis. ^bSchematic illustrations of flow modes are as follows:



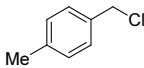
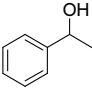
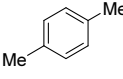
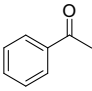
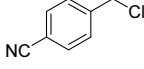
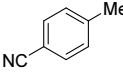
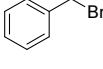
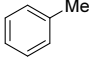
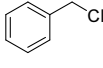
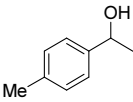
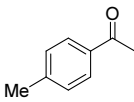
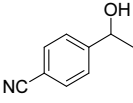
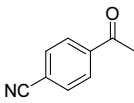
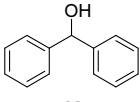
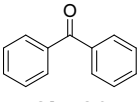
2-3-7 Generality of the self-supported paired electrosynthetic system

Finally, to demonstrate the generality of this self-supported paired electrosynthetic system, the electrochemical reactions of other halides and alcohols were carried out using parallel laminar flow mode.

As shown in entry 1 of Table 2-4, when α -chloro-*p*-xylene (**1c**) was used as a cathodic substrate, conversion of 1-phenylethanol (**1b**) and yields of *p*-xylene (**2c**) and acetophenone (**2b**) were low, although only conversion of **1c** was relatively high. In this case, probably cathodic product **2c** was easily oxidized at the anode due to its lower oxidation potential and the oxidation of **2c** would interfere the desired **1b** oxidation. In contrast, conversions and yields were improved when the cathodic substrate was replaced by 4-cyanobenzyl chloride (**1d**) (entry 2). This was ascribed to a higher oxidation potential of **2d**, which has a powerful electron-withdrawing group on the benzene ring, and hence, the desired oxidation of **1b** proceeded smoothly without interference from **2d** oxidation.

In entry 3, benzyl bromide (**1e**) was employed as a cathodic substrate instead of chlorides, but yields of both products were less satisfactory. In this case, bromide ion derived cathodically from **1e** would be oxidized at the anode to give Br^+ species (Br^+ , Br_3^- , Br_2 , etc.), and then, they were reduced at the cathode to regenerate bromide ion. Thus, part of the electricity seemed to be consumed for redox reaction of Br^-/Br^+ . In fact, electrolyte solution collected in a vessel after the electrolysis showed bright yellow color and the color turned slightly colorless after several hours. This indicates the existence of Br^+ species. It should be noted that chloride ion has higher oxidation potential than that of bromide ion and anodically generated Cl_2 would be removed to gas phase. Therefore, the system would be less affected by the redox reaction of Cl^-/Cl_2 than that of Br^-/Br^+ .

Table 2-4. Self-supported paired electrosynthesis of toluene derivative and ketone using a two inlet microreactor.^a

Entry	Substrate		Conversion (%)		Yield (%)	
	Halide	Alcohol	Halide	Alcohol	Toluene derivative	Ketone
1	 1c	 1b	76	20	 2c, 14	 2b, 6
2	 1d	1b	79	66	 2d, 65	2b, 60
3	 1e	1b	61	59	 2a, 32	2b, 32
4	 1a	 1f	45	87	2a, 41	 2f, 72
5	1a	 1g	79	5	2a, 21	 2g, 1
6	1a	 1h	48	43	2a, 29	 2h, 20
7	1a	1f	93	>99	2d, 87	2f, 61

^aExperiments were carried out under the following conditions. Electrode distance: 80 μm , current density: 0.4 mA cm^{-2} . Acetonitrile solutions of halide compound and alcohol were introduced through the cathode side inlet and anode side inlet, respectively. Flow rates of each solution were 5 $\mu\text{L min}^{-1}$ and the total flow rate was 10 $\mu\text{L min}^{-1}$. Conversions and yields were determined by HPLC analysis.

On the other hand, when 1-(*p*-tolyl)ethanol (**1f**) was used as an anodic substrate instead of **1b**, the desired anodic reaction proceeded effectively with a high yield of 4'-methylacetophenone (**2f**), while anodic oxidation of 4-(1-hydroxyethyl)benzotrile (**1g**) hardly proceeded (entries 4 and 5). These are apparently ascribed to the oxidation potentials of **1f** and **1g**, and the former and latter oxidation potentials are lower and higher, respectively, than that of **1b**.

Benzhydrol (**1h**) was used in entry 6 and relatively low yields were obtained in this case. Benzene ring of **1h** affected as electron-withdrawing group and the anodic reaction was difficult to proceed like entry 5.

The best result was obtained in the substrates combination of **1d** and **1f** (entry 7). In this case, the paired electrosynthesis proceeded with excellent conversions (93% for **1d** and over 99% for **1f**) and good yields (87% for **2d** and 61% for **2f**).

From these results, it can be stated that the feasibility of the reactions depends greatly on the oxidation potentials and reduction potentials of substrates and products.

2-4 Conclusion

Electroorganic synthesis has attracted much interest as an environmentally friendly process for recent decades. However, commercial application of electroorganic synthesis as a green sustainable process has been limited by some problems such as separation and waste problems of supporting electrolyte. From this point of view, a novel microreactor system for electroorganic synthesis without intentionally added supporting electrolyte was developed in this chapter. This system enables to use acetonitrile as solvent for self-supported system for the first time. In addition, the successful operation of this system provides knowledge about the mechanism of self-supported system. This also provides practical knowledge about how to design self-supported system even in aprotic solvent. It should be noted that the methodology of this self-supported microreactor system can be applied to a variety of electroorganic synthesis that make a significant contribution to synthetic chemistry toward green sustainable chemistry.

2-5 References

- [1] United States Environmental Protection Agency, Green Chemistry: <http://www.epa.gov/greenchemistry/>
- [2] P.T. Anastas, J.C. Warner, in *Green Chemistry: Theory and Practice*, Oxford University Press, New York, **1998**, p.30.
- [3] a) *Organic Electrochemistry*, fourth ed. (Eds. H. Lund, O. Hammerich), Marcel Dekker, New York, **2001**; b) J. Yoshida, K. Kataoka, R. Horcajada, A. Nagaki, *Chem. Rev.* **2008**, *108*, 2265.
- [4] a) E. Raoult, J. Sarrazin, A. Tallec, *J. Appl. Electrochem.* **1984**, *14*, 639; b) E. Raoult, J. Sarrazin, A. Tallec, *J. Appl. Electrochem.* **1985**, *15*, 85; c) J. Jorissen, *Electrochim. Acta* **1996**, *41*, 553.
- [5] a) K. Chiba, Y. Kono, S. Kim, Y. Kitano, M. Tada, *Proc. Electrochem. Soc.* **2002**, 10; b) K. Chiba, Y. Kono, S. Kim, K. Nishimoto, Y. Kitano, M. Tada, *Chem. Commun.* **2002**, 1766; c) K. Hayashi, S. Kim, Y. Kono, M. Tamura, K. Chiba, *Tetrahed. Lett.* **2006**, *47*, 171.
- [6] a) F. Beck, H. Guthke, *Chem. Ing. Technol.* **1969**, *41*, 943; b) L. Ebersson, K. Nyberg, H. Sternerup, *Chem. Scrip.* **1973**, *3*, 12; c) H. Pütter in *Organic Electrochemistry*, fourth ed. (Eds.: H. Lund, O. Hammerich), Marcel Dekker, New York, **2001**, p.1259.
- [7] C.A. Paddon, G.J. Pritchard, T. Thiemann, F. Marken, *Electrochem. Commun.* **2002**, *4*, 825.
- [8] R. Horcajada, M. Okajima, S. Suga, J. Yoshida, *Chem. Commun.* **2005**, 1303.
- [9] a) D. Horii, M. Atobe, T. Fuchigami, F. Marken, *Electrochem. Commun.* **2005**, *7*, 35; b) D. Horii, M. Atobe, T. Fuchigami, F. Marken, *J. Electrochem. Soc.* **2005**,

153, D143.

- [10] a) C.J.T. Grotthuss, *Ann. Chim.* **1806**, 58, 54; b) N. Agmon, *Chem. Phys. Lett.* **1995**, 244, 456; c) K.-D. Kreuer, *Chem. Mater.* **1996**, 8, 610; d) J.A. Morrone, K.E. Haslinger, M.E. Tuckerman, *J. Phys. Chem. B* **2006**, 110, 3712; e) R. D. Lisi, M. Goffredi, V. T. Liveri, *J. Chem. Soc., Faraday Trans. 1* **1978**, 74, 1096.
- [11] P. He, P. Watts, F. Marken, S.J. Haswell, *Angew. Chem. Int. Ed.* **2006**, 45, 4146.
- [12] a) M.M. Baizer in *Organic Electrochemistry*, (Eds. H. Lund, M.M. Baizer), Marcel Dekker, New York, **1991**, p.1421; b) C.A. Paddon, M. Atobe, T. Fuchigami, P. He, P. Watts, S.J. Haswell, G.J. Pritchard, S.D. Bull, F. Marken, *J. Appl. Electrochem.* **2006**, 36, 617.
- [13] For selected examples, see: a) M.M. Baizer, R.C. Hallcher, *J. Electrochem. Soc.* **1976**, 123, 809; b) H. Pütter, H. Hannebaum, DE19, (13-11-1997), 618, 854; c) E. Steckhan, T. Arns, W.R. Heineman, G. Hilt, D. Hoormann, J. Jorissen, L. Kroner, B. Lewall, H. Pütter, *Chemosphere* **2001**, 43, 63; d) K. Park, P.N. Pintauro, M.M. Baizer, K. Nobe, *J. Electrochem. Soc.* **1985**, 132, 1850; e) A.F. Jalbout, S.H. Zhang, *Acta. Chim. Slovacia* **2002**, 49, 917; f) M. Ishifune, H. Yamashita, M. Matsuda, H. Ishida, N. Yamashita, Y. Kera, S. Kashimura, H. Masuda, H. Murase, *Electrochim. Acta* **2001**, 46, 3259; g) S. Kim, R. Uchiyama, Y. Kitano, M. Tada, K. Chiba, *J. Electroanal. Chem.* **2001**, 507, 152; h) G. Hilt, *Angew. Chem. Int. Ed.* **2003**, 42, 1720; i) W. Li, T. Nonaka, T.C. Chou, *Electrochemistry* **1999**, 67, 4; j) W. Li, T. Nonaka, *J. Electrochem. Soc.* **1999**, 146, 592; k) W. Li, T. Nonaka, *Electrochim. Acta* **1999**, 44, 2605; l) Y. Shen, M. Atobe, W. Li, T. Nonaka, *Electrochim. Acta* **2003**, 48, 1041.

- [14] B.M. Matute, M. Edin, K. Bogár, F.B. Kaynak, J.-E. Bäckvall, *J. Am. Chem. Soc.* **2005**, *127*, 8817.
- [15] A.M. Couper, D. Pletcher, F.C. Walsh, *Chem. Rev.* **1990**, *90*, 837.
- [16] a) S. Rondinini, P.R. Mussini, P. Mutini, G. Sello, *Electrochim. Acta* **2001**, *46*, 3245; b) J. Simonet, *J. Electroanal. Chem.* **2005**, *583*, 34; c) C. Bellomunno, D. Bonanomi, L. Falcicola, M. Longhi, P.R. Musini, L.M. Doubova, G.D. Silvestro, *Electrochim. Acta* **2005**, *50*, 2331; d) A.A. Isse, S. Gotardello, C. Maccato, A. Gennaro, *Electrochem. Commun.* **2006**, *8*, 1707.
- [17] It has been reported that toluene was electro-oxidized to give polymeric products: L.F. D'Elia, R. Ortiz, *Port. Electrochim. Acta* **2005**, *23*, 481.
- [18] a) G.W. Morrow in *Organic Electrochemistry*, fourth ed. (Eds.: H. Lund, O. Hammerich), Marcel Dekker, New York, **2001**, p.589; b) O.R. Brown, S. Chandra, J.A. Harrison, *J. Electroanal. Chem.* **1972**, *34*, 505; c) E.A. Mayeda, L.L. Miller, J.F. Wolf, *J. Am. Chem. Soc.* **1972**, *94*, 6812.
- [19] a) W. T. Dixon, R.O.C. Norman, *J. Chem. Soc.* **1963**, 3119; b) D.J. Edge, B.C. Gilbert, R.O.C. Norman, P.R. West, *J. Chem. Soc. (B)*, **1971**, 189.
- [20] a) D. Hori, T. Fuchigami, M. Atobe, *J. Am. Chem. Soc.* **2007**, *129*, 11692; b) D. Horii, F. Amemiya, T. Fuchigami, M. Atobe, *Chem.-Eur. J.* **2008**, *14*, 10382.

Chapter 3

Electrochemical Conversion of Primary Amine to Secondary Amine Using a Microreactor: Analogous System of Photocatalytic Redox Combined Synthesis

A $[S/\pm e^-/I/\mp e^-/P]$ type electrochemical conversion of benzylamine to dibenzylamine using a microreactor has been investigated as an analogue of photocatalytic redox combined reaction. By comparison with a conventional batch type reactor, a clear advantage of this electrochemical microreactor system was successfully demonstrated. In addition, reaction conditions such as electrode distance, flow rate, and current density were optimized.

3-1 Introduction

In this section, a paired electrochemical reaction system using a microreactor is described as an analogue of the heterogeneous photocatalytic reaction system. The reaction feature and reaction paths of heterogeneous photocatalysis will be firstly summarized below, then an analogous electrochemical system will be discussed.

3-1-1 *Heterogeneous photocatalysis*

A new era in heterogeneous photocatalysis was opened in 1972 by the pioneering work of Fujishima and Honda.^[1] They discovered the photocatalytic splitting of water on TiO₂ electrodes, and since then, there has been a great research interest about heterogeneous photocatalysis which can be applied, such as solar energy conversion, photosynthesis of organic compounds, water sterilization and organic contaminants degradation, and photodynamic therapy of cancer.^[2]

In a heterogeneous photocatalysis system, generally, the reaction is a redox reaction driven by photoexcited electrons (e^-) in the conduction band (CB) and simultaneously generated positive holes (h^+) in the valence band (VB) of semiconducting materials *via* light absorption. The oxidation of a substrate by electron transfer into the h^+ in the valence band (formation of the radical cation) is accompanied by a reduction of another substrate *via* electron transfer from the conduction band (formation of the radical anion) (Figure 3-1).

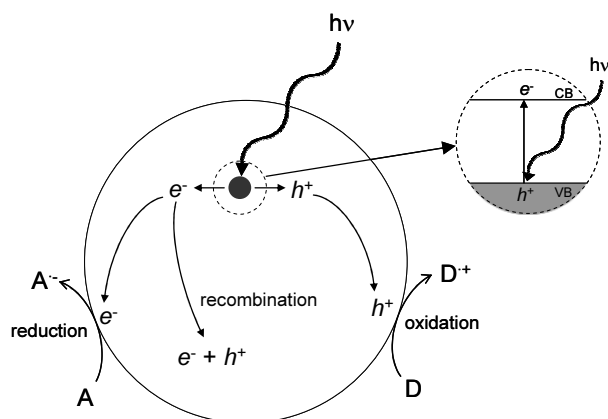


Figure 3-1. Schematic illustration of photoexcitation in a semiconductor particulate as heterogeneous photocatalyst followed by deexcitation events.

In the presence of molecular oxygen (O_2) under ordinary atmospheric conditions, the reduction of O_2 by e^- is mainly occurred to give the resulting products such as super-oxide anion,^[3] hydroperoxy radical,^[4] and hydroxyl radical^[5]. Since all of them are oxidants, the photocatalytic oxidation of substrates under aerated conditions is proceeded by both h^+ and these oxidants derived from e^- . On the basis of the mechanism, the degradation of organic contaminants in water is widely carried out by photocatalytic oxidation with TiO_2 particles. The reduction of dissolved O_2 couples with this oxidation, resulting complete oxidation and mineralization of organic pollutants in water. Although the desired oxidation reaction becomes O_2 reduction rate limited, the quantum efficiency of photoassisted oxidation is increased by modification of the TiO_2 surface by a catalyst for O_2 reduction such as VIII metals.^[6] Consequently, photocatalytic reactions with metal-deposited TiO_2 particles and films have also been studied extensively.^[7] In these metal deposited photocatalysts, it is considered that the deposited metal acts as a reduction site, increasing the charge separation efficiency and thus expediting the transportation of photogenerated electrons in the conduction band of TiO_2 to the outer system.

On the other hand, when the photocatalytic reactions are carried out under deaerated

conditions, both reduction and oxidation by e^- and h^+ , respectively, can be utilized for conversion of organic substrates.^[2h, 8] Yanagida's group reported photocatalytic reductions of aromatic ketones and olefins by using CdS semiconductor particulate with visible light irradiation in the presence of triethylamine in methanol (Figure 3-2).^[9] These reactions afforded corresponding alcohols and dihydro compounds, respectively, in moderate to good yields, accompanying sacrificial oxidation of triethylamine by h^+ . As shown in Figure 3-3, Baciocchi reported that an oxidative pathway was conversely adopted in the synthesis of diarylethanes.^[10] Benzyltrimethylsilanes were photocatalytically oxidized by TiO_2 in the presence of silver sulfate to give the corresponding diarylethanes in 50-74% yields. Silver salts were required to trap the photogenerated electrons on the TiO_2 , so that the recombination rate of e^- and h^+ in the semiconductor was slowed down. Molecular oxygen was found to be a less efficient sacrificial oxidizing agent than silver salts under aerated condition.

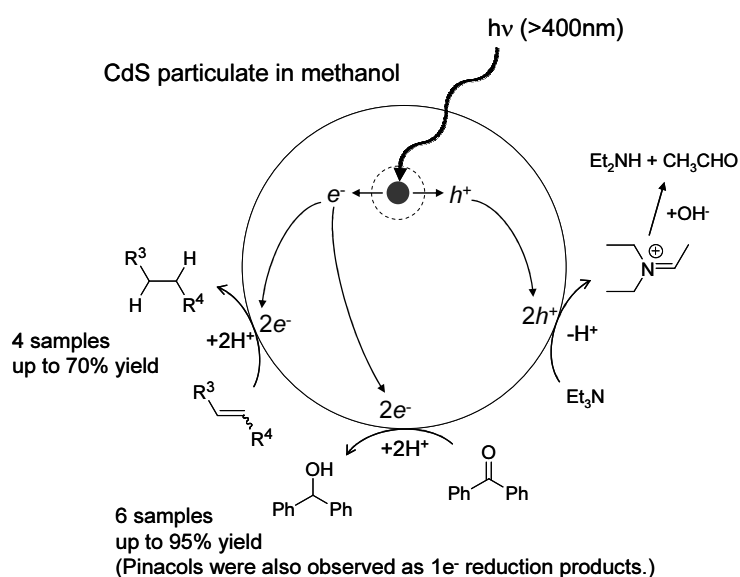


Figure 3-2. Schematic illustration of CdS catalyzed photoreduction of ketones and olefins with triethylamine in methanol.

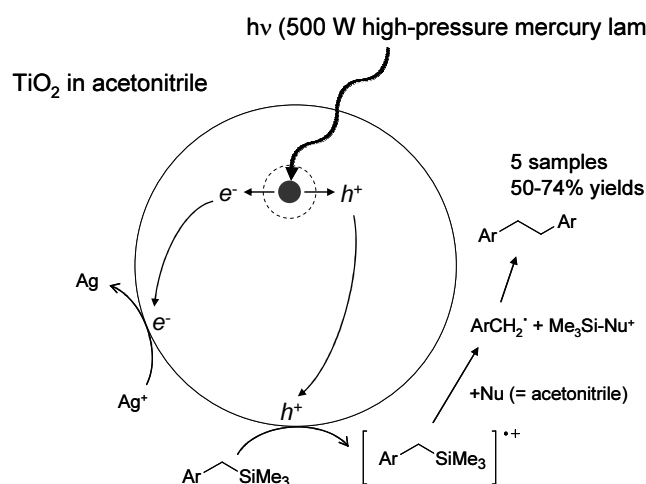


Figure 3-3. Schematic illustration of TiO₂ catalyzed photooxidation of benzyltrimethylsilanes with Ag₂SO₄ in acetonitrile.

3-1-2 Photocatalytic redox combined synthesis

In heterogeneous photocatalysis under deaerated condition, a reduction by e^- and an oxidation by h^+ are proceed separately at each site on the particle. Photocatalytic redox combined synthesis purposely utilizes both of this simultaneous reduction and oxidation for the synthesis of desired compound(s). The sites for reduction and oxidation on the particle would be located nearby, enabling induction of a redox combined reaction. Many examples of photocatalytic redox combined synthesis have been reported until today.^[11]

As a typical example, Figure 3-4 shows a photocatalytic L-pipecolic acid (L-PCA) synthesis based on the concept of photocatalytic redox combined synthesis reported by Ohtani and co-workers.^[12] This reaction involves successive oxidation of one of the amino groups in L-(S)-lysine (L-Lys) into imines by h^+ , hydrolysis of the imines into aldehyde, condensation of them with the remaining amino group into a cyclic Schiff base (CSB), and reduction of Schiff base into pipecolic acid by e^- . Photocatalytic redox combined synthesis like this elegant and integrated sequential scheme can be regarded as a powerful tool for synthetic organic chemistry, and therefore, further

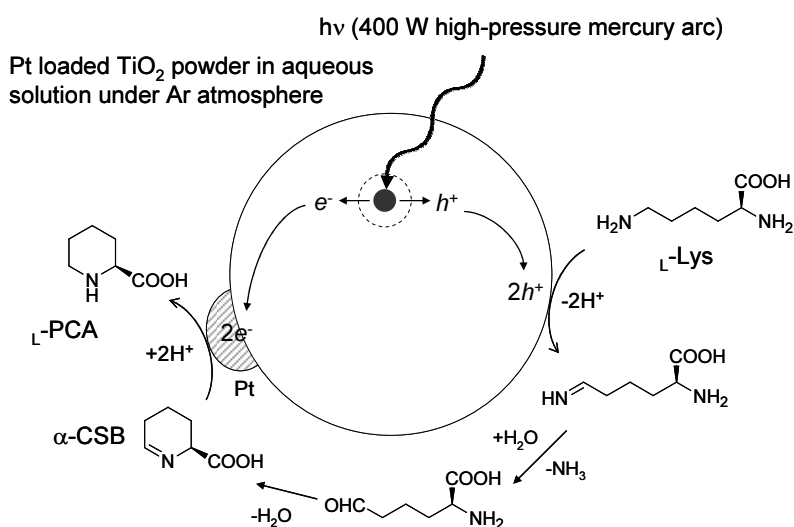


Figure 3-4. Proposed mechanism of the photocatalytic redox combined synthesis of L-pipecolic acid (L-PCA) from L-(S)-lysine (L-Lys) using platinum (Pt) loaded TiO₂ powders.

extensive studies would be highly desirable.

3-1-3 $[S/\pm e^-/I/\mp e^-/P]$ type paired electrosynthesis as an analogue of photocatalytic redox combined synthesis

The schematic concept of photocatalytic redox combined synthesis like Figure 3-4 is fairly similar to $[S/\pm e^-/I/\mp e^-/P]$ type paired electrosynthesis.^[13] In $[S/\pm e^-/I/\mp e^-/P]$ type paired electrosynthesis, a single starting substrate (*S*) is reduced or oxidized at the electrode to an intermediate (*I*), which is further oxidized or reduced at the counter electrode to give the corresponding single final product (*P*). The use of undivided cell should be inevitable. Figure 3-5 shows a typical example for this type of paired electrosynthesis reported by Nonaka and co-workers.^[14] *S*, *I*, and *P* in Figure 3-5 correspond to 2,3-butanediol, acetoin, and methyl ethyl ketone, respectively. 2,3-Butanediol is firstly oxidized to give acetoin by BrO⁻ which is anodically generated from Br⁻ (NaBr as supporting electrolyte) and then, obtained acetoin is reduced to give methyl ethyl ketone as a final product. This simultaneous intentional

utilization of cathodic reduction and anodic oxidation can be considered as a schematic analogue of photocatalytic redox combined synthesis. Thus, similar reaction schemes can be also applied both electrochemical and photocatalytic systems for efficient synthesis of specific compounds.

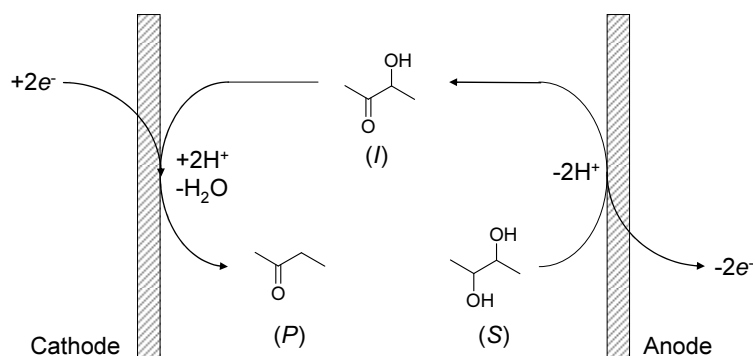


Figure 3-5. $[S/\pm e^-//\mp e^-/P]$ type paired electrochemical synthesis of methyl ethyl ketone from 2,3-butanediol. The redox mediator of anodic oxidation is omitted in this figure.

3-1-4 Objective and strategy of this chapter

In photocatalytic redox combined synthesis, the reduction site and the oxidation site locate very closely (nano-micro meter order). This feature enables to proceed a smooth sequential redox reaction on the heterogeneous photocatalyst. In contrast, in $[S/\pm e^-//\mp e^-/P]$ type paired electrochemical synthesis, the distance between the anode and cathode is centimeter order when the reaction is carried out in a conventional laboratory scale batch type reactor. Hence, electrochemically generated intermediates need specific time to diffuse from the electrode surface to the counter electrode surface, and complete conversion to the final product would be difficult to achieve by passing the theoretical amount of electricity.

Compare to the conventional batch type reactor, an electrochemical microreactor has a possibility to achieve an efficient substrate conversion to the final product in $[S/\pm e^-//\mp e^-/P]$ type paired electrochemical synthesis. As described in the general introduction in Chapter

1, significantly short electrode distance enables fast molecular diffusion to the counter electrode, offering similar circumstances of the surface of photoexcited semiconductor particulate. Undesired side-reactions (anodic oxidation of solvent, cathodic hydrogen evolution, etc.) would be avoided in this case, so that the current efficiency of the system may be improved compared to the case using conventional batch type reactor.

With this consideration in mind, the goal of this chapter is to demonstrate a clear advantage of electrochemical microreactor in $[S/\pm e^-/I] \mp e^-/P$ type paired electrosynthesis toward conventional batch type reactor. This demonstration would not only enhance the practical value of our electrochemical microreactor but also show a possibility of the electrochemical microreactor as an analogous system of photocatalytic redox combined reaction system.

As a model reaction of this chapter, an electrochemical conversion of benzylamine to dibenzylamine was employed (Figure 3-6). Oxidative condensation of benzylamines to *N*-benzylidene benzylamines has been widely studied^[15] because benzylimines are useful synthetic intermediates that can undergo a large variety of transformations of the C=N double bond including hydrogenations, [2+2] cycloadditions and nucleophilic additions such as Strecker reaction.^[16] Furthermore, by following cathodic hydrogenation of benzylimines, it would be possible to obtain symmetric and asymmetric secondary amines with once passing through the electrochemical microreactor. Needless to say, *N*-alkylation of primary amines has also been studied extensively because nitrogen containing compounds play a central role in Nature and also in industries.^[17] Since additional oxidative/reductive reagents or catalysts are not required in this electrochemical conversion, a fast and clean *N*-alkylation system can be provided by this sequential two step procedure using the electrochemical

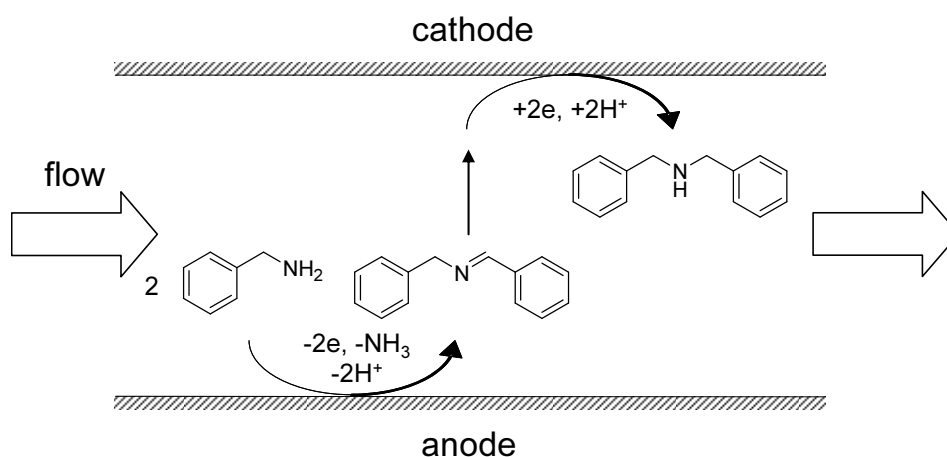


Figure 3-6. Schematic representation of the electrochemical conversion of benzylamine to dibenzylamine in ethanol using the electrochemical microreactor.

microreactor.

In this chapter, the above system has been demonstrated and compared with a conventional batch type reactor. In addition, reaction conditions such as electrode distance, flow rate, and current density have been also optimized.

3-2 Experimental Section

3-2-1 Instrumentation

Nuclear magnetic resonance (^1H NMR) spectra were measured on JEOL JNM EX-270 spectrometer operating at 270 MHz (^1H NMR) in CDCl_3 . All ^1H NMR chemical shifts were reported in ppm relative to internal references of TMS at δ 0.00. EI mass spectra were measured with a Shimadzu GCMS-QP5050A mass spectrometer. Cyclic voltammetry was performed by using a computer-controlled electrochemical analyzer (ALS/CH Instruments 630C). Preparative electrolyses were carried out with a HOKUTO DENKO HA-501 Potentiostat/Galvanostat. High performance liquid chromatography (HPLC) analysis was performed by an internal standard method with Shimadzu LC-20AD liquid chromatograph equipped with a UV detector (SPD-10AV, Shimadzu) and in-line two columns (Inertsil[®] ODS-80A, GL Sciences).

3-2-2 Materials

Benzylamine, dibenzylamine, 4-methoxytoluene, sodium ethoxide, tetra-*n*-butylammonium perchlorate ($n\text{-Bu}_4\text{NClO}_4$), tetra-*n*-butylammonium tetrafluoroborate ($n\text{-Bu}_4\text{NBF}_4$), tetra-*n*-ethylammonium perchlorate ($n\text{-Et}_4\text{NClO}_4$), and sodium dodecyl sulfate were purchased from Tokyo Chemical Industry. *N*-Benzyldenebenzylamine, ammonium chloride, and triethylamine were purchased from Wako Pure Chemical Industries. Ethanol, methanol, and acetic acid were purchased from Kanto Chemical. Tetra-*n*-butylammonium hexafluorophosphate ($n\text{-Bu}_4\text{NPF}_6$) was purchased from Sigma-Aldrich. Tetra-*n*-hexylammonium perchlorate ($n\text{-Hex}_4\text{NClO}_4$) was purchased from Fluka Chemie. All chemicals were used as received.

3-2-3 Microreactor

Figure 3-7 shows schematic illustration of the microreactor. The microreactor had a geometry with platinum (Pt) anode (3 cm width, 3 cm length, Nilaco) and graphite cathode (3 cm width, 3 cm length, IGS-743, Nippon Techno-Carbon) directly facing each other. A spacer (adhesive tape, 80 μm thickness, Nitto Denko) was used to leave a rectangular channel exposed, and the two electrodes were simply sandwiched together (the area of the electrode channel was 3 cm^2). After connecting Teflon tubing to inlet and outlet, the reactor was sealed with epoxy resin.

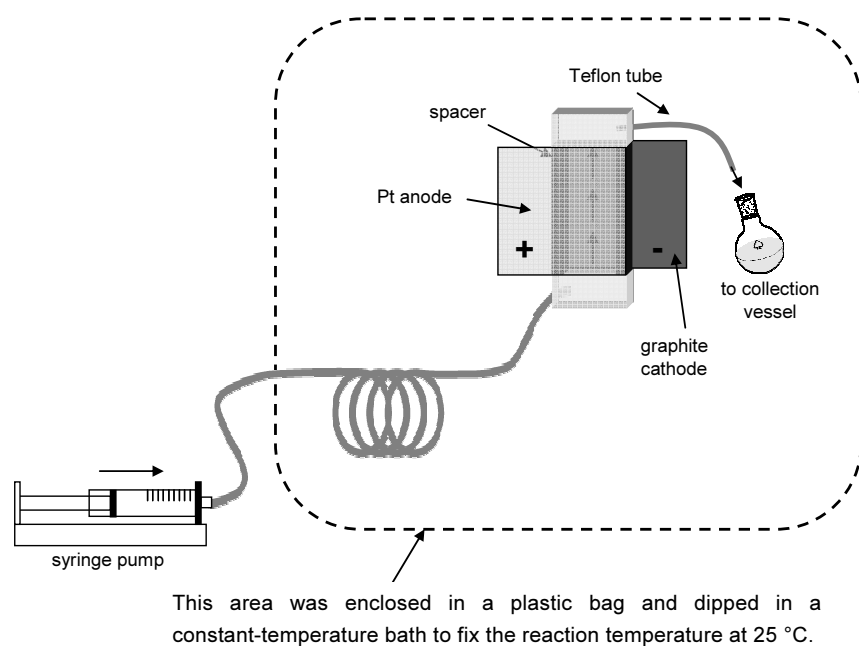


Figure 3-7. Schematic illustration of the microreactor.

3-2-4 General procedure for preparative electrolysis

KdScientific model 100 syringe pump was used to pump the reaction solution. The solution contains 30 mM of benzylamine, 250 mM of tetra-*n*-butylammonium perchlorate ($n\text{-Bu}_4\text{NClO}_4$) as supporting electrolyte, 30 mM of sodium ethoxide, and

ethanol as solvent. The reaction temperature was fixed at 25 °C by using a constant-temperature bath. All reactions were conducted galvanostatically. The collected reaction mixture was analyzed by HPLC (The eluent was acetonitrile/water (50:50 v/v) mixture containing 20 mM of sodium dodecyl sulfate, 40 mM of triethylamine, and 4vol% of acetic acid. Retention times were 9.9 min. for *N*-benzylidenebenzylamine, 24.5 min. for 4-methoxytoluene as internal standard, and 47 min. for dibenzylamine, respectively. The eluent flow rate was 1.0 mL min⁻¹ and compounds were detected by UV detector at 254 nm. Products were also identified by authentic samples using ¹H NMR and mass spectroscopy.

3-3 Results and Discussion

3-3-1 Linear sweep voltammetry

At first, the electrochemical behaviors of the substrate and intermediate were examined. The linear sweep voltammograms for benzylamine (**1**) and *N*-benzylidenebenzylamine (**2**) were measured in 250 mM *n*-Bu₄NClO₄-30 mM EtONa-EtOH at a platinum (Pt) disk electrode. As shown in Figure 3-8, specific wave changes were observed in the voltammograms of **1**. Wave I (*ca.* 1.6 V *vs.* SCE) was decreased with increasing the concentration of **1**, while wave II (*ca.* 2.2 V *vs.* SCE) was increased with increasing the concentration. The increase of wave II with almost linear relationship between the peak current and the concentration of **1** indicates that this wave was derived from the oxidation of **1**. Meanwhile, the concentration of **1** may also affect the circumstances of the Pt electrode surface. In fact, the shape of background voltammogram (condition without **1**) was far different from those of Figure 3-8. It is well known that many problems such as auto-inhibition and poisoning phenomena arise when pure platinum electrode is used for direct ethanol oxidation, resulting in high overpotentials. Since the reaction mechanism involves many adsorbed intermediates (containing poisoning species) and by-products such as carbon monoxide, carbon dioxide, ($\cdot\text{CHO}$)_{ads}, ($\cdot\text{COOH}$)_{ads}, CH₃CHO, and CH₃COOH, the surface circumstances on the Pt electrode is extremely complex.^[18] The presence of **1** in the electrolytic medium might cause drastic changes on the Pt electrode surface, so that the current of wave I depended on the concentration of **1**.

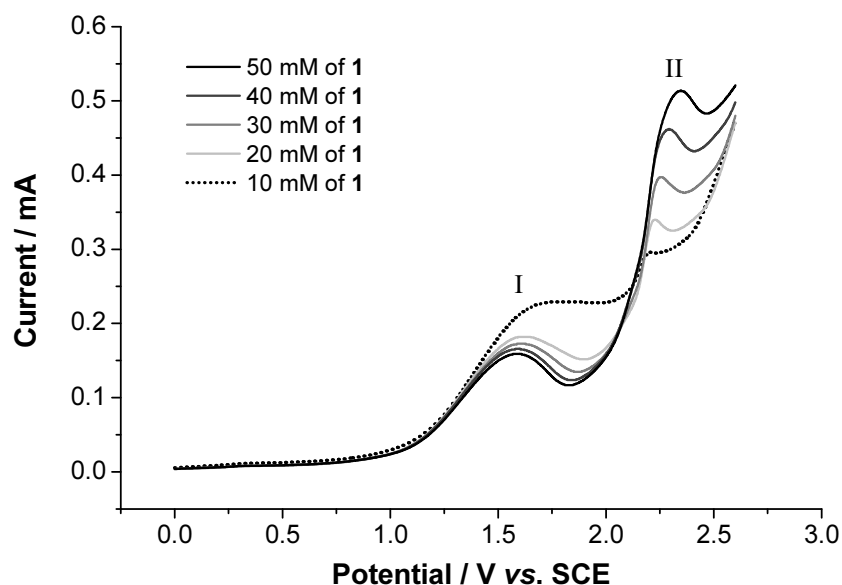


Figure 3-8. Linear sweep voltammograms of benzylamine (**1**) in 250 mM $n\text{-Bu}_4\text{NClO}_4$ -30 mM EtONa-EtOH recorded at a Pt disk electrode (3 mm diameter). The scan rate was 50 mV s^{-1} .

Figure 3-9 shows the linear sweep voltammograms of *N*-benzylidenebenzylamine (**2**) in 250 mM $n\text{-Bu}_4\text{NClO}_4$ -30 mM EtONa-EtOH recorded at a graphite disk electrode. The reduction peak current of **2** was clearly observed in *ca.* -2.1 V vs. SCE in the case of 10 mM of **2**. Since graphite electrode shows a relatively high overpotential for the hydrogen evolution reaction, the desired cathodic reduction of intermediate **2** would be occurred preferentially even in a preparative scale electrolysis using a microreactor.

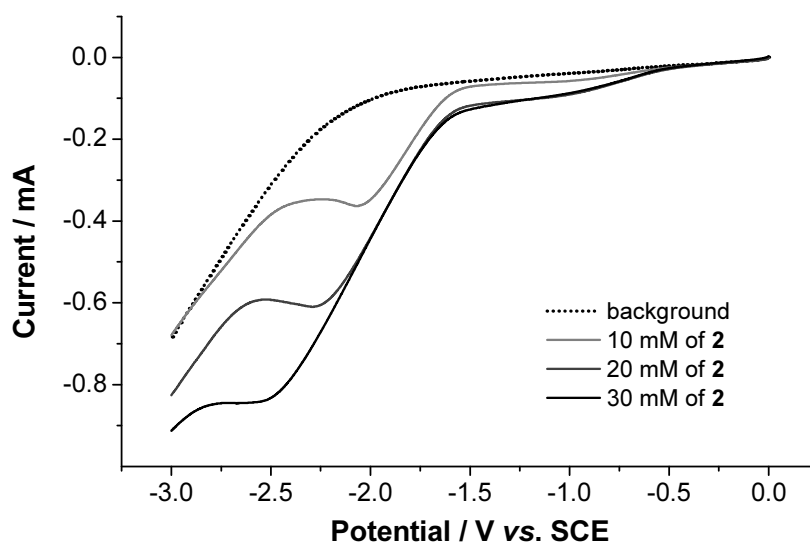
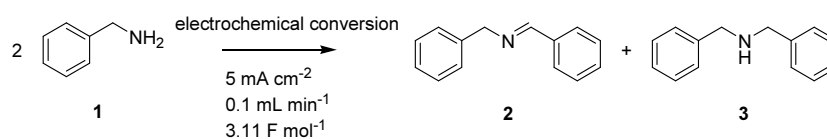


Figure 3-9. Linear sweep voltammograms of *N*-benzylidenebenzylamine (**2**) in 250 mM *n*-Bu₄NClO₄-30 mM EtONa-EtOH recorded at a graphite disk electrode (3 mm diameter). The scan rate was 50 mV s⁻¹.

3-3-2 Preparative electrolysis for the conversion of benzylamine to dibenzylamine using a microreactor

Next, preparative electrolysis for the conversion of benzylamine (**1**) to dibenzylamine (**3**) was carried out using a microreactor with Pt anode and graphite cathode combination. As shown in entry 1 of Table 3-1, when acetonitrile was used as solvent, the desired reaction did not proceed because the cell voltage was drastically increased with the electrolysis time. This was attributed to the passivation of the electrode surface by electropolymerization. In fact, a small amount of white precipitate was observed in the collected medium and electrode surface. On the other hand, when alcohols were used as solvent, the desired $[S/\pm e^-/I/\mp e^-/P]$ type paired reaction was proceeded with low cell voltages (3.3-3.6 V, entries 2 and 3). Although the yields of desired product **3** were fairly low, these preliminary results showed the possibility of this system as an analogue of photocatalytic redox combined reaction system.

Table 3-1. The effect of solvent in the electrochemical conversion of **1** to **3** using the microreactor.^a



Entry	Solvent	Total yield (%) ^b	Product ratio ^b
		2 + 3	2 : 3
1 ^c	MeCN	-	-
2 ^d	MeOH	54	93 : 7
3 ^d	EtOH	55	84 : 16

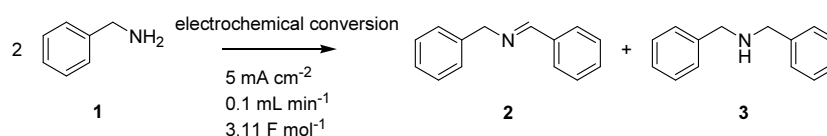
^aThe microreactor was consisted of a Pt anode and graphite cathode combination. The electrode distance was 80 μm . 250 mM of *n*-Bu₄NBF₄ was used as supporting electrolyte. All reactions were carried out at 25 °C. ^bYields and product ratios were determined by HPLC analysis. Yields were based on the theoretical amount of dimeric product. ^cThe cell voltage was too high to continue the electrolysis. ^d30 mM of sodium ethoxide was added.

Consequently, the supporting electrolyte for this electrochemical reaction system was then optimized (Table 3-2). Only small amounts of NH₄Cl, *n*-Bu₄NPF₆, and *n*-Et₄NClO₄ could dissolve in ethanol, so that saturated conditions were employed for cases using these electrolytes. The best result was obtained by the use of *n*-Bu₄NClO₄, as shown in entry 4.

From the results of GC-MS analyses of collected samples, the conversion of **1** was fairly good in all cases, but the progress of the desired $[S/\pm e^-/I/\mp e^-/P]$ type paired reaction was greatly affected by the kind of supporting electrolytes used. Generally, the choice of anion part of the supporting electrolyte is an important factor in anodic reactions in which the choice may influence the product distribution, while the choice of cation part influences on cathodic reactions.^[19] Nevertheless, in our case, anion part affected both the anodic and cathodic reactions. The comparison of the total yields in

entries 2 and 4 indicates that the use of ClO_4^- gave better result than that of BF_4^- in the anodic oxidation of **1** to **2**. In addition, the comparison of the product ratios in entries 2 and 4 suggests that the choice of ClO_4^- was also preferred than that of BF_4^- in the cathodic reduction of **2** to **3**. Besides, the product ratios of entries 4, 5, and 6 showed comparable values, indicating that the kind of tetraalkylammonium cation parts little affected the efficiency of cathodic reduction of **2** to **3**. However, the comparison of total yields in entries 4, 5, and 6 suggest that the kind of tetraalkylammonium cation parts clearly affected the efficiency of anodic oxidation of **1** to **2**. Hence, the effects of supporting electrolyte are significantly complex and it is still unclear what factors of

Table 3-2. The effect of supporting electrolyte in the electrochemical conversion of **1** to **3** using the microreactor.^a



Entry	Supporting electrolyte	Total yield (%) ^b	Product ratio ^b
		2 + 3	2 : 3
1 ^c	NH_4Cl	33	94 : 6
2	$n\text{-Bu}_4\text{NBF}_4$	55	84 : 16
3 ^c	$n\text{-Bu}_4\text{NPF}_6$	71	63 : 37
4	$n\text{-Bu}_4\text{NClO}_4$	97	58 : 42
5 ^c	$n\text{-Et}_4\text{NClO}_4$	82	61 : 39
6	$n\text{-Hex}_4\text{NClO}_4$	61	62 : 38

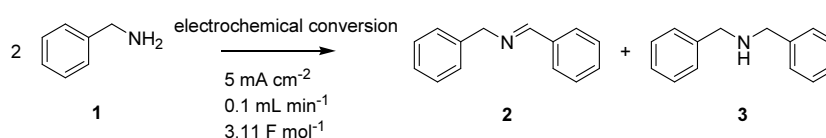
^aThe microreactor was consisted of a Pt anode and graphite cathode combination. The electrode distance was 80 μm . The concentration of supporting electrolyte was 250 mM unless otherwise indicated. 30 mM of sodium ethoxide was added and ethanol was used as solvent. All reactions were carried out at 25 °C. ^bYields and product ratios were determined by HPLC analysis. Yields were based on the theoretical amount of dimeric product. ^cSaturated solution was used because of the low solubility of the supporting electrolyte.

the supporting electrolyte play key roles in this system. Some additional investigations would be required for this issue.

Additionally, many bubbles (probably hydrogen gas) were observed at the outlet of the microreactor in any cases, which would be derived from the cathodic reduction of solvent. Owing to this cathodic gas evolution as a side-reaction, the desired cathodic reduction would be partially suppressed.

Subsequently, the cathode material of the microreactor was investigated (Table 3-3). Although both grassy carbon (GC) and zinc (Zn) electrodes have relatively high over potential for the hydrogen evolution reaction, these electrodes exhibited lower performance compared to that of graphite electrode. Graphite electrode has large superficial area in a specific size, which reduces the actual current density. This feature might improve the efficiency of the reduction of **2** to **3**.

Table 3-3. The effect of cathode material in the electrochemical conversion of **1** to **3** using the microreactor.^a



Entry	Cathode material	Total yield (%) ^b	Product ratio ^b
		2 + 3	2 : 3
1	graphite	97	58 : 42
2	GC	66	67 : 33
3	Zn	81	84 : 16

^aA Pt plate was used as the anode material. 250 mM of *n*-Bu₄NClO₄ was used as supporting electrolyte. Electrode distance was 80 μm. 30 mM of sodium ethoxide was added and ethanol was used as solvent. All reactions were carried out at 25 °C. ^bYields and product ratios were determined by HPLC analysis. Yields were based on the theoretical amount of dimeric product.

3-3-3 Comparison with a conventional batch type reactor

The desired $[S/\pm e^-/I/\mp e^-/P]$ type paired reaction using the microreactor was successfully demonstrated in the previous section. Thus, in the next step, a comparison with a conventional batch type reactor was carried out. The electrode distance of the microreactor was fixed at 80 μm , while that of a conventional batch type reactor was set as approximately 1.5 cm. As shown in Figure 3-10, the desired amine **3** was hardly obtained by using a conventional batch type reactor, and the reaction proceeded to give the intermediate imine **2** selectively in excellent yield. This result clearly shows that significantly short electrode distance of the microreactor enables a highly efficient sequential redox reaction, remarkably increasing the desired product **3** ratio. From these results, it can be stated that this $[S/\pm e^-/I/\mp e^-/P]$ type paired reaction system using the microreactor successfully works like a photocatalytic redox combined reaction system.

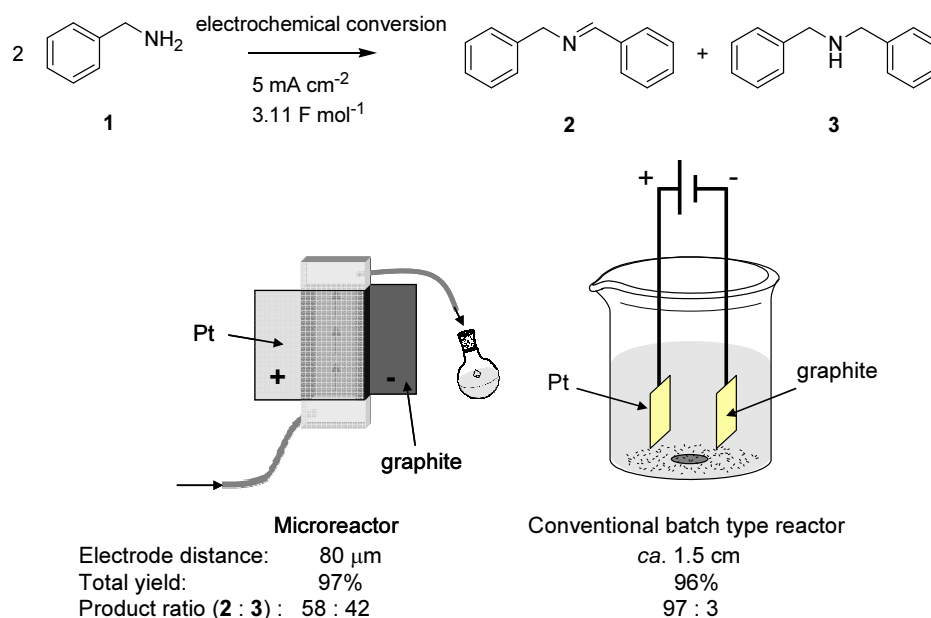


Figure 3-10. Comparison of the preparative electrolysis results between the microreactor and a conventional batch type reactor. Reactions were carried out in 250 mM of $n\text{-Bu}_4\text{NClO}_4$ -30 mM EtONa-EtOH at 25 $^\circ\text{C}$.

3-3-4 Effect of electrode distance

As described in the chapter 2, our electrochemical microreactor has many parameters and these parameters should be investigated systematically for the system optimization.

Thus, the effect of electrode distance on the $[S/\pm e^-/I/\mp e^-/P]$ type paired reaction system was then investigated. It was expected that the narrower electrode distance (50 μm) enhanced the desired redox reaction efficiency compared to the original electrode distance (80 μm). However, the narrower electrode distance decreased the product yields, as shown in Figure 3-11. On the other hand, the broader electrode distance (130

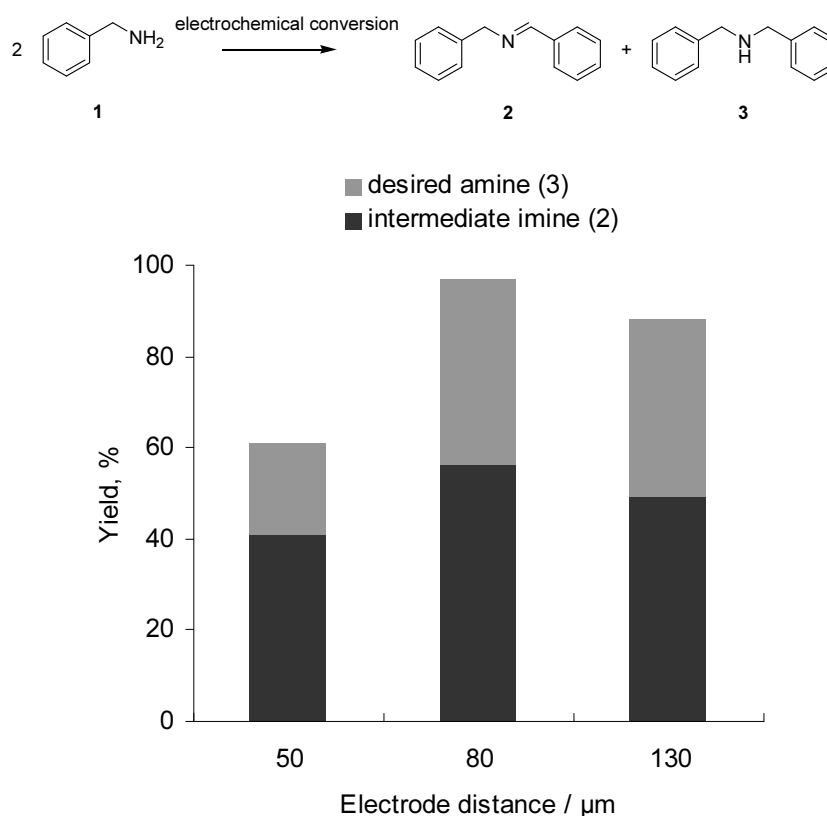


Figure 3-11. The effect of the electrode distance on the conversion of benzylamine (1) to dibenzylamine (3) via *N*-benzylidenebenzylamine (2). Flow rate was fixed at 0.1 mL min⁻¹. Current density was set as 5.0 mA cm⁻². 3.11 F mol⁻¹ of charge was passed. Yields were determined by HPLC analysis and based on the theoretical amount of dimeric product.

μm) resulted in a similar product yields. Therefore, the mass diffusion efficiencies of the substrate and intermediate would be enough at this range of electrode distance. Extremely narrow or broad electrode distance should be avoided to suppress unfavorable effects.

3-3-5 Effect of flow rate

Subsequently, the effect of flow rate on the $[S/\pm e^-/I/\mp e^-/P]$ type paired reaction system was investigated. As shown in Figure 3-12, when faster flow rate ($0.155 \text{ mL min}^{-1}$, 2.00 F mol^{-1}) was used, the yield of desired amine **3** was significantly decreased while

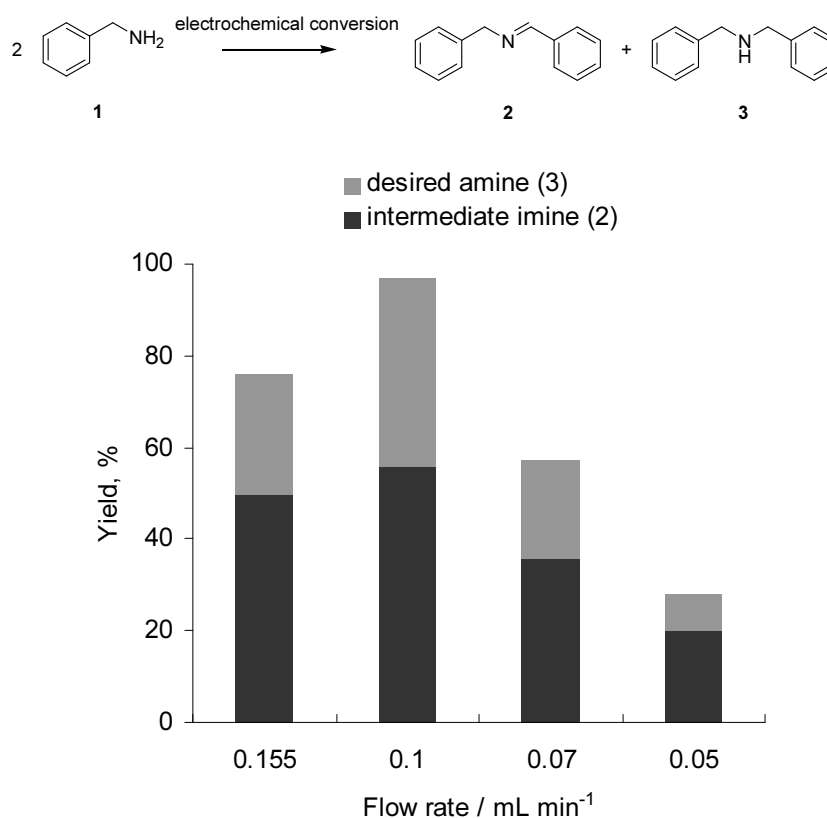


Figure 3-12. The effect of the flow rate on the conversion of benzylamine (**1**) to dibenzylamine (**3**) via *N*-benzylidenebenzylamine (**2**). Electrode distance was set as $80 \mu\text{m}$. Current density was set as 5.0 mA cm^{-2} . The amount of charge passed depends on the flow rate (2.00 to 6.22 F mol^{-1}). Yields were determined by HPLC analysis and based on the theoretical amount of dimeric product.

the yield of intermediate imine **2** was slightly decreased. This was attributed that the cathodic reduction of **2** was not enough to follow the anodic production of **2** in this condition. On the other hand, slower flow rate conditions also gave unfavorable results. In this case, it can be presumed that the over-oxidation of **3** at the anode would be occurred to give some by-products. Moreover, intermediate **2** would be reproduced by the over-oxidation of **3**.

3-3-6 *Effect of current density*

Next, the effect of current density on the $[S/\pm e^-/I/\mp e^-/P]$ type paired reaction system was investigated. As shown in Figure 3-13, the selectivity of the anodic oxidation of **1** to **2** was getting worse by applying higher current density. Over-oxidation of **3** would be also enhanced.

From the results of the system optimization, it can be concluded that the improvement of product **3** yield by optimizing some parameters has certain limitations due to the side-reactions of **1** and/or over-oxidation of **3**.

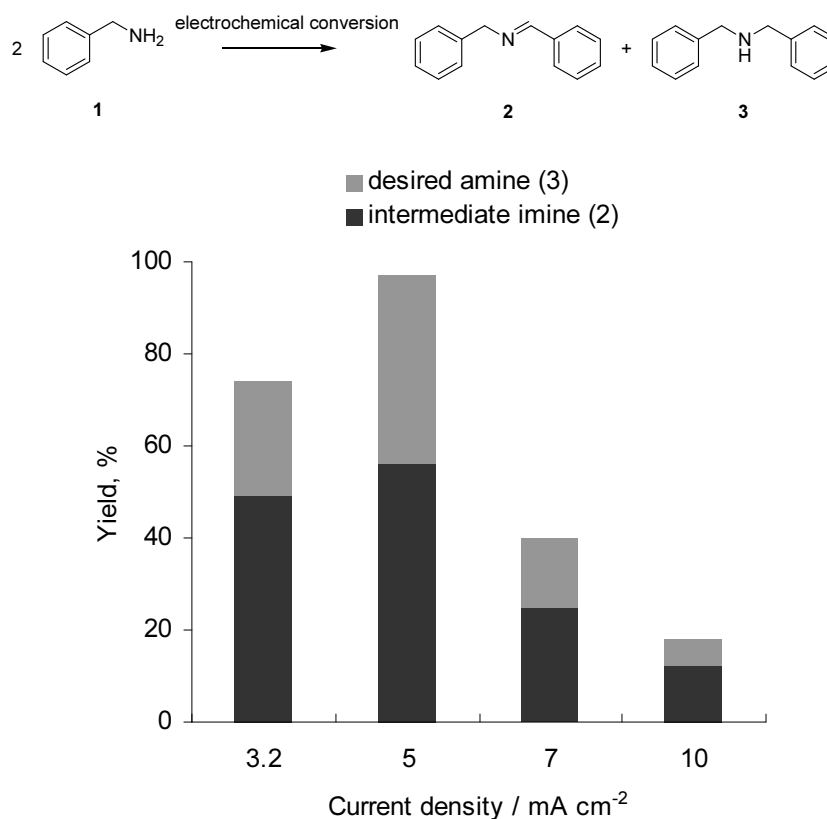


Figure 3-13. The effect of the current density on the conversion of benzylamine (**1**) to dibenzylamine (**3**) via *N*-benzylidenebenzylamine (**2**). Electrode distance was set as 80 μm . Flow rate was fix at 0.1 mL min^{-1} . The amount of charge passed depends on the current density (2.00 to 6.22 F mol^{-1}). Yields were determined by HPLC analysis and based on the theoretical amount of dimeric product.

3-3-7 Improvement of the microreactor: Suppression of the over-oxidation of product amine **3** to intermediate imine **2**

In order to confirm the over-oxidation of product amine **3** to **2**, the electrolyte solution with **3** was introduced into the reactor instead of the solution with starting material **1** (Figure 3-14 (a)). As a result, 26% of intermediate imine **2** was obtained and 65% of **3** was recovered. Hence, this result clearly indicates the reproduction of **2** by the over-oxidation of **3** at the anode. Since the recovery yield was up to 91%, the over-oxidation of **3** would give not only **2** but also some unknown by-products. In addition, when the electrolyte solution with **2** was introduced into the reactor, 74% of **2**

was converted into **3** (Figure 3-14(b)). This suggests that it is possible to improve the yield of **3** by further optimization of this system such as cell structure modification.

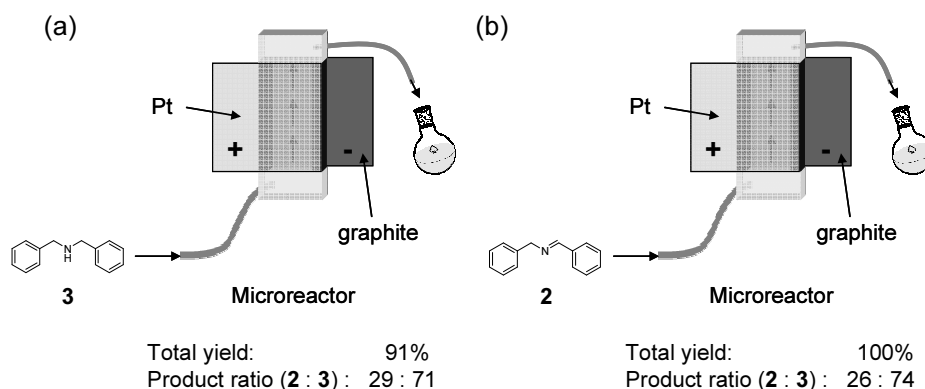


Figure 3-14. Preparative electrolysis results of the microreactor. Reactions were carried out in 250 mM of $n\text{-Bu}_4\text{NClO}_4$ -30 mM EtONa-EtOH at 25 °C. The electrode distance was 80 μm . The flow rate was 0.1 mL min^{-1} . The current density was 5 mA cm^{-2} . 3.11 F mol^{-1} of charge was passed. (a) 30 mM of dibenzylamine (**3**) was used as a starting material. (b) 30 mM of *N*-benzylidenebenzylamine (**2**) was used as a starting material.

In the first modification, a microreactor with longer length was designed (Figure 3-16 (a)). This newly designed microreactor has a twice length of electrodes compared to the original one, and the electrode area is 6 cm^2 . It was expected that the cathodic reduction of **2** to **3** would be enhanced by this new microreactor and the production of amine **3** would be more favored in this reactor. However, the reaction using this reactor resulted in poor yields of **2** and **3**. Therefore, it can be considered that the over-oxidation of **3** at the anode occurs simultaneously with the conversion of **1** to **2**, and after the complete consumption of **1**, the anodic over-oxidation of **3** to **2** and cathodic reduction of **2** to **3** become balanced in the reactor (The balanced ratio is approximately **2** : **3** = 60 : 40). Thus, the yield of **3** would be hardly improved by the elongation of cell length (the increase of charge passed). This consideration was indirectly supported by the results of linear sweep voltammograms of **3**. As shown in

Figure 3-15, the oxidation peak current of **3** was observed at *ca.* 1.5 V vs. SCE. Hence, product amine **3** would be more easily oxidized than substrate amine **1** when both **1** and **3** exist at the anode surface. Further improvement of the microreactor design should be attempted in order to obtain higher **3** selectively.

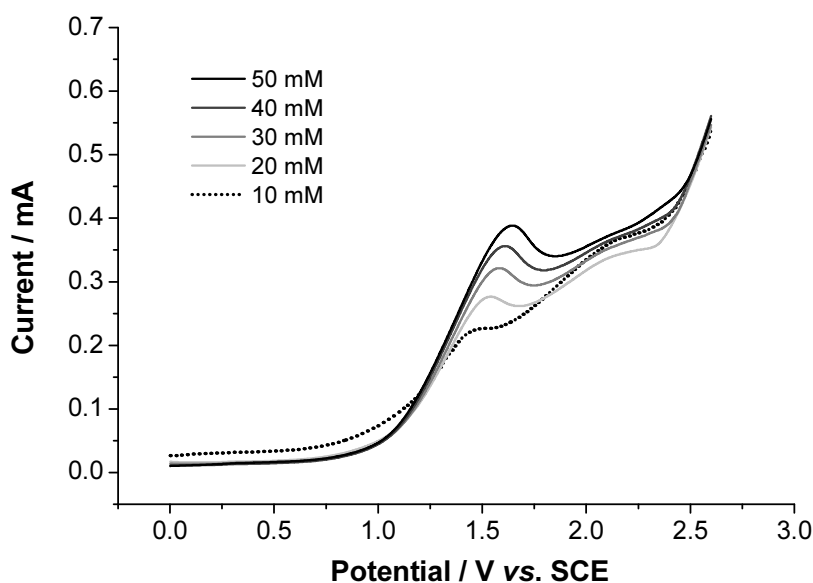


Figure 3-15. Linear sweep voltammograms of dibenzylamine (**3**) in 250 mM *n*-Bu₄NClO₄-EtOH recorded at a Pt disk electrode (3 mm diameter). The scan rate was 50 mV s⁻¹.

Besides, when the polarity of the electrochemical cell was reversed (graphite anode and Pt cathode combination), the reaction yielded **2** quantitatively (Figure 3-16 (b)). In this case, the hydrogen evolution reaction was dominantly occurred at the cathode due to the extremely low overpotential for the hydrogen evolution reaction of Pt, and therefore, intermediate imine **2** was ejected quantitatively without being reduced by the cathode. As described in the introduction section, compound **2** is a highly valuable synthetic intermediate which can be utilized for a large variety of organic transformations. Hence, this result opens a new aspect of the electrochemical

microreactor as a high throughput imine production system.

Finally, a specially designed microreactor was used for the desired $[S/\pm e^-/I/\mp e^-/P]$ type paired reaction. As shown in Figure 3-16 (c), the former part of this reactor was consisted of a Pt plate anode and Pt plate cathode combination, and the latter part of this reactor was consisted of a Pt plate anode and graphite plate cathode combination. The electrolyses of each part of the reactor were conducted independently. In this special microreactor, it was expected that intermediate imine **2** was mainly generated at the former part, and promptly transported to the latter part without being reduced to **3**. In the latter part, transported **2** would be efficiently reduced to give the desired product **3**. In this way, a similar situation of Figure 3-14 (b) would be realized at the latter part in this reactor, and the product **3** would be produced favorably.

As a result, this special microreactor electrolysis turned out to be a slight improvement of product **3** ratio. This result suggests that the concept of this design is certainly reasonable, however, the completely selective formation of the desired product is still difficult.

Chapter 3 Electrochemical Conversion of Primary Amine to Secondary Amine Using a Microreactor: Analogous System of Photocatalytic Redox Combined Synthesis

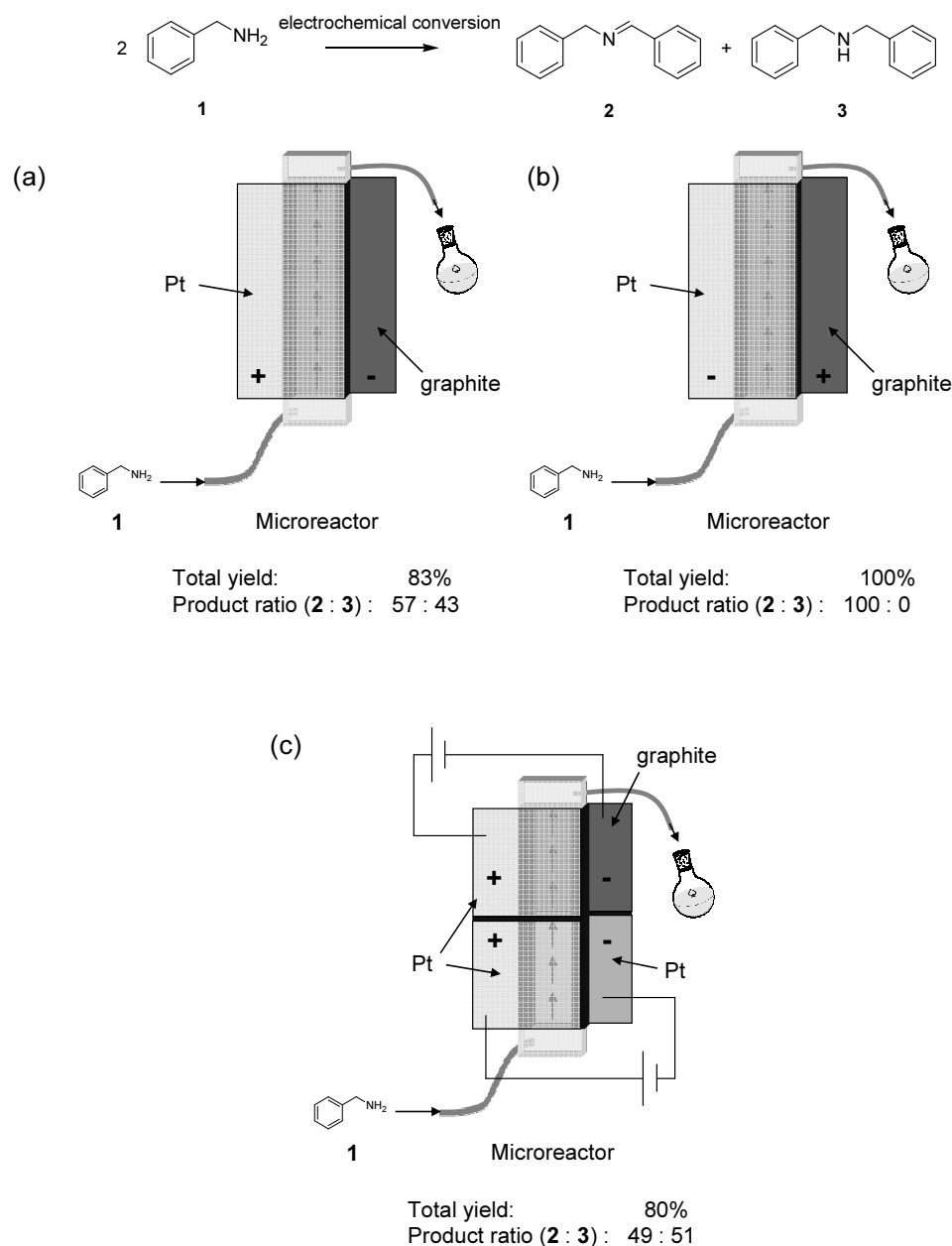


Figure 3-16. Preparative electrolysis results of the newly designed microreactors. Reactions were carried out in 250 mM of $n\text{-Bu}_4\text{NClO}_4$ -30 mM EtONa-EtOH at 25 °C. The electrode distance was fixed at 80 μm . The flow rate was 0.1 mL min^{-1} . The current density was 5 mA cm^{-2} . 6.22 F mol^{-1} of charge was passed. (a) 6 cm length Pt plate anode and 6 cm length graphite plate cathode were used. (b) 6 cm length graphite plate anode and 6 cm length Pt plate cathode were used. (c) The former part of the cell was a Pt plate anode and Pt plate cathode combination. The latter part of the cell was a Pt plate anode and graphite plate cathode combination. Each electrode plate was 3 cm length. The two anode plates were separated by spacer tape (80 μm) for insulation (the two cathode plates were also separated in the same way). The former part and latter part of the cell were connected to different galvanostats, respectively, and the electrolyses were conducted independently.

3-4 Conclusion

The $[S/\pm e^-/I/\mp e^-/P]$ type paired electrochemical conversion of benzylamine by using a microreactor was successfully carried out to provide dibenzylamine. The key feature of the method is an extremely narrow electrode distance of the microreactor. This sequential redox reaction hardly proceeded in the conventional batch type reactor. These results clearly show a significant advantage of the electrochemical microreactor for $[S/\pm e^-/I/\mp e^-/P]$ type paired electrosynthesis. In addition, it can be regarded that the two electrode surfaces facing each other with extremely narrow electrode distance works as an analogous reaction field of photocatalytic redox combined reaction system.

Experimental results also revealed that over-oxidation of dibenzylamine to *N*-benzylidenebenzylamine was occurred in the microreactor. This re-production reaction retreats a dibenzylamine selectivity, limiting the practical utility of this reaction system. A specially designed microreactor was applied to overcome this problem, showing the possibility of dibenzylamine selectivity improvement.

This system can tolerate a wide range of sequential redox reaction system and offers a new dimension in the electrochemical microreactor system and their applications in electroorganic synthesis.

3-5 References

- [1] A. Fujishima, K. Honda, *Nature* **1972**, *37*, 238.
- [2] Selected examples and reviews, see: a) A.J. Bard, *Science* **1980**, *207*, 139; b) E. Borgarello, J. Kiwi, E. Pelizzetti, M. Visca, M. Grätzel, *J. Am. Chem. Soc.* **1981**, *91*, 4305; c) M. Fujihira, Y. Satoh, T. Osa, *Nature* **1981**, *293*, 203; d) R. Cai, K. Hashimoto, Y. Kubota, A. Fujishima, *Bull. Chem. Soc. Jpn.* **1991**, *64*, 1268; e) R. Cai, Y. Kubota, T. Shuin, H. Sakai, K. Hashimoto, A. Fujishima, *Cancer Res.* **1992**, *52*, 2346; f) A.L. Linsebigler, G. Lu, J.T. Yates Jr., *Chem. Rev.* **1995**, *95*, 735; g) A. Maldotti, A. Molinari, R. Amadelli, *Chem. Rev.* **2002**, *102*, 3811; h) N. Hoffmann, *Chem. Rev.* **2008**, *108*, 1052.
- [3] T. Hirakawa, H. Kominami, B. Ohtani, Y. Nosaka, *J. Phys. Chem. B* **2001**, *105*, 6993.
- [4] P. Pichat, C. Guillard, C. Maillard, L. Amalric, J.C. D'Oliveira, *Trace Met. Environ.* **1993**, *3*, 207.
- [5] R.I. Bickley, R.K.M. Jayanty, V. Vishwanathan, J.A. Navio, *NATO ASI Ser., Ser. C* **1986**, *174*, 555.
- [6] C.-M. Wang, A. Heller, H. Gerischer, *J. Am. Chem. Soc.* **1992**, *114*, 5230.
- [7] a) W.W. Dunn, Y. Aikawa, A.J. Bard *J. Am. Chem. Soc.* **1981**, *103*, 3456; b) M.A. Fox, C.C. Chen, *J. Am. Chem. Soc.* **1983**, *105*, 4497; c) S. Nishimoto, B. Ohtani, T. Kagiya, *J. Chem. Soc., Faraday Trans.* **1985**, *81*, 2467; d) A. Wold, *Chem. Mater.* **1993**, *5*, 280.
- [8] Selected examples and reviews, see: a) S. Teratani, J. Nakamichi, K. Taya, K. Tanaka, *Bull. Chem. Soc. Jpn.* **1982**, *55*, 1688; b) F. Mahdavi, T.C. Bruton, Y. Li, *J. Org. Chem.* **1993**, *58*, 744; c) K.H. Park, H.S. Joo, K.I. Ahn, K. Jun, *Tetrahed.*

- Lett.* **1995**, *36*, 5943; d) B. Ohtani, Y. Goto, S.-I. Nishimoto, T. Inui, *J. Chem. Soc., Faraday Trans.* **1996**, *92*, 4291; e) M. Fagnoni, D. Dondi, D. Ravelli, A. Albini, *Chem. Rev.* **2007**, *107*, 2725.
- [9] T. Shiragami, C. Pac, S. Yanagida, *J. Phys. Chem.* **1990**, *94*, 504.
- [10] a) E. Baciocchi, C. Rol, G.C. Rosato, G.V. Sebastiani, *J. Chem. Soc., Chem. Commun.* **1992**, *59*; b) E. Baciocchi, C. Rol, G.V. Sebastiani, L. Taglieri, *J. Org. Chem.* **1994**, *59*, 5972.
- [11] Examples of photocatalytic redox combined synthesis, see: a) S. Nishimoto, B. Ohtani, T. Yoshikawa, T. Kagiya, *J. Am. Chem. Soc.* **1983**, *105*, 7180; b) B. Ohtani, H. Osaki, S. Nishimoto, T. Kagiya, *J. Am. Chem. Soc.* **1986**, *108*, 308; c) B. Ohtani, H. Osaki, S. Nishimoto, T. Kagiya, *Tetrahed. Lett.* **1986**, *27*, 2019; d) K. Shibata, T. Mimura, M. Matsui, T. Sugiura, H. Minoura, *J. Chem. Soc., Chem. Commun.* **1988**, 1318; e) H. Minoura, Y. Katoh, T. Sugiura, Y. Ueno, M. Matsui, K. Shibata, *Chem. Phys. Lett.* **1990**, *173*, 220; f) R. Künne, C. Feldmer, H. Kisch, *Angew. Chem. Int. Ed.* **1992**, *31*, 1039; g) R. Künne, C. Feldmer, F. Knoch, H. Kisch, *Chem. Eur. J.* **1995**, *1*, 441; h) H. Keck, W. Schindler, F. Knoch, H. Kisch, *Chem. Eur. J.* **1997**, *3*, 1638; i) L. Cermenati, C. Richter, A. Albini, *Chem. Commun.* **1998**, 805; j) A. Reinheimer, R. van Eldik, H. Kisch, *J. Phys. Chem. B* **2000**, *104*, 1014; k) H. Kisch, W. Lindner, *Chem. Unserer Zeit.* **2001**, *35*, 250.
- [12] a) B. Ohtani, S. Tsuru, S. Nishimoto, T. Kagiya, *J. Org. Chem.* **1990**, *55*, 5551; b) B. Ohtani, K. Iwai, H. Kominami, T. Matsuura, Y. Kera, S. Nishimoto, *Chem. Phys. Lett.* **1995**, *242*, 315; c) B. Pal, S. Ikeda, H. Kominami, Y. Kera, B. Ohtani,

J. Catal. **2003**, *217*, 152.

- [13] Reviews of the paired electrosynthesis and examples of $[S/\pm e^-/I/\mp e^-/P]$ type paired electrosynthesis, see: a) W. Li, T. Nonaka, T.-C. Chou, *Electrochemistry* **1999**, *67*, 4; b) C.A. Paddon, M. Atobe, T. Fuchigami, P. He, P. Watts, S.J. Haswell, G.J. Pritchard, S.D. Bull, F. Marken, *J. Appl. Electrochem.* **2006**, *36*, 617; c) R. Hazard, *Bull. Soc. Chim. Fr.* **1975**, *3-4*, 679; d) H.J. Wille, D. Knittle, B. Kastening, J. Mergel, *J. Appl. Electrochem.* **1980**, *10*, 489; e) H. Maekawa, K. Nakano, T. Hirashima, I. Nishiguchi, *Chem. Lett.* **1991**, 1661; f) H. Horio, K. Momota, K. Kato, M. Morita, Y. Matsuda, *Electrochim. Acta* **1996**, *41*, 1; g) H. Ohmori, H. Maeda in *New Challenges in Organic Electrochemistry* (ed. T. Osa), Gordon and Breach Science Publishers, Amsterdam, **1998**, Chapter 2.2.
- [14] M.M. Baizer, T. Nonaka, K. Park, Y. Saito, K. Nobe, *J. Appl. Electrochem.* **1984**, *14*, 197.
- [15] Selected examples of oxidative condensation of benzylamine, see: a) S. Ito, K. Sasaki, Y. Yanagi, *Bioelectrochemistry and Bioenergetics* **1982**, *9*, 313; b) K. Nakayama, M. Hamamoto, Y. Nishiyama, Y. Ishii, *Chem. Lett.* **1993**, 1699; c) K. Ohkubo, T. Nanjo, S. Fukuzumi, *Bull. Chem. Soc. Jpn.* **2006**, *79*, 1489; d) S.M. Landge, V. Atanassova, M. Thimmaiah, B. Török, *Tetrahed. Lett.* **2007**, *48*, 5161; e) M. Langeron, A. Chiaroni, M.-B. Fleury, *Chem. Eur. J.* **2008**, *14*, 996; f) A. Grirrane, A. Corma, H. Garcia, *J. Catal.* **2009**, *264*, 138; g) K.-W. Chi, H.Y. Hwang, J.Y. Park, C.W. Lee, *Synth. Met.* **2009**, *159*, 26.
- [16] a) D. Enders, U. Reinhold, *Tetrahed. Asym.* **1997**, *8*, 1895; b) C. Palomo, J.M. Aizpurua, I. Ganboa, M. Oiarbide, *Eur. J. Org. Chem.* **1999**, 3223; c) H. Miyabe,

M. Ueda, T. Naito, *Synlett* **2004**, 1140; d) V.I. Tararov, A. Boerner, *Synlett* **2005**, 203; e) G.K. Friestad, A.K. Mathies, *Tetrahed.* **2007**, 63, 2541; f) J. Gawronski, N. Wascinska, J. Gajewy, *Chem. Rev.* **2008**, 108, 5227; g) S.J. Connon, *Angew. Chem. Int. Ed.* **2008**, 47, 1176.

- [17] Selected recent reviews, examples, and applications of *N*-alkylation, see: a) F. Fabienne, V. Frederic, L. Marc in *Fine chemicals through heterogeneous catalysis* (eds. R.A. Sheldon, H. van Bekkum), Wiley-VCH, Weinheim; New York, **2001**, p.461; b) C.A. Olsen, H. Franzyk, J.W. Jaroszewski, *Synthesis* **2005**, 16, 2631; c) G. Guillena, D.J. Ramón, M. Yus, *Chem. Rev.* **2010**, 110, 1611; d) J. Chen, X. Chen, M. Bois-Choussy, J. Zhu, *J. Am. Chem. Soc.* **2006**, 128, 87; e) R. Goikhman, T.L. Jacques, D. Sames, *J. Am. Chem. Soc.* **2009**, 131, 3042; f) L.M. Salonen, C. Bucher, D.W. Banner, W. Haap, J.-L. Mary, J. Benz, O. Kuster, P. Seiler, W.B. Schweizer, F. Diederich, *Angew. Chem. Int. Ed.* **2009**, 48, 811; g) M.H.S.A. Hamid, C.L. Allen, G.W. Lamb, A.C. Maxwell, H.C. Maytum, A.J.A. Watson, J.M.J. Williams, *J. Am. Chem. Soc.* **2009**, 131, 1766.
- [18] a) E. Pastor, T. Iwashita, *Electrochim. Acta* **1994**, 39, 547; b) N. Fujiwara, K.A. Friedrich, U. Stimming, *J. Electroanal. Chem.* **1999**, 472, 120; c) C. Lamy, A. Lima, V. LeRhun, F. Delime, C. Coutanceau, J.-M. Léger, *J. Power Sources* **2002**, 105, 283; d) J. Datta, S. Singh, S. Das, N. R. Bandyopadhyay, *Bull. Mater. Sci.* **2009**, 32, 643.
- [19] H. Lund, in *Organic Electrochemistry*, fourth ed. (Eds. H. Lund, O. Hammerich), Marcel Dekker, New York, **2001**, p.223.

Chapter 4

Product Selectivity Control by Using a Liquid-Liquid Parallel Laminar Flow in a Microreactor

A novel strategy for product selectivity control by using a liquid-liquid parallel laminar flow in a microreactor has been demonstrated. The combined use of suitable flow mode in the microreactor and corresponding cathode material enables chemoselective cathodic reduction to control the product regioselectivity in cathodic carbonyl allylation. Additionally, the formation of clear substrate concentration gradient in the microreactor channel was supported by the estimation of substrate diffusion coefficient and computational simulation of the flow.

4-1 Introduction

4-1-1 Product selectivity control

In the field of synthetic chemistry, there has been a great interest about the control of product selectivity. Product selectivity is defined as the ratio of the desired product to all products in a chemical reaction which gives a mixture of desired product and some byproducts. The development of a novel method or strategy for product selectivity control have been regarded as fundamental but permanent subjects of synthetic chemistry because product selectivity often becomes problematic especially in a industrial production. Hence, considerable synthetic importance and theoretical interest can be found in the methods for product selectivity control.

With this view in mind, in this study, a new method for product selectivity control has been demonstrated. Before discussion of such a novel method, conventional ways of product selectivity control are described below.

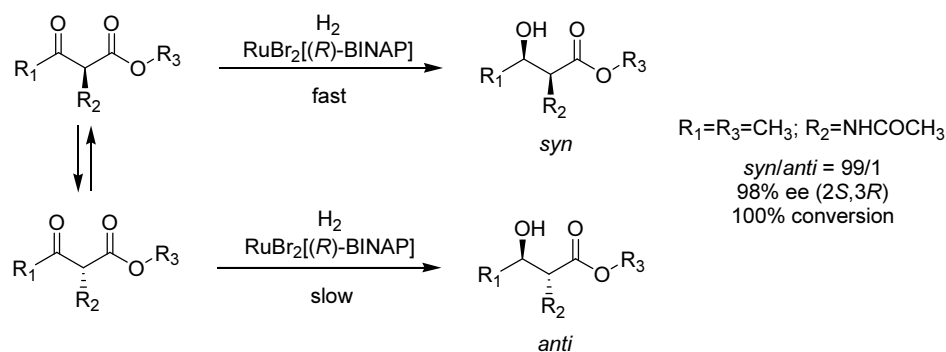
Generally, product selectivity is controlled by using suitable reactant(s) and suitable reaction conditions. Successful regio-, chemo- and stereo-selective reactions by using organometallic catalysts can be regarded as one of the most typical and well-controlled reactions.

Thus, in this section, factors for product selectivity control are classified. They are usually divided into chemical factors and physical factors. Chemical factors are based on characteristics and interactions of reaction molecules and solvents such as steric effect, resonance effect, and solvent effect. Physical factors are related to the reaction fields or systems which are specially designed for each reaction, and ultrasonic irradiation system and micro-flow system are typical examples. Most of the methods for product selectivity control are considered from the view of these two factors, and some of these are exemplified in the next section.

4-1-2 Product selectivity control induced by chemical factors

Steric effect

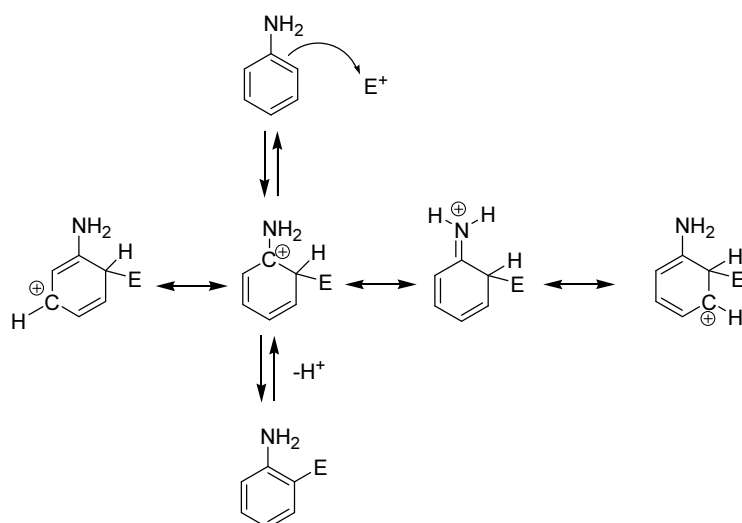
Steric effect is widely exploited by many researchers to change the reaction pattern and to suppress the undesired side reactions. One of the most typical example of steric effect for controlling product selectivity is kinetic resolution. In the kinetic resolution, generally, two enantiomers show different reaction rate in a chemical reaction to yield an excess amount of the less reactive enantiomer as a result of different steric hindrance between each enantiomer and an optically active reactant.



Scheme 4-1. Stereoselective hydrogenation *via* dynamic kinetic resolution.^[1] The remarkably high *syn* selection is rationalized in terms of the sterically constrained transition state between the substrate and the ruthenium catalyst.

Resonance effect

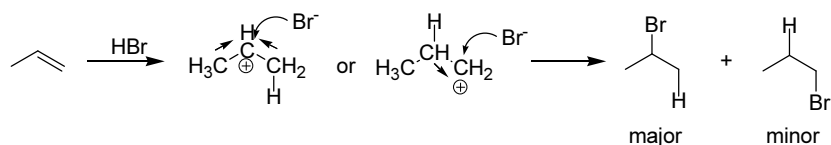
The classical example of resonance effect is found in electrophilic aromatic substitution reaction. For example, the amino group of aniline acts as a strong *ortho/para*-director, enhancing the proportion of the corresponding *ortho*- and *para*-products in an electrophilic substitution reaction.



Scheme 4-2. Electrophilic substitution reaction of aniline at *para*-position. The nitrogen atom can donate electron density to the π system of benzene ring (forming an iminium ion), giving four resonance structures. This substantially enhances the selectivity of *para*-substituted product.

Inductive effect

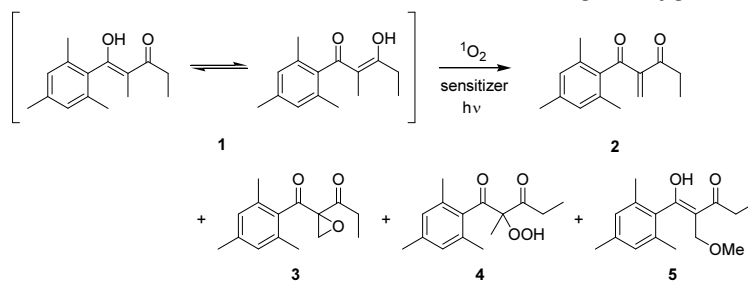
Markovnikov's rule is partially caused by inductive effect. This rule states the product selectivity in an addition reaction of a protic acid (HX) to an alkene. The acid hydrogen (H) attaches to the carbon atom with fewer alkyl substituents, while the halide (X) group attacks the carbon atom with more alkyl substituents. This selectivity is partially ascribed to that the inductive stabilization of the carbocation intermediate can be occurred at more substituted carbon atoms. Another explanation is given by hyperconjugation between carbocation and C-H σ bonds.



Scheme 4-3. Markovnikov's rule in the reaction of propene with hydrobromic acid.

Solvent effect

Solvents can often influence reaction rates through the reaction equilibrium. This leads that the product distribution of a reaction alters considerably with changes of solvent. For example, the product distribution in the reaction of singlet oxygen with 1,3-diketone (**1**) is remarkably affected by solvent effects, as shown in Table 4-1.^[2] The observed solvent effect on the selectivity of this reaction product can be rationalized by the consideration of the transition states with solvent polarity.

Table 4-1. Product distribution in the reaction of singlet oxygen with **1**.

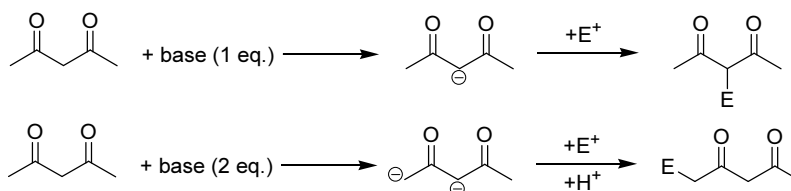
Solvent	Sensitizer*	Distribution (%)			
		2	3	4	5
CCl ₄	TPP	75	25	-	-
benzene	TPP	26	65	9	-
acetone	TPP	14	56	30	-
acetonitrile	MB	45	14	41	-
methanol	MB	-	6	25	40

*TPP: tetraphenylporphine, MB: Methylene Blue

Amount of reactant

In organic synthesis, the amount of reactants also affects the product selectivity in a chemical reaction. Suitable amount of reactants should be added to a reaction system with suitable adding speed and order. One example of this type of product selectivity change is carbon-carbon bond formation reaction of acetylacetone with electrophiles (Scheme 4-4). In this reaction, when one equivalent of base is added to the substrate

solution, carbanion is generated at the C3 position of the substrate, and then the carbanion is caught by electrophile to give C3 substituted product. On the other hand, when two equivalents of base are used, dianion is generated and one equivalent of electrophile reacts at C1 position predominantly to give the C1 substituted product.^[3]



Scheme 4-4. Carbon-carbon bond formation reaction of acetylacetone with an electrophile.

Others

Other chemical factors such as noncovalent interaction, hyperconjugation, hydrogen bond, electron orbital interaction and electron density can also affect the product selectivity. It should be noted that the product selectivity control induced by these factors is mainly provided by intentional changes of transition state stability or intermediate stability of the reaction molecule(s) during a reaction.

4-1-3 Product selectivity control induced by physical factors

Numerous reports have been paid attention to the product selectivity, however, many conventional methods for product selectivity control have focused relatively on chemical factors (One exception is the product selectivity change induced by temperature control). In contrast, some recent studies have reported the product selectivity control induced by physical factors. The term of physical factors used here denotes the significant changes in a reaction field. Researchers could purposely change the reaction route or reaction pattern by the change of external circumstances for a

reaction instead of the change of reactant, catalyst, or solvent. These novel strategies are cited below.

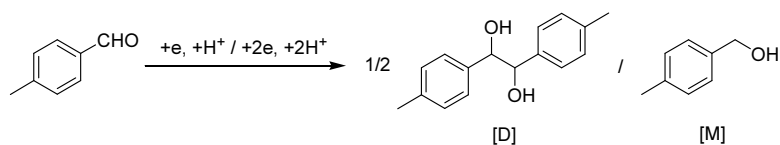
Temperature

Temperature control has historically been regarded as an important factor for product selectivity control although it can be classified into a physical factor. For example, low temperature condition generally affords good enantiomer excess in a kinetic resolution.

Ultrasonic irradiation

Ultrasonic irradiation on chemical reactions significantly affects the product distribution due to cavitation and agitation in homogeneous and heterogeneous reaction systems, respectively. Electroreduction of *p*-methylbenzaldehyde under ultrasonic irradiation is one of the typical example for product selectivity control by ultrasound (Table 4-2).^[4] In this case, ultrasonic irradiation drastically promoted the formation of hydrodimeric product toward hydromonomeric product.

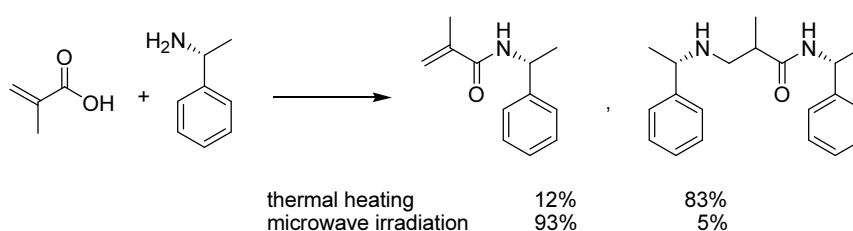
Table 4-2. Electroreduction of *p*-methylbenzaldehyde.



Stirring mode	Current efficiency for [D] + [M]	Selectivity [D] / [M]
still	35%	0.0
mechanical	74%	1.0
ultrasonic	77%	>99

Microwave irradiation

Since microwave irradiation offers a convenient method of local heating and activation, it can be considered as an alternative method to traditional thermal heating. Microwave irradiation can also provide a more selective and much faster reaction. Scheme 4-5 shows a selectivity enhancement of the condensation reaction by the use of microwave irradiation.^[5]



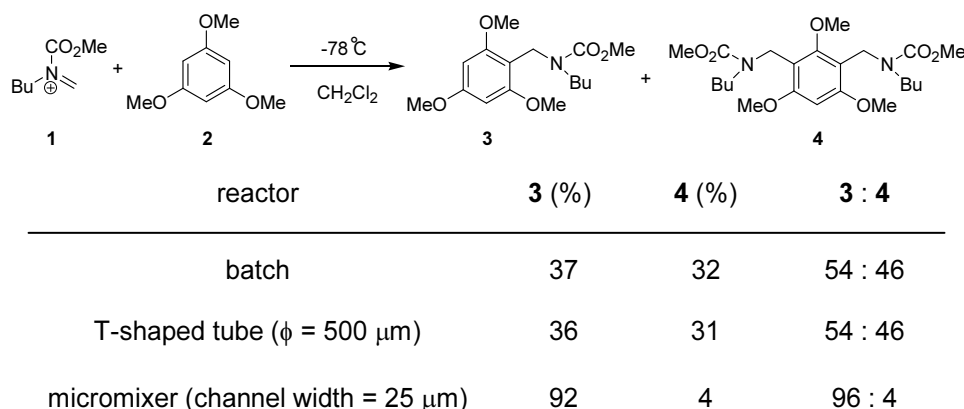
Scheme 4-5. Reaction comparison between conventional thermal heating and microwave irradiation in a methacrylamide formation reaction from methacrylic acid and (*R*)-1-phenyl-ethylamine.

Site isolation

The concept of site isolation was proposed about 30 years ago by Cohen and Patchornik, and since then, this concept has received an much attention.^[6] Site isolation is originally defined that the attachment of opposing reagents to the respective insoluble polymers suppresses their mutual destruction in a one-pot multistep reaction (Scheme 4-6). Therefore, this concept can be also regarded as a method of product selectivity control. One specific example is the use of polymer-supported carbon nucleophiles in electrochemical generation of carbocations for a direct oxidative carbon-carbon bond formation reaction (Scheme 4-7).^[7] Site isolation between an anode and polymer-supported carbon nucleophiles was achieved to suppress the oxidation of carbon nucleophiles at the anode. Thus, the desired final

Micro-flow system

In the method using a micro-flow system (microreactor or micromixer system), the product selectivity of a reaction can be significantly improved by the extremely fast and efficient mixing and heat transfer stemming from small size and high surface-to-volume ratio of microstructures. One typical example is the selective formation of a Friedel-Crafts monoalkylation product by using a micromixer (Scheme 4-8).^[8] This type of selectivity change can be regarded as “disguised chemical selectivity” which was proposed by Rys.^[9]



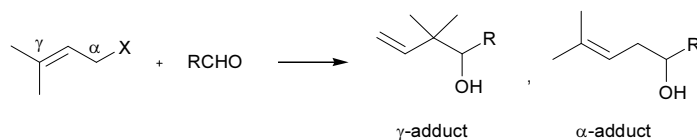
Scheme 4-8. Reaction comparison between three types of reactors in a Friedel-Crafts alkylation reaction of aromatic compound **2** with *N*-acyliminium ion **1**.

Moreover, micro-flow systems are fully compatible with space integration. The term of space integration represents a sequence of reactions which is conducted in one flow by adding components at different places (flow synthesis).^[10] This method is more flexible as far as choice of reagents which is concerned due to stepwise addition of components. Therefore, a wide variety of selective product formation in a sequence of reactions would be proposed by the method based on space integration using micro-flow systems.

4-1-4 Objective and strategy of this chapter

In the above sections, conventional methods and recent novel strategies for product selectivity control are cited and classified into the two factors. Further research on the method of product selectivity control is still worthwhile. As indicated in the general introduction (see. Chapter 1), this thesis aims to propose novel reaction systems which are realized only by using an electrochemical microreactor. Thus, the goal of this chapter is to propose a novel strategy for product selectivity control realized by using an electrochemical microreactor. This strategy can be also regarded as a type of space integration (product selectivity control induced by physical factor), however, the methodology is fully different from those of reported examples. The basis and details of this strategy are described below.

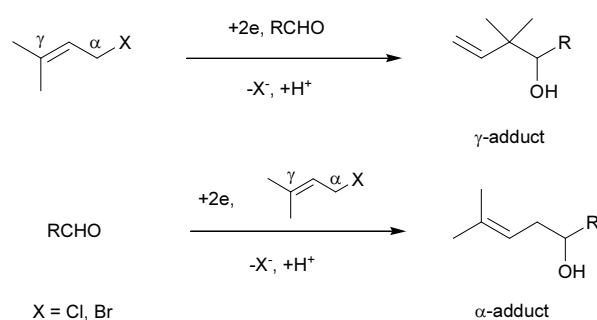
Firstly, in order to demonstrate this novel strategy, cathodic carbonyl allylation was employed for the model reaction. Carbonyl allylation is one of the most important and most utilized reactions in organic synthesis.^[11] This reaction usually provides two regioisomers, γ - and α -adducts, and both products are very useful and valuable as the framework for the synthesis of natural compounds and pharmaceuticals (Scheme 4-9). Therefore, the development of a facile regioselective synthesis for either γ - or α -adducts is highly important.



Scheme 4-9. Carbonyl allylation between allylic halides and aldehydes.

Among the several methods employed for this cross-coupling reaction, the electrochemical method serves as a straightforward and powerful method, and cathodic

carbonyl allylation has been reported by many researchers since 1972.^[12] Although the regioselectivity of this reaction is influenced by electrode materials, the concentration of supporting electrolytes and current density, Tokuda *et al.* clarified that the regioselectivity was mainly related to the difference in the reduction potentials between the two starting substrates.^[13] Electrochemical carbonyl allylation can produce either γ - or α -adducts depending on whether the aldehyde or allylic halide is reduced by the cathode. If the aldehyde has a higher reduction potential, the γ -adduct is produced but if the reduction potential of the allylic halide is higher, the α -adduct is favored. Therefore, control of the product selectivity (regioselectivity in this reaction) requires that either the allylic halides or aldehydes should be reduced chemoselectively, regardless of their reduction potentials.



Scheme 4-10. The reaction pathway of cathodic carbonyl allylation between an allylic halide and an aldehyde.

To perform chemoselective cathodic reduction, a liquid-liquid parallel laminar flow in a microreactor was employed in this study. The channel of the microreactor is sufficiently small to ensure stable and laminar flow of solutions.^[14] As shown in Figure 4-1, when two solutions (allylic halide solution and aldehyde solution) are introduced through respective inlets (inlet 1 and inlet 2) of the microreactor, a stable liquid-liquid interface can be formed, and mass transfer between the input streams occurs only by

means of diffusion. Therefore, the substrate introduced through inlet 1 could be predominantly reduced, whereas the reduction of the inlet 2 substrate could be avoided. Consequently, chemoselective cathodic reduction would proceed and an intentional cross-coupling product would be obtained regioselectively. In other words, product selectivity control would be realized by simply switching the reagent flows.

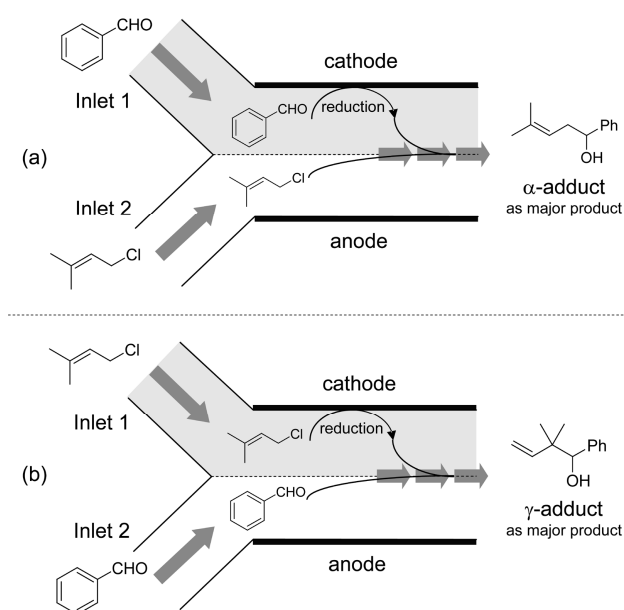


Figure 4-1. Chemoselective cathodic reduction using parallel laminar flow in the microreactor. (a) Flow mode for the selective reduction of benzaldehyde (**2a**). (b) Flow mode for the selective reduction of 1-chloro-3-methyl-2-butene (**1a**).

The demonstration of the above strategy, reaction conditions, diffusion estimation and computational simulation of the liquid-liquid parallel laminar flow in the microreactor channel, and versatility of this system were investigated in this chapter.

4-2 Experimental Section

4-2-1 Instrumentation

Nuclear magnetic resonance (^1H NMR, ^{13}C NMR) spectra were measured on JEOL JNM EX-270 spectrometer operating at 270 MHz (^1H NMR), 67.8 MHz (^{13}C NMR) in CDCl_3 . All ^1H NMR chemical shifts were reported in ppm relative to internal references of TMS at δ 0.00. ^{13}C NMR chemical shifts were reported in ppm relative to carbon resonance in chloroform- d_1 at δ 77.00. EI mass spectra were measured with a Shimadzu GCMS-QP5050A mass spectrometer. IR spectra were recorded on a Shimadzu FTIR-8100A spectrometer. Cyclic voltammetry and chronoamperometry were performed by using a computer-controlled electrochemical analyzer (ALS/CH Instruments 630C). Preparative electrolyses were carried out with a HOKUTO DENKO HA-501 Potentiostat/Galvanostat. GC analyses were performed with a Shimadzu GC-2014 gas chromatograph with Tween 80 (2 m column). Computational fluid dynamics (CFD) simulations for liquid-liquid parallel laminar flow in a microreactor were carried out by using commercial CFD package Fluent 6.3 (ANSYS Inc.).

4-2-2 Materials

1-Chloro-3-methyl-2-butene (**1a**) was purchased from Aldrich and purified by distillation before use. Hexamethylphosphoric triamide (HMPA), tetrabutylammonium perchlorate ($n\text{-Bu}_4\text{NClO}_4$), benzaldehyde (**2a**), 4-(trifluoromethyl)benzaldehyde (**2b**), 2-naphthaldehyde (**2c**), *p*-tolualdehyde (**2d**) and 3-furaldehyde (**2e**) were purchased from Tokyo Chemical Industry and used as received.

4-2-3 Microreactor

Figure 4-2 shows schematic illustration of the microreactor. The microreactor consisted of two plates. Each plate was glued the electrode plate (cathode plate (Pt or Ag, Nilaco) or anode plate (graphite, IGS-743, Nippon Techno-Carbon), 3 cm width, 3 cm length) and glass plate (2.6 cm width, 3 cm length) together. A slit was provided on anode side for introducing solution B of Figure 4-2 into the reactor. A spacer (both sides adhesive tape, 20 μm thickness, Nitto Denko) was used to leave a rectangular channel exposed, and the two plates were simply sandwiched together. After connecting Teflon tubing to inlets and outlet, the reactor was sealed with epoxy resin. The dimensions of the channel were 1 cm width, 20 μm depth, and 6 cm total length and area of the two electrodes was 3 cm^2 .

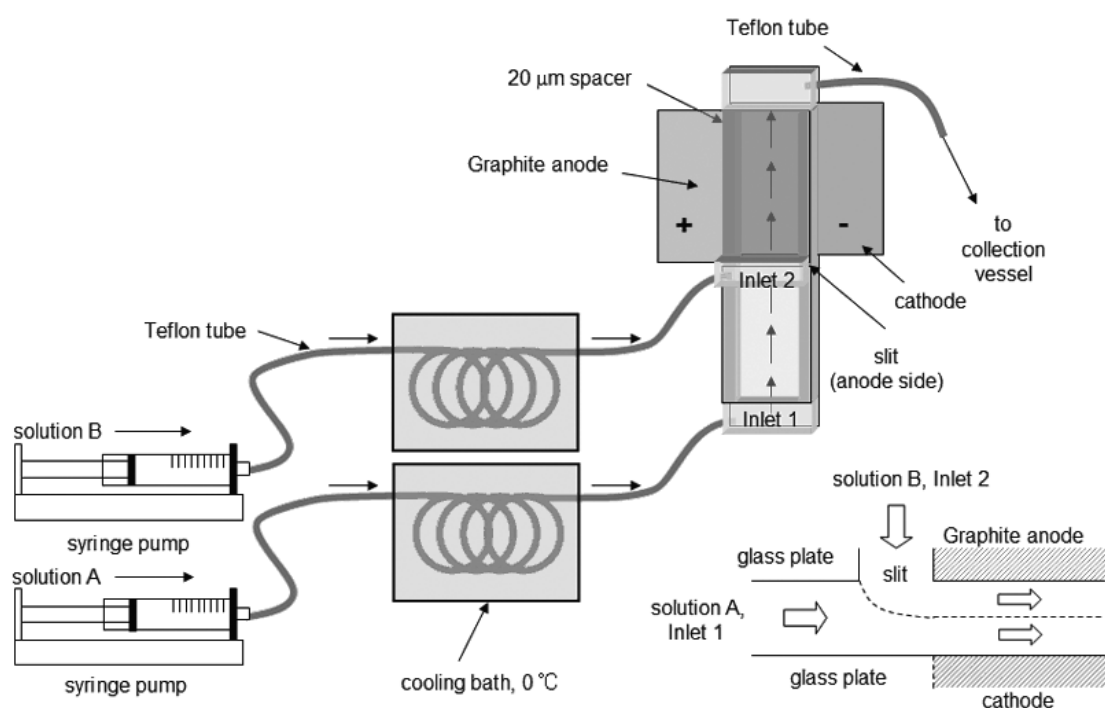


Figure 4-2. Schematic illustration of the microreactor.

4-2-4 CFD simulation settings

A T-type planer (2D) geometry and boundary conditions used are shown in Figure 4-3. The quadrilateral mesh was generated by using the pre-processor Gambit 2.4 software (ANSYS Inc.). The physical properties and simulation parameters used in the present work are listed in Table 4-3. A uniform inlet velocity was set at the two inlets and input streams were assumed to develop into laminar flows. In application of Fluent 6.3, Navier-Stokes equations and species transport equations were solved simultaneously. No heat transfer and no reaction between transported species were presumed. A no-slip boundary condition was used at the walls where the velocity is zero.

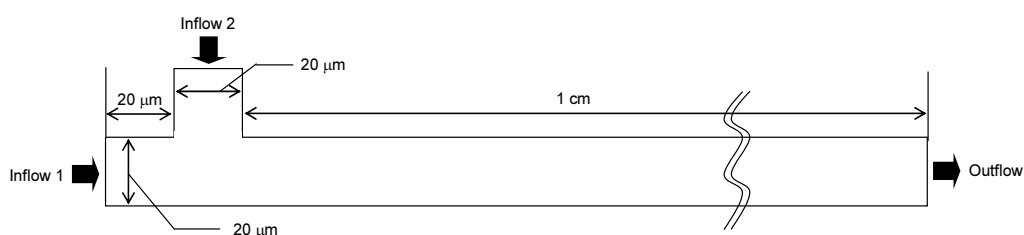


Figure 4-3. Schematic illustration of the geometry and the boundary conditions used in the CFD simulation.

Table 4-3. Simulation settings and physical properties of liquids used for the simulations.

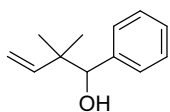
Property	Value
Mesh number	1,046,000
Inlet velocity (Inflow 1 and Inflow 2)	$8.33 \times 10^{-4} \text{ m s}^{-1}$
Mass fraction of benzaldehyde (Inflow 1)	0
Mass fraction of benzaldehyde (Inflow 2)	0.206
Molecular weight (HMPA)	$179.2 \text{ kg kmol}^{-1}$
Molecular weight (benzaldehyde)	$106.12 \text{ kg kmol}^{-1}$
Density (HMPA)	1030 kg m^{-3}
Density (benzaldehyde)	1041.5 kg m^{-3}
Dynamic viscosity ^a	$1.11 \times 10^{-2} \text{ Pa s}$

^aObtained by rheology measurements, see: Figure 4-14.

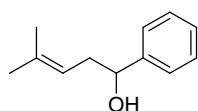
4-2-5 General procedure for preparative electrolysis

KdScientific model 100 syringe pumps were used to pump the reaction solutions. Two solutions were flowed through a cooling bath (0 °C) before introducing into the cell. All reactions were conducted galvanostatically. Conditions of the cathodic cross-coupling reaction between **1** and **2** in the microreactor are described in footnotes *a* of Table 1 in the main text. The reaction mixture was analyzed by GC. For isolation of the products, the reaction mixture (5 mL) was added to a 50 mL of water and the aqueous layer was extracted three times with a 30 mL of diethyl ether. The combined organic fractions were washed with brine, dried over Na₂SO₄ and concentrated in *vacuo*. The residue was purified by column chromatography on silica gel with hexane/AcOEt. ¹H NMR yields of the crude mixture was determined with an internal standard (MeNO₂). All products except for **4b** were identified by authentic samples and literatures (**3a**,^[13b] **4a**,^[13b] **3e**,^[13b] **4e**,^[13b] **3b**,^[15] **4c**,^[16] **3c**,^[17] **3d**^[17] and **4d**^[18]) using ¹H NMR and mass spectroscopy. Compound **4b** was identified by using ¹H and ¹³C NMR, IR, mass, and high-resolution mass spectroscopy.

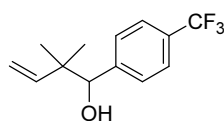
4-2-6 Spectroscopic data

**2,2-Dimethyl-1-phenyl-but-3-en-1-ol (3a)**

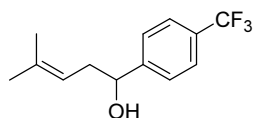
colorless oil; ¹H NMR (270 MHz, CDCl₃) δ 7.29(s, 5H), 5.92(dd, *J* = 17.3, 10.5 Hz, 1H), 5.16-5.04(m, 2H), 4.43(s, 1H), 1.02(s, 3H), 0.96(s, 3H); MS (EI) *m/z* (relative intensity) 176([M⁺], 0.26), 107(100), 79(93), 70(98).

**4-Methyl-1-phenyl-pent-3-en-1-ol (4a)**

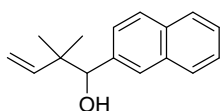
colorless oil; ^1H NMR (270 MHz, CDCl_3) δ 7.40-7.23(m, 5H), 5.20-5.14(m, 1H), 4.68(dd, $J = 8.1, 5.7$ Hz, 1H), 2.55-2.38(m, 2H), 1.83(bs, 1H), 1.72(s, 3H), 1.61(s, 3H); MS (EI) m/z (relative intensity) 176($[\text{M}^+]$, 4.3), 107(99), 79(95), 70(100).

**2,2-Dimethyl-1-(4-trifluoromethyl-phenyl)-but-3-en-1-ol (3b)**

colorless oil; ^1H NMR (270 MHz, CDCl_3) δ 7.56(d, $J = 8.1$ Hz, 2H), 7.41(d, $J = 8.1$ Hz, 2H), 5.88(dd, $J = 17.6, 10.8$ Hz, 1H), 5.20-5.05(m, 2H), 4.48(s, 1H), 2.11(bs, 1H), 1.02(s, 3H), 0.96(s, 3H); MS (EI) m/z (relative intensity) 244($[\text{M}^+]$, 0.01), 225(9), 175(98), 147(33), 127(88), 70(100).

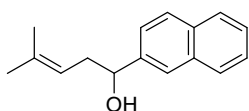
**4-Methyl-1-(4-trifluoromethyl-phenyl)-pent-3-en-1-ol (4b)**

colorless oil; IR (neat NaCl, v/cm^{-1}) 3370, 2920, 1620, 1420, 1330, 1170, 1130, 1070, 1020, 890; ^1H NMR (270 MHz, CDCl_3) δ 7.60(d, $J = 8.10$ Hz, 2H), 7.48(d, $J = 8.10$ Hz, 2H), 5.18-5.12(m, 1H), 4.75(t, $J = 5.67$, 1H), 2.48-2.42(m, 2H), 2.08(bs, 1H), 1.74(s, 3H), 1.61(s, 3H); ^{13}C NMR (67.8 MHz, CDCl_3) δ 148.00, 136.45, 125.95, 125.11(q, $J = 3.9$ Hz), 118.85, 73.31, 38.37, 25.94, 18.01; MS (EI) m/z (relative intensity) 244($[\text{M}^+]$, 0.09), 225(3), 175(62), 147(10), 127(49), 70(100); HRMS (EI) m/z Calcd. for $\text{C}_{13}\text{H}_{13}\text{F}_3\text{O}$ $[\text{M}^+ - 2\text{H}]$: 242.0913 Found: 242.0912.



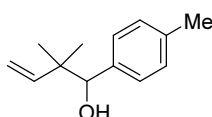
2,2-Dimethyl-1-naphthalen-2-yl-but-3-en-1-ol (3c)

pale yellow oil; ^1H NMR (270 MHz, CDCl_3) δ 7.84-7.74(m, 4H), 7.48-7.42(m, 3H), 5.97(dd, $J = 17.6, 10.8$ Hz, 1H), 5.18-5.06(m, 2H), 4.60(s, 1H), 2.14(bs, 1H), 1.06(s, 3H), 1.01(s, 3H); MS (EI) m/z (relative intensity) 226($[\text{M}^+]$, 4.6), 157(100), 129(92), 102(3), 77(6).



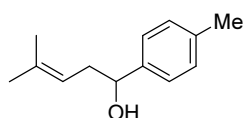
4-Methyl-1-naphthalen-2-yl-pent-3-en-1-ol (4c)

pale yellow oil; ^1H NMR (270 MHz, CDCl_3) δ 7.84-7.81(m, 4H), 7.51-7.42(m, 3H), 5.23-5.16(m, 1H), 4.85(dd, $J = 7.6, 5.4$ Hz, 1H), 2.58-2.51(m, 2H), 2.11(bs, 1H), 1.73(s, 3H), 1.63(s, 3H); MS (EI) m/z (relative intensity) 226($[\text{M}^+]$, 5.1), 208(12), 193(21), 178(16), 157(100), 129(96), 115(4), 89(5), 77(6).



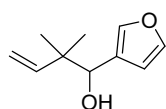
2,2-Dimethyl-1-p-tolyl-but-3-en-1-ol (3d)

colorless oil; ^1H NMR (270 MHz, CDCl_3) δ 7.20-7.10(m, 4H), 5.92(dd, $J = 17.5, 10.9$ Hz, 1H), 5.15-5.04(m, 2H), 4.40(s, 1H), 2.34(s, 3H), 1.01(s, 3H), 0.95(s, 3H); MS (EI) m/z (relative intensity) 190($[\text{M}^+]$, 0.29), 121(100), 93(81), 77(64), 70(69).



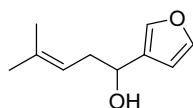
4-Methyl-1-*p*-tolyl-pent-3-en-1-ol (4d)

colorless oil; ^1H NMR (270 MHz, CDCl_3) δ 7.25(d, $J = 8.07$ Hz, 2H), 7.15(d, $J = 8.07$ Hz, 2H), 5.20-5.14(m, 1H), 4.64(dd, $J = 7.91$ Hz, 5.27, 1H), 2.58-2.29(m, 2H), 2.34(s, 3H), 1.94(bs, 1H), 1.73(s, 3H), 1.62(s, 3H); MS (EI) m/z (relative intensity) 190($[\text{M}^+$], 1.3), 172(10), 157(16), 142(11), 121(100), 93(80), 77(57), 70(58).



1-Furan-3-yl-2,2-dimethyl-but-3-en-1-ol (3e)

yellow oil; ^1H NMR (270 MHz, CDCl_3) δ 7.36-7.734(m, 2H), 6.37-6.36(m, 1H), 5.91(dd, $J = 17.3, 10.8$ Hz, 1H), 5.17-5.07(m, 2H), 4.40(s, 1H), 1.03(s, 3H), 1.00(s, 3H); MS (EI) m/z (relative intensity) 166($[\text{M}^+$, 8]), 133(1), 97(100), 70(90).



1-Furan-3-yl-4-methyl-pent-3-en-1-ol (4e)

yellow oil; ^1H NMR (270 MHz, CDCl_3) δ 7.39-7.37(m, 2H), 6.42-6.41(m, 1H), 5.20-5.12(m, 1H), 4.66(dd, $J = 7.26, 5.79$ Hz, 1H), 2.55-2.37(m, 2H), 1.85(bs, 1H), 1.73(s, 3H), 1.65(s, 3H); MS (EI) m/z (relative intensity) 166($[\text{M}^+$], 10.9), 148(4.4), 133(3.5), 119(4.1), 97(100), 70(95).

4-3 Results and Discussion

4-3-1 Cyclic voltammetry in the microreactor

First of all, in order to confirm that substrate was prevented from reaching the counter electrode surface by the use of liquid-liquid parallel laminar flow, cyclic voltammograms (CVs) were measured for the reduction of benzaldehyde (**2a**) in the microreactor. A reduction peak of **2a**, as shown in Figure 4-4(b), was clearly observed at -1.89 V vs. Ag wire when an electrolytic stream containing **2a** entered only through inlet 1 of Figure 4-1 (cathode side inlet). On the other hand, the peak current was significantly decreased when an electrolytic solution with **2a** was introduced through inlet 2 (anode side inlet), and a solution without **2a** was introduced through inlet 1 (Figure 4-4(c)). This result indicated that the use of liquid-liquid parallel laminar flow did prevent **2a** from reaching the cathode when it was introduced through inlet 2.

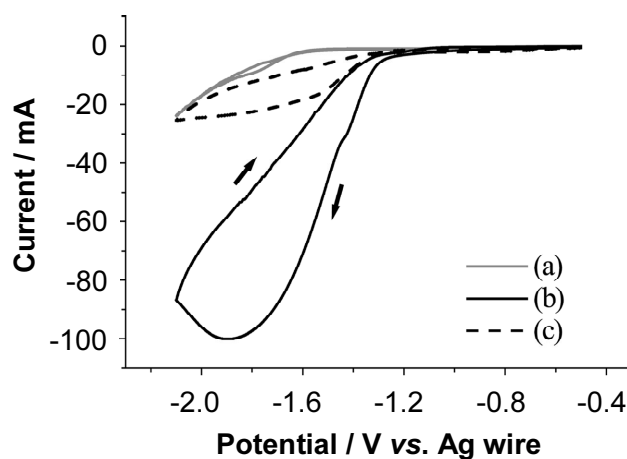


Figure 4-4. Cyclic voltammograms for the reduction of benzaldehyde (**2a**) in 200 mM *n*-Bu₄NClO₄-hexamethylphosphoric triamide (HMPA) using a microreactor with a Pt cathode. Ag wire as a reference electrode was placed externally, downstream near the outlet of the microreactor. The scan rate was 100 mV s⁻¹. (a) HMPA solution without **2a** was introduced through inlet 1 of Figure 4-1 at a flow rate of 0.02 mL min⁻¹ (background). (b) HMPA solution with **2a** (1M) was introduced through inlet 1 at a flow rate of 0.02 mL min⁻¹. (c) HMPA solution with **2a** (2M) was introduced through inlet 2, and HMPA solution without **2a** was introduced through inlet 1, both at a flow rate of 0.01 mL min⁻¹.

4-3-2 Reduction potentials of substrates

Next, reduction potentials of substrates were measured by cyclic voltammetry in 0.2 M *n*-Bu₄NClO₄/hexamethylphosphoric triamide (HMPA) medium recorded at (a) platinum (Pt), (b) glassy carbon (GC), and (c) silver (Ag) electrodes. As shown in Figure 4-5(a), benzaldehyde (**2a**) was reduced at *ca.* -2.22 V *vs.* SCE (peak potential), while 1-chloro-3-methyl-2-butene (**1a**) was reduced at *ca.* 3.02 V *vs.* SCE at Pt electrode. As mentioned in the above, the regioselectivity of this model reaction is mainly influenced by the difference in the reduction potentials between two starting substrates. When aldehydes are more readily reduced than allylic halides, the reduction yields α -adducts preferentially. Thus, it can be predicted that the α -adduct would be obtained as a major product at the bulk electrolysis using Pt electrode. From the result of Figure 4-5(b), GC electrode would also show similar product selectivity. On the other hand, as shown in Figure 4-5(c), **1a** and **2a** were reduced at almost same potentials (*ca.* -2.23 V *vs.* SCE) at the Ag electrode. This was ascribed to a electrocatalytic activity of the Ag electrode for the reduction of organic halides.^[19] Therefore, it is expected that a nearly equal amount of γ -adduct and α -adduct are obtained at the bulk electrolysis using Ag electrode.

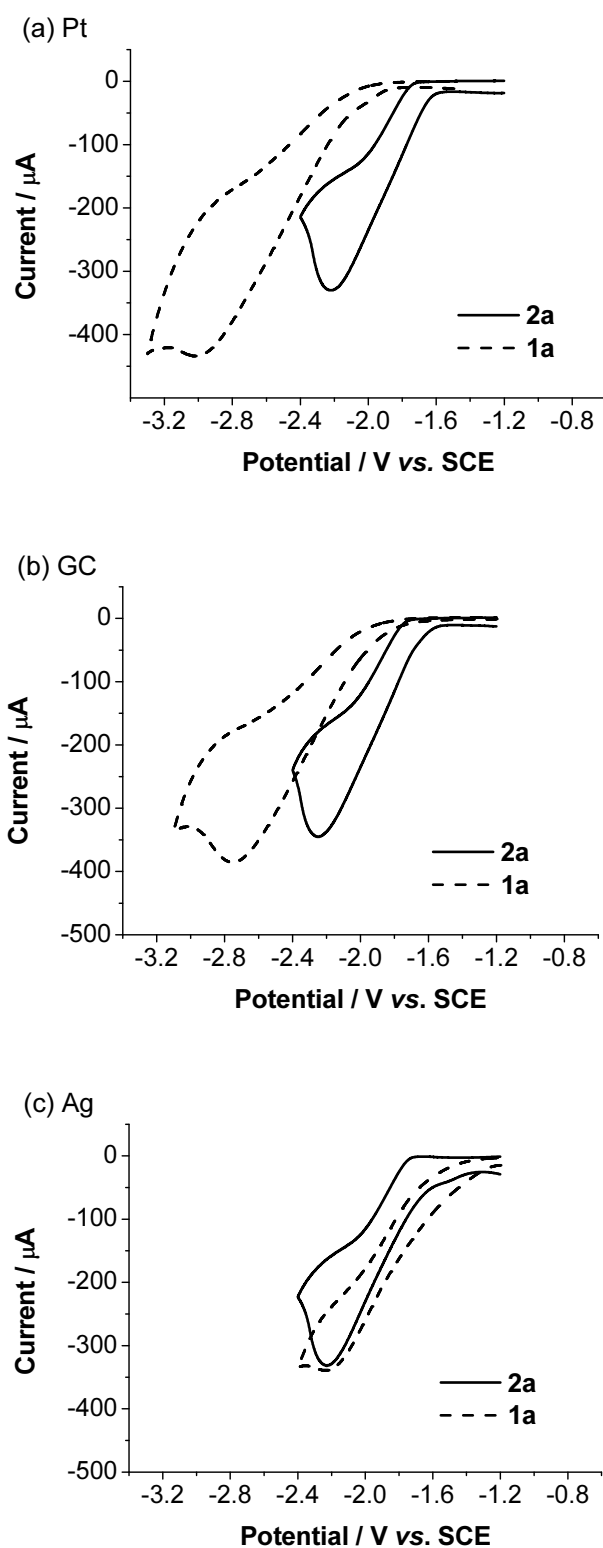


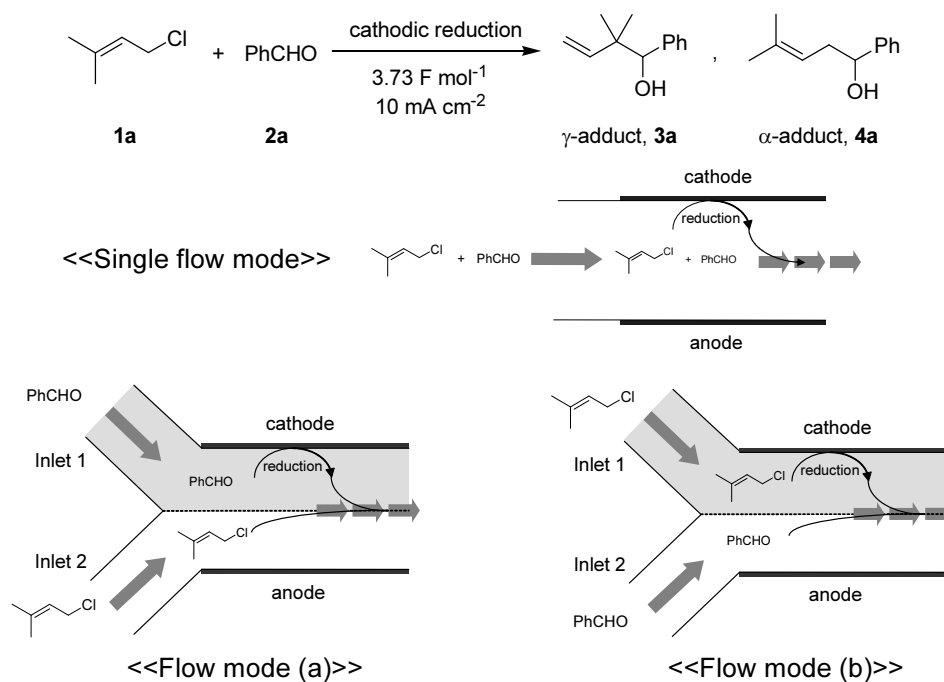
Figure 4-5. Cyclic voltammograms of 50 mM 1-chloro-3-methyl-2-butene (**1a**) / HMPA and 50 mM benzaldehyde (**2a**) / HMPA recorded at (a) Pt, (b) GC, and (c) Ag disk electrodes (3 mm diameter). The scan rate was 100 mV s^{-1} .

4-3-3 Preparative experiments of the cathodic cross-coupling reaction

Subsequently, preparative experiments of the cathodic cross-coupling reaction were carried out using a 1-chloro-3-methyl-2-butene (**1a**) and benzaldehyde (**2a**) substrate combination. Since the reduction potential of **2a** is much lower than that of **1a** at the Pt electrode, α -adduct was obtained as a major product when the reaction was carried out using a conventional batch type reactor with the Pt electrode (Table 4-4, entry 1). Similar results were obtained by using the microreactor with single flow mode (see the figure of Table 4-4) and the Pt and GC electrodes (entry 2 and entry 3). In contrast, as shown in entry 4, the yield of γ -adduct was increased by using the Ag electrode. These experimental results well reflect the results of CVs in Figure 4-4.

Then, in order to improve the γ -adduct selectivity, 1-bromo-3-methyl-2-butene was used instead of **1a** in entry 5 because allylic bromide has lower reduction potential than that of allylic chloride. However, the total yield was significantly decreased though γ -adduct was obtained dominantly. In this case, bromide ion derived cathodically from 1-bromo-3-methyl-2-butene would be oxidized at the anode to give Br^+ species, and then, they were reduced at the cathode to regenerate bromide ion. Thus, a large part of the electricity seemed to be consumed for the redox reaction of Br^-/Br^+ .

As shown in entry 6, the selectivity of α -adduct was improved by using the microreactor with the flow mode (a). The 90% of substrate **1a** was converted in this condition, however, hydrobenzoin, benzyl alcohol and homo-coupling products of **1a** were also detected as by-products. (The oxidation of HMPA was occurred simultaneously in the anode because HMPA has a lower oxidation potential.) Since these homo-coupling side-reaction would be occurred simultaneously in entry 6, the yield was improved by decreasing the concentration of **2a** as shown in entry 7. (The

Table 4-4. Cathodic carbonyl allylation between **1a** and **2a** using the microreactor.^a

Entry	Cathode material	Flow mode	Total yield (%) ^b	
			3a + 4a	Selectivity ^b 3a : 4a
1 ^c	Pt	Batch type reactor	69	29 : 71
2	Pt	Single flow mode	64	17 : 83
3	GC	Single flow mode	54	15 : 85
4	Ag	Single flow mode	63	45 : 55
5 ^d	Ag	Single flow mode	10	>99 : <1
6	Pt	Flow mode (a)	44	9 : 91
7 ^e	Pt	Flow mode (a)	55	8 : 92
8	Pt	Flow mode (b)	58	41 : 59
9	Ag	Flow mode (a)	60	47 : 53
10	Ag	Flow mode (b)	75 (67) ^f	87 : 13

^aExperimental conditions: The concentration of **1a** in HMPA was 500 mM, and that for **2a** was 2 M. *n*-Bu₄NClO₄ was used as a supporting electrolyte in all solutions (200 mM). Flow rates of each solution were 0.01 mL min⁻¹ and the total flow rate was 0.02 mL min⁻¹. All reactions were performed at 0 °C. ^bDetermined by GC analysis. ^cReported in the literature.^[13b] ^d1-bromo-3-methyl-2-butene was used instead of **1a**. ^eThe concentration of **2a** was 1 M. ^fIsolated yield in parenthesis.

current efficiency for **4a** was 27.1% and the productivity was 26.8 mg h⁻¹.) On the other hand, the use of the flow mode (b) significantly increased the γ -adduct selectivity (entry 8). These results indicated that our concept for chemoselective cathodic reduction by using a parallel laminar flow in the microreactor works.

As shown in entry 9, the use of the Ag electrode with flow mode (a) couldn't enhance α -adduct selectivity compared to the result in entry 4. However, the selectivity was reversed and γ -adduct was obtained as a major product when the electrolysis was performed by a combination use of the Ag electrode and flow mode (b) (entry 10, the current efficiency for **3a** was 33.4% and the productivity was 32.9 mg h⁻¹). It should be noted that this was opposite selectivity compared to that obtained in entry 7.

4-3-4 Estimation of diffusion coefficient for 2a and CFD simulations of the liquid-liquid parallel laminar flow in the microreactor

The effect of a liquid-liquid parallel laminar flow mode in the microreactor and the application to the preparative electrolysis were investigated experimentally in the previous sections (section 4-3-1 and 4-3-3). In addition to these experiments, it is important to verify the formation of liquid-liquid parallel laminar flow in the microreactor channel and the substrate diffusion behavior in such a flow mode. Therefore, in this section, the diffusion coefficient for the substrate (benzaldehyde (**2a**)) in HMPA medium was estimated and the spatial distribution of the substrate in the microreactor was investigated by computational fluid dynamics (CFD) simulations.

Estimation of diffusion coefficient by Stokes-Einstein equation and diffusion length by Fick's second law

Firstly, the diffusion coefficient for **2a** in HMPA was estimated from Stokes-Einstein equation:

$$D = \frac{kT}{6\pi r \eta} \quad \text{Equation 4-1}$$

where D is the diffusion coefficient of the species, η is the dynamic viscosity of the medium, k is the Boltzmann constant, T is the absolute temperature, and r is the effective radius of the diffusing species. If the effective radius of the diffusing species modeled as a sphere was set as 0.28 nm (comparable size of organic compound), which value was obtained from the literature,^[20] the diffusion coefficient for **2a** (D_{BA}) was roughly estimated as:

$$D_{BA} = 2.4 \times 10^{-6} \text{ cm}^2 \text{ s}^{-1}$$

by using above equation with:

$$\eta = 3.245 \times 10^{-3} \text{ Pa s}$$

which was obtained from the dynamic viscosity of HMPA in the same literature.

A residence time (t) in the reactor was 18 s corresponding to a total flow rate of 0.02 mL min⁻¹. Therefore, the diffusion length (x) of **2a** was estimated as:

$$x = (Dt)^{1/2} = 66 \text{ } \mu\text{m}$$

by using Fick's second law. As the channel depth is 20 μm , this suggests that the **2a** molecule reaches to the cathode surface in approximately one thirds of the channel length from the anode surface. Thus, the concentration of **2a** on the cathode surface would be diluted compared to that under the single flow mode of Table 4-3.

However, this estimation is fairly rough due to including some approximations and cannot fully support the formation of liquid-liquid parallel laminar flow in the

microreactor channel. Thus, in the next step, CFD simulation of the flow was conducted.

CFD simulations at several orders of diffusion coefficient

Under the experimental conditions used in this study, different simulations were carried out by varying the diffusion coefficient for **2a** (D_{BA}) from 5×10^{-6} to 1×10^{-8} $\text{cm}^2 \text{s}^{-1}$. This range of diffusion coefficient roughly covers from the diffusion of general small organic compounds in the low viscosity solvent to their diffusion in high viscosity medium such as ionic liquids. For example, the diffusion coefficient for ferrocene in acetonitrile ($\eta = 0.345 \times 10^{-4} \text{ Pa s}$ [21]) was estimated as $2.3 \times 10^{-5} \text{ cm}^2 \text{ s}^{-1}$ [22], while the value for methyl viologen in a typical ionic liquid 1-*n*-butyl-3-methylimidazolium hexafluorophosphate ([bmim][PF₆], $\eta = 2.33 \times 10^{-1} \text{ Pa s}$ [23]) was estimated as $1.1 \times 10^{-8} \text{ cm}^2 \text{ s}^{-1}$ [24].

Figures 4-6, 4-8, 4-10 and 4-12 show schematic visualizations of the CFD simulation results for **2a** diffusion in the microreactor channel from inlets to 1.0 mm down stream position, and Figures 4-7, 4-9, 4-11 and 4-13 show corresponding distribution plots for **2a** concentration at the specific positions, respectively. In Figures 4-6 and 4-7, when D_{BA} was set as $5 \times 10^{-6} \text{ cm}^2 \text{ s}^{-1}$, **2a** immediately diffused to the cathode surface and the input streams were completely mixed each other even at 1 mm down stream position. This tendency was not significantly improved when D_{BA} was set as $1 \times 10^{-6} \text{ cm}^2 \text{ s}^{-1}$, as shown in Figures 4-8 and 4-9. Thus, these results indicate that the D_{BA} value obtained by Stokes-Einstein equation in the previous section ($= 2.4 \times 10^{-6} \text{ cm}^2 \text{ s}^{-1}$) cannot support the results of CV measurements in Figure 4-4.

In contrast, when D_{BA} was set as $1 \times 10^{-7} \text{ cm}^2 \text{ s}^{-1}$, the concentration gradient clearly remained even at 1 cm down stream position, as shown in Figure 4-10 and 4-11. In this

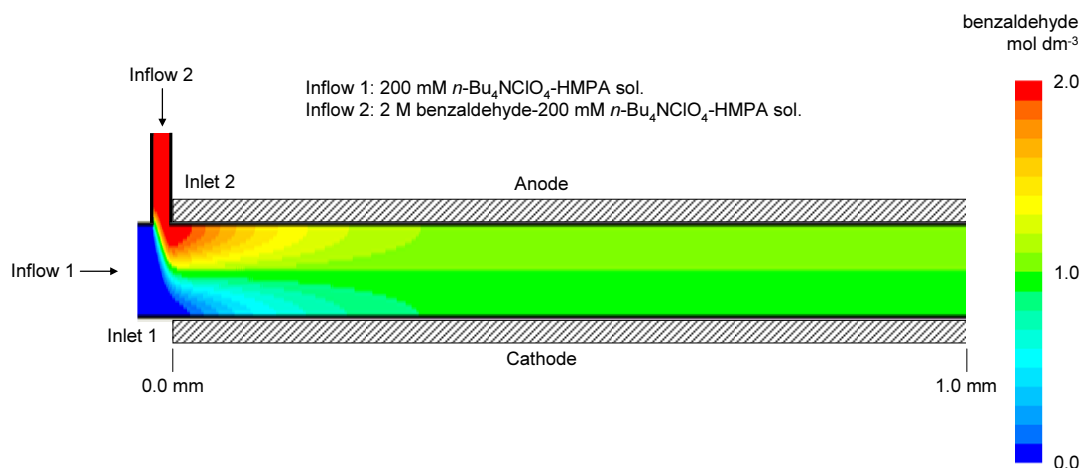


Figure 4-6. Schematic visualization of the CFD simulation result for benzaldehyde diffusion in the microreactor channel from inlets to 1.0 mm down stream position. D_{BA} was set as $5 \times 10^{-6} \text{ cm}^2 \text{ s}^{-1}$. Each flow rate was fixed at 0.01 mL min^{-1} . The electrode distance was set as $20 \text{ }\mu\text{m}$ (The vertical scale is different from the horizontal scale. Both two inlets have $20 \text{ }\mu\text{m}$ width.).

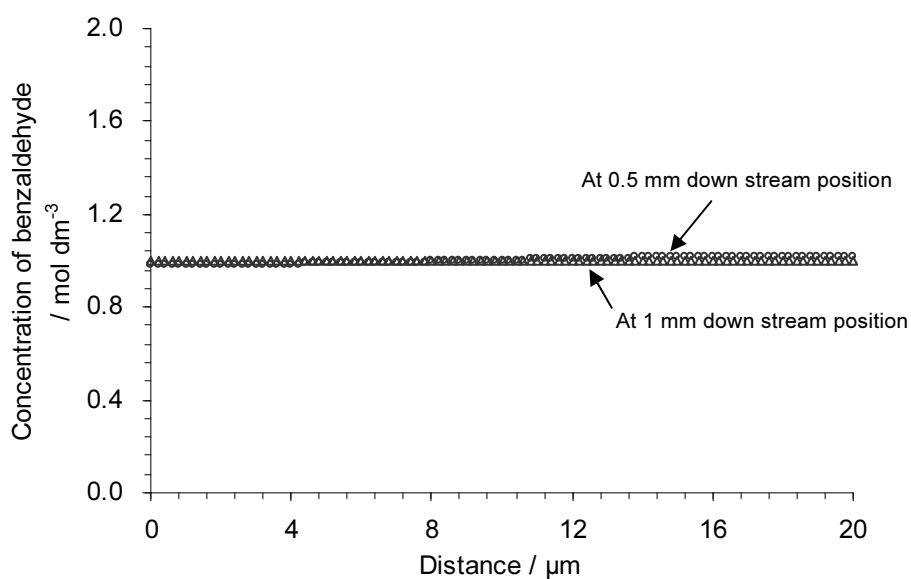


Figure 4-7. Distribution plots for **2a** concentration at specific positions of the microreactor channel corresponding to the CFD simulation of Figure 4-6. D_{BA} was set as $5 \times 10^{-6} \text{ cm}^2 \text{ s}^{-1}$. X axis shows the distance from the cathode surface.

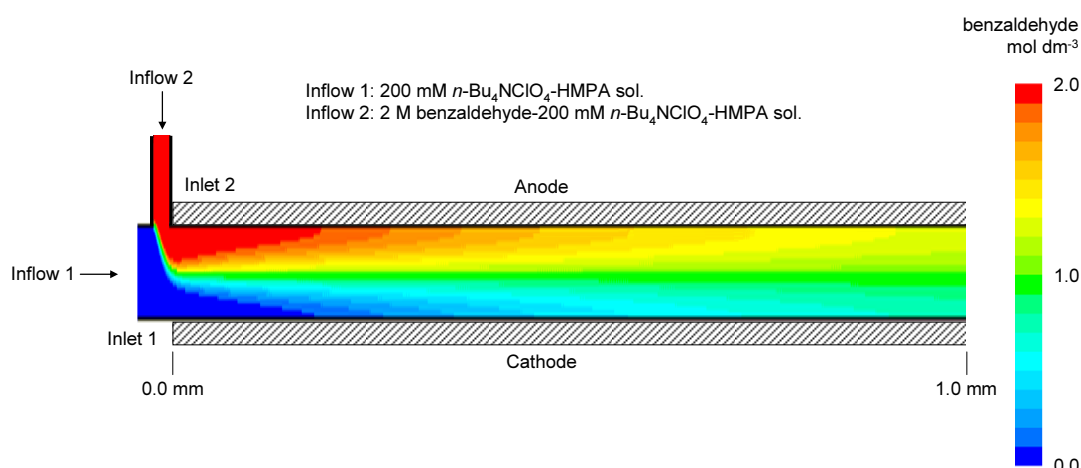


Figure 4-8. Schematic visualization of the CFD simulation result for benzaldehyde diffusion in the microreactor channel from inlets to 1.0 mm down stream position. D_{BA} was set as $1 \times 10^{-6} \text{ cm}^2 \text{ s}^{-1}$. Each flow rate was fixed at 0.01 mL min^{-1} . The electrode distance was set as $20 \mu\text{m}$ (The vertical scale is different from the horizontal scale. Both two inlets have $20 \mu\text{m}$ width.).

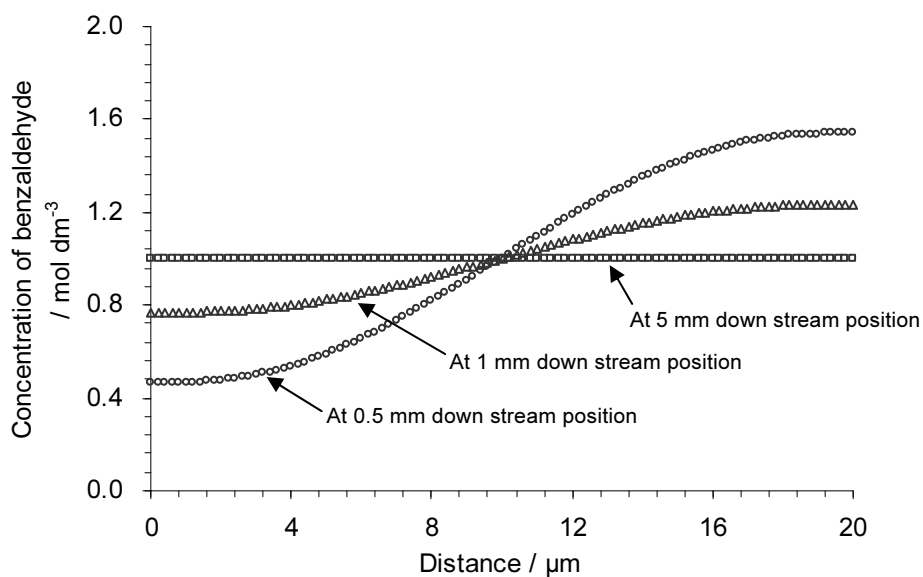


Figure 4-9. Distribution plots for **2a** concentration at specific positions of the microreactor channel corresponding to the CFD simulation of Figure 4-8. D_{BA} was set as $1 \times 10^{-6} \text{ cm}^2 \text{ s}^{-1}$. X axis shows the distance from the cathode surface.

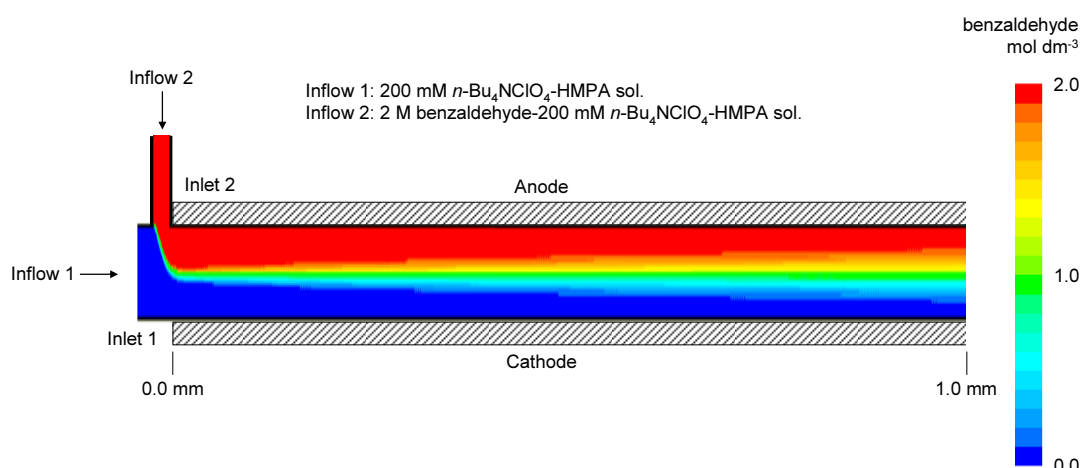


Figure 4-10. Schematic visualization of the CFD simulation result for benzaldehyde diffusion in the microreactor channel from inlets to 1.0 mm down stream position. D_{BA} was set as $1 \times 10^{-7} \text{ cm}^2 \text{ s}^{-1}$. Each flow rate was fixed at 0.01 mL min^{-1} . The electrode distance was set as $20 \mu\text{m}$ (The vertical scale is different from the horizontal scale. Both two inlets have $20 \mu\text{m}$ width.).

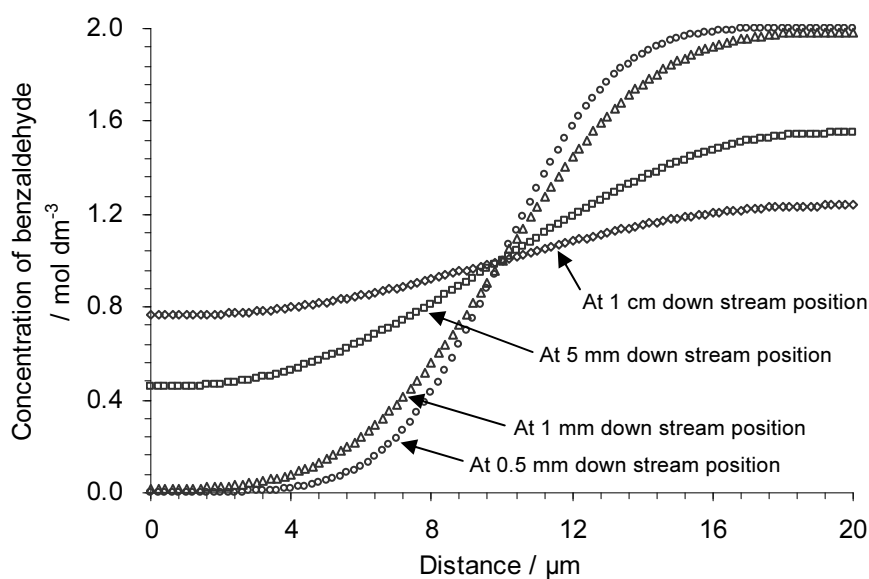


Figure 4-11. Distribution plots for **2a** concentration at specific positions of the microreactor channel corresponding to the CFD simulation of Figure 4-10. D_{BA} was set as $1 \times 10^{-7} \text{ cm}^2 \text{ s}^{-1}$. X axis shows the distance from the cathode surface.

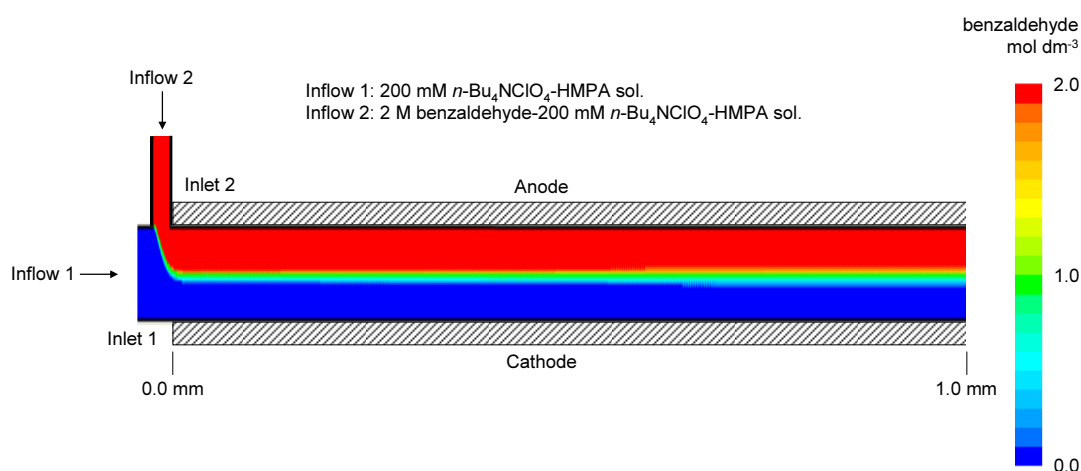


Figure 4-12. Schematic visualization of the CFD simulation result for benzaldehyde diffusion in the microreactor channel from inlets to 1.0 mm down stream position. D_{BA} was set as $1 \times 10^{-8} \text{ cm}^2 \text{ s}^{-1}$. Each flow rate was fixed at 0.01 mL min^{-1} . The electrode distance was set as $20 \text{ }\mu\text{m}$ (The vertical scale is different from the horizontal scale. Both two inlets have $20 \text{ }\mu\text{m}$ width.).

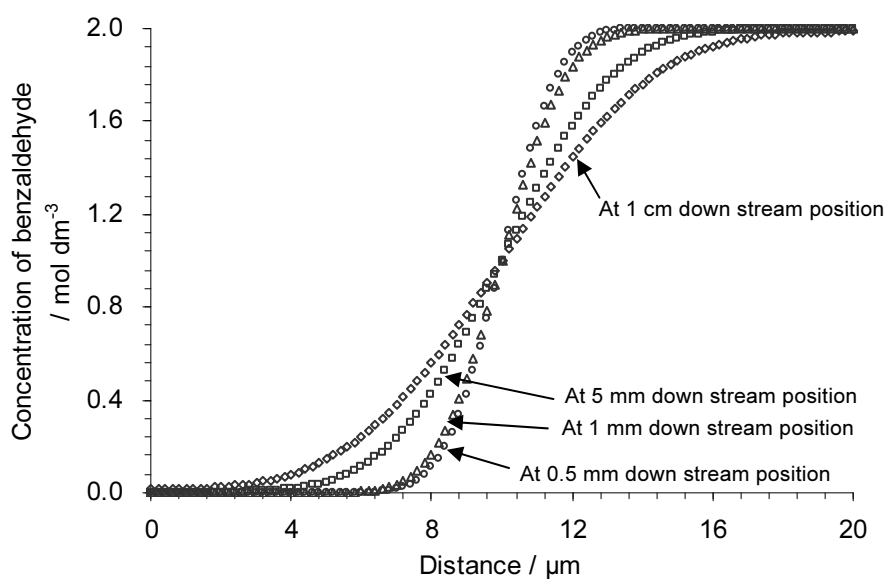


Figure 4-13. Distribution plots for **2a** concentration at specific positions of the microreactor channel corresponding to the CFD simulation of Figure 4-12. D_{BA} was set as $1 \times 10^{-8} \text{ cm}^2 \text{ s}^{-1}$. X axis shows the distance from the cathode surface.

case, the concentration of **2a** on the cathode surface was diluted especially in the former part of the cell. Furthermore, the concentration distribution was drastically changed in the order of D_{BA} value lower than $1 \times 10^{-8} \text{ cm}^2 \text{ s}^{-1}$. In this order of D_{BA} value, **2a** hardly diffuse to the cathode surface and the concentration of **2a** on the cathode surface is extremely low (Figures 4-12 and 4-13). The resulting **2a** concentration profiles are qualitatively in agreement with the experimental results obtained in Figure 4-4. Therefore, from these results, it can be stated that the real D_{BA} value in the $n\text{-Bu}_4\text{NClO}_4\text{-HMPA}$ medium would be found in the range from 1×10^{-8} to $1 \times 10^{-7} \text{ cm}^2 \text{ s}^{-1}$. It is also noteworthy that the results of this CFD simulations clearly support the formation of concentration gradient of substrate in the microreactor channel over a specific length.

Estimation of diffusion coefficient by Wilke-Chang equation

In order to estimate more precise value of diffusion coefficient for **2a**, Wilke-Chang equation was then employed. Wilke-Chang equation, which is a modified form of Stokes-Einstein equation obtained experimentally, is probably the most widely used to estimate diffusion coefficient in liquid phase systems.^[25] The equation is:

$$D_{BA} = 7.4 \times 10^{-8} \frac{(\phi M_{\text{sol}})^{1/2} T}{\eta_{\text{sol}} V_{BA}^{0.6}} \quad \text{Equation 4-2}$$

where ϕ is the association factor of solvent, M_{sol} is the molecular weight of solvent, T is the absolute temperature, η_{sol} is the viscosity of solvent, and V_{BA} is the molal volume of **2a** at its normal boiling temperature. M_{sol} of HMPA is $179.20 \text{ g mol}^{-1}$. T was set as 273.15 K ($0 \text{ }^\circ\text{C}$) in this system. ϕ was set as 0.7 which the value is derived from the association factor of aromatic hydrocarbon.

In order to obtain η_{sol} in Equation 4-2, the rheology of $n\text{-Bu}_4\text{NClO}_4\text{-HMPA}$ medium

was measured experimentally. Figure 4-14 shows the relationships between shear rate ($\dot{\gamma}$) and shear stress (τ) of three samples (sample A: 200 mM *n*-Bu₄NCIO₄-HMPA sol., sample B: 1 M **2a**-200 mM *n*-Bu₄NCIO₄-HMPA sol., sample C: 2 M **2a**-200 mM *n*-Bu₄NCIO₄-HMPA sol.) at 0 °C. Linear relationships were observed in each sample, suggesting that these mediums are Newtonian fluids. Thus, the viscosity (μ) of these samples was estimated by following equation:

$$\tau = \mu \cdot \dot{\gamma} \quad \text{Equation 4-3}$$

and determined as 1.27×10^{-2} , 1.13×10^{-2} and 1.11×10^{-2} Pa s for samples A, B and C, respectively. These results suggest that the concentration of **2a** slightly affects their viscosity. The viscosity of sample A (1.27×10^{-2} Pa s) was employed as η_{sol} in Equation 4-2.

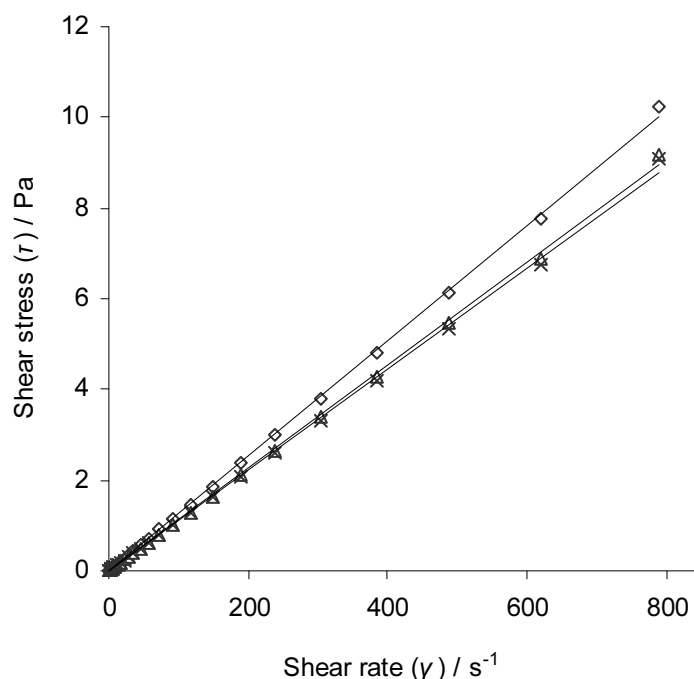


Figure 4-14. The relationships between shear rate ($\dot{\gamma}$) and shear stress (τ) of *n*-Bu₄NCIO₄-HMPA mediums recorded by a rheometer at 0 °C. Rhombic plots: sample A, 200 mM *n*-Bu₄NCIO₄-HMPA sol., $\tau / \dot{\gamma} = 1.27 \times 10^{-2}$ Pa s. Triangle plots: sample B, 1 M **2a**-200 mM *n*-Bu₄NCIO₄-HMPA sol., $\tau / \dot{\gamma} = 1.13 \times 10^{-2}$ Pa s. X shape plots: sample C, 2 M **2a**-200 mM *n*-Bu₄NCIO₄-HMPA sol., $\tau / \dot{\gamma} = 1.11 \times 10^{-2}$ Pa s. Plots are average values of three times measurements.

The molal volume of **2a** at normal boiling point (V_{BA}) was estimated by Le Bas method.^[26] The molecular formula of **2a** is C_7H_6O , and additive volumes of carbon atom, hydrogen atom, oxygen atom, and ring structure are 14.8, 3.7, 7.4, -15.0 $cm^3 g^{-1} mol^{-1}$, respectively. Therefore, the V_{BA} value was determined as:

$$V_{BA} = 7 \times 14.8 + 6 \times 3.7 + 7.4 - 15.0 = 118.2 \text{ cm}^3 \text{ g}^{-1} \text{ mol}^{-1}$$

Consequently, by using Equation 4-2 with these values, the diffusion coefficient for **2a** was estimated as:

$$D_{BA} = 1.02 \times 10^{-6} \text{ cm}^2 \text{ s}^{-1}$$

Although the estimation by Wilke-Chang equation gave slightly lower value of D_{BA} compared to that estimated by Stokes-Einstein equation, this value is still far different from the value expected by CV results and CFD simulations. This may be attributed to the following facts: i) Wilke-Chang equation is supposed to estimate at very low concentration of solute condition, not suited for extremely high concentration condition like 2 M. ii) Wilke-Chang equation would not be applied for the estimation in high viscosity medium like $1.27 \times 10^{-2} \text{ Pa s}$. iii) The association factor of HMPA (ϕ) would be significantly different from the real value. From these results, it can be stated that it is rather difficult to estimate the precise D_{BA} value in the $n\text{-Bu}_4\text{NClO}_4\text{-HMPA}$ medium by using prediction equations.

Experimental measurement of diffusion coefficient by potential step chronoamperometry and steady-state cyclic voltammetry

In the next step, the diffusion coefficient for **2a** (D_{BA}) was measured experimentally by potential step chronoamperometry and steady-state cyclic voltammetry. Although there are some methods available for measuring molecular diffusion coefficient in a solution such as optical scattering^[27] and NMR spectrometry^[28], the electrochemical

measurements have some advantages which they can be carried out by using common apparatus with short experimental time. This method needs fast electron transfer between an electrode and target molecules, and the use of adequate amount of supporting electrolyte is inevitable.

Initially, to determine D_{BA} value and the number of electrons (n) for the **2a** reduction, the potential step chronoamperometry was performed using 10 mM **2a**/0.2 M *n*-Bu₄NClO₄-HMPA solution with a sample time of 0.001 s recorded at the Pt disk electrode (3 mm diameter). The sample was pre-treated by holding the potential at a point corresponding to zero faradaic current (0.00 V vs. SCE) for 2 s, after which the potential was stepped to a potential higher than the **2a** reduction peak potential (-2.6 V vs. SCE) and the current measured for 10 s at 0 °C. The time-dependent current response obtained on the first step was showed in Figure 4-15 and corresponding Cottrell plot was showed in Figure 4-16 (The Cottrell plot was corrected by subtraction of the background current.).

The current was almost linear with the reciprocal of the square root of time from 2.23 to 0.31 s^{-1/2}. The relationship between D_{BA} and n was then obtained by fitting to the following Cottrell equation:

$$I = \frac{nFAD_{BA}c}{(\pi D_{BA}t)^{1/2}} = 9.82 \times 10^{-5} t^{-1/2} \quad \text{Equation 4-4}$$

where, I , F , A and c are the current, the Faraday constant, the geometric surface area of the working electrode, and the concentration of **2a**, respectively.

Next, in order to determine D_{BA} and n values, another relationship between D_{BA} and n was estimated by steady-state cyclic voltammetry using a Pt micro disk electrode (100 μm diameter) with a slow scan rate. Figure 4-17 shows the CV for the reduction of 10 mM **2a** in 0.2 M *n*-Bu₄NClO₄-HMPA solution recorded at 0 °C, and the

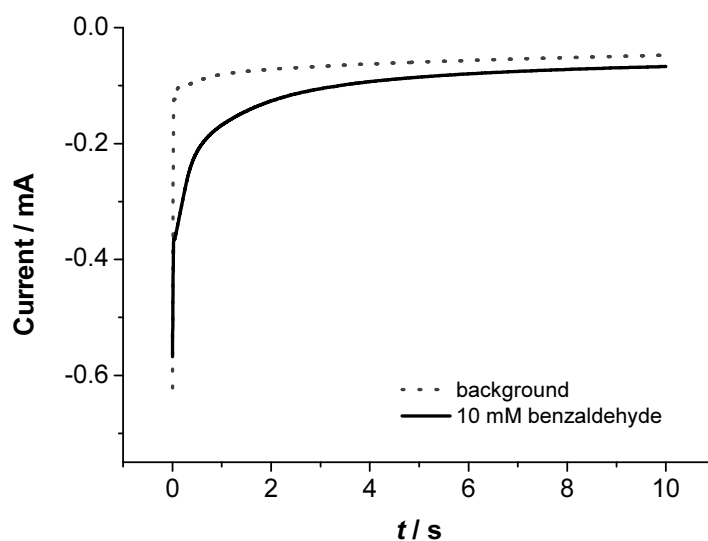


Figure 4-15. Potential step chronoamperogram for the reduction of 10 mM benzaldehyde in HMPA containing 0.2 M $n\text{-Bu}_4\text{NClO}_4$ recorded at the Pt disk electrode at 0 °C. The potential was stepped from 0.0 to -2.6 V vs. SCE.

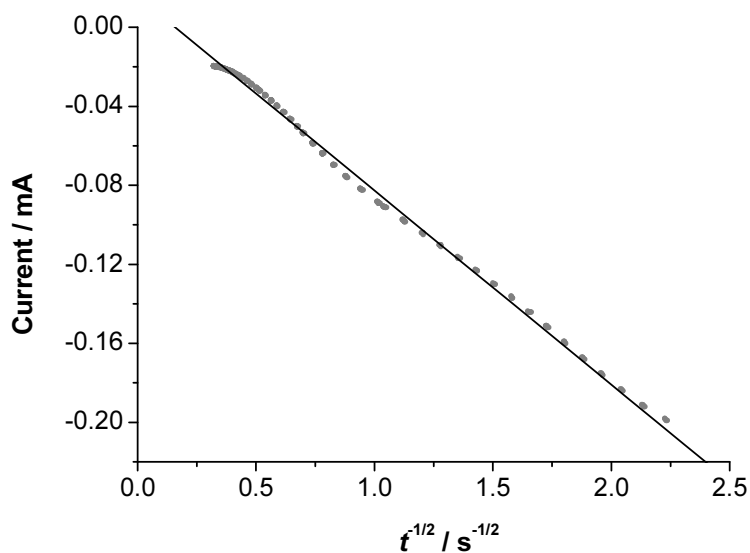


Figure 4-16. Cottrell plot (dot line) of current vs. $t^{1/2}$ corresponding to the chronoamperogram of Figure 4-15. The plot was corrected by subtraction of the background current. Fitting line is also given as a solid line which the slope is $-9.82 \times 10^{-5} \text{ A s}^{1/2}$.

measured diffusion limiting current was obtained as 7.63×10^{-8} A (This limiting current was corrected by subtraction of the background current.). Thus, the relationship between D_{BA} and n was obtained by fitting to the following equation:

$$I_{\text{lim}} = 4nFcD_{\text{BA}}a = 7.63 \times 10^{-8} \text{ A} \quad \text{Equation 4-5}$$

where a is the radius of the micro disk electrode.

Then, from the simultaneous equations of Equations 4-4 and 4-5, D_{BA} and n were determined as $2.40 \times 10^{-6} \text{ cm}^2 \text{ s}^{-1}$ and 1.65, respectively. This D value is close to that obtained by hydrodynamic estimation in the previous sections, suggesting that such estimation can be successfully applied under the low **2a** concentration condition. Nevertheless, the real D_{BA} value under high concentration condition (2 M **2a**) is still not confirmed.

Thus, subsequently, additional steady-state cyclic voltammetry was carried out for the reduction of 2 M **2a** in 0.2 M $n\text{-Bu}_4\text{NClO}_4\text{-HMPA}$ solution at 0 °C. As shown in

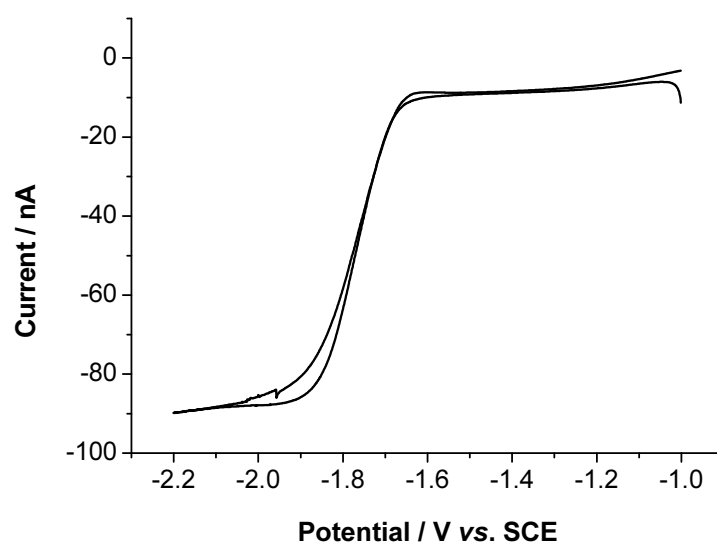


Figure 4-17. Steady-state cyclic voltammogram for the reduction of 10 mM **2a** at the Pt micro disk electrode (100 μm diameter) in 0.2 M $n\text{-Bu}_4\text{NClO}_4\text{-HMPA}$ solution at 0 °C. The scan rate was 10 mV s^{-1} .

Figure 4-18, the diffusion limiting current was obtained as 2.10×10^{-8} A. Then, by using n value of 1.65 obtained in the above and the following equation:

$$I_{\text{lim}} = 4 \times 1.65 \times FcD_{\text{BA}}a = 2.10 \times 10^{-8} \text{ A} \quad \text{Equation 4-6}$$

the real D_{BA} value under high concentration condition (2 M **2a**) was determined as:

$$D_{\text{BA}} = 1.32 \times 10^{-7} \text{ cm}^2 \text{ s}^{-1}$$

This D_{BA} value is approximately one order of magnitude lower than that under low concentration condition, indicating that the concentration of **2a** greatly affects their D_{BA} values and the diffusion manner of liquid-liquid parallel laminar flow in the microreactor channel.

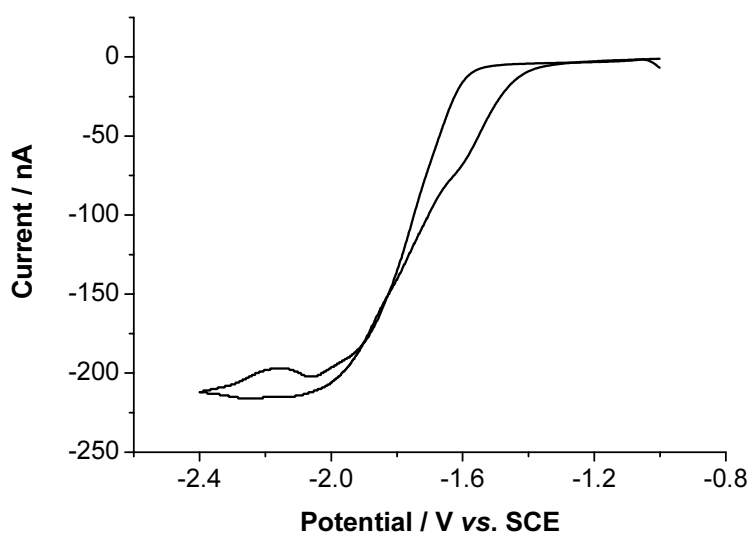


Figure 4-18. Steady-state cyclic voltammogram for the reduction of 2 M **2a** at the Pt micro disk electrode (25 μm diameter) in 0.2 M $n\text{-Bu}_4\text{NClO}_4\text{-HMPA}$ solution at 0 $^\circ\text{C}$. The scan rate was 10 mV s^{-1} .

Figures 4-19 and 4-20 show computational simulation results of liquid-liquid parallel laminar flow in the microreactor channel using the D_{BA} value obtained at Equation 4-6. Although the concentration gradient for **2a** still remains even at 1 cm

down stream position from inlets, this result slightly reflects the results of CV measurements in Figure 4-4. As stated in the previous section, the CFD simulations using several orders of diffusion coefficient suggest that the D_{BA} value would be found in the range from 1×10^{-8} to $1 \times 10^{-7} \text{ cm}^2 \text{ s}^{-1}$. However, the electrochemically measured D_{BA} value was a little larger than such predicted values. This minor difference between the predicted D_{BA} value and measured D_{BA} value would indicate that some unknown factors may affect the **2a** diffusion in the microreactor channel and reduce the D_{BA} value. Actually, a decrease of molecular diffusion in micro-nano channels have been observed in the literature.^[29] This phenomenon can be attributed to the increased number of interactions between medium and the channel walls, which can no longer be neglected when the channel size reaches a critical value. Therefore, it might be possible that such interactions reduce the D_{BA} value and the clear concentration gradient of **2a** is kept in the microreactor channel. It might be necessary for more accurate simulation to combine a new diffusion model, representing interaction between substrate and wall, with macro-scale models, which were based on Navier-Stokes equations and species transport equations.

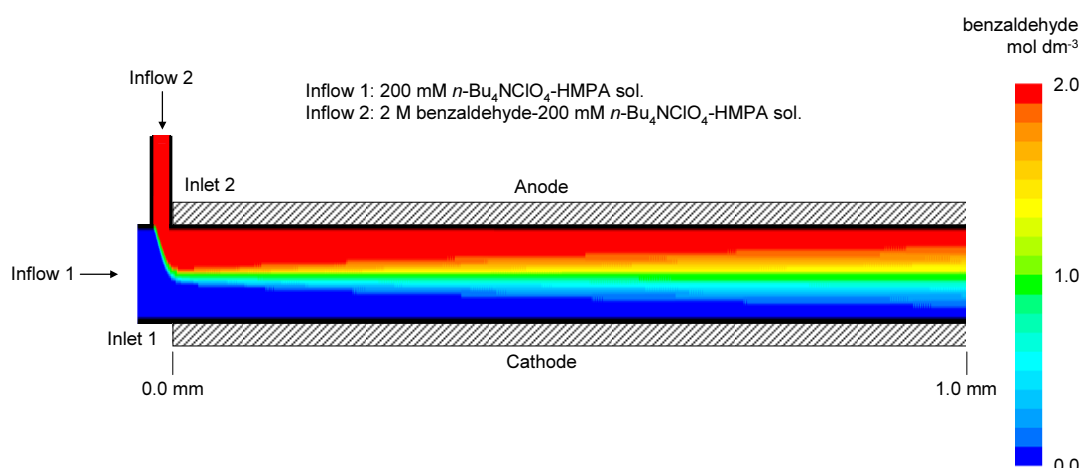


Figure 4-19. Schematic visualization of the CFD simulation result for benzaldehyde diffusion in the microreactor channel from inlets to 1.0 mm down stream position. D_{BA} was set as $1.32 \times 10^{-7} \text{ cm}^2 \text{ s}^{-1}$. Each flow rate was fixed at 0.01 mL min^{-1} . The electrode distance was set as $20 \text{ }\mu\text{m}$ (The vertical scale is different from the horizontal scale. Both two inlets have $20 \text{ }\mu\text{m}$ width.).

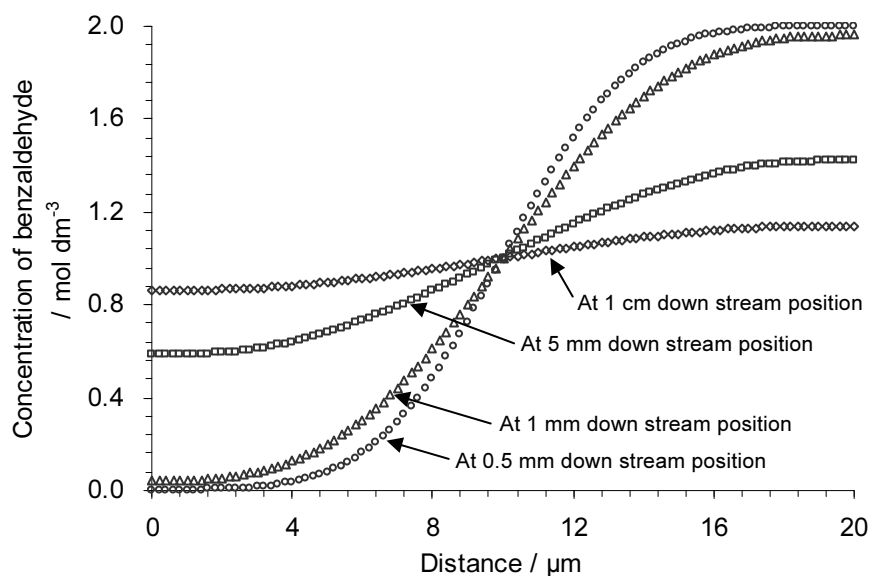


Figure 4-20. Distribution plots for **2a** concentration at specific positions of the microreactor channel corresponding to the CFD simulation of Figure 4-19. D_{BA} was set as $1.32 \times 10^{-7} \text{ cm}^2 \text{ s}^{-1}$. X axis shows the distance from the cathode surface.

Influence of the flow rate difference between input streams on the substrate diffusion

Finally, the influence of the flow rate difference between input streams on the **2a** diffusion was investigated by CFD simulation. In Figures 4-21 and 4-22, the flow rate of inflow 2 was set twice as fast as the rate of inflow 1. The **2a** diffusion was enhanced in this condition, and the concentration of **2a** on the cathode surface increased faster than that calculated in Figures 4-19 and 4-20. In contrast to this, the flow rate of inflow 1 was set twice as fast as the rate of inflow 2, as shown in Figures 4-23 and 4-24. The **2a** diffusion was fairly decreased and the concentration change of **2a** on the cathode surface was depressed. These simulations apparently show that the substrate diffusion at the liquid-liquid parallel laminar flow in the microreactor channel is significantly affected not only by diffusion coefficient but also by the flow rate difference between input streams.

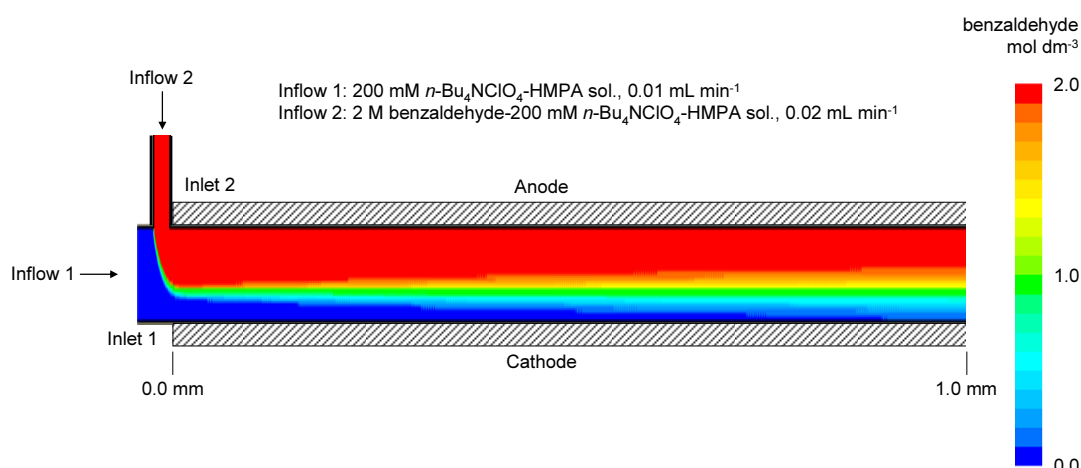


Figure 4-21. Schematic visualization of the CFD simulation result for benzaldehyde diffusion in the microreactor channel from inlets to 1.0 mm down stream position. D_{BA} was set as $1.32 \times 10^{-7} \text{ cm}^2 \text{ s}^{-1}$. The flow rate of Inflow 1 was fixed at 0.01 mL min^{-1} , and that of Inflow 2 was fixed at 0.02 mL min^{-1} . The electrode distance was set as $20 \mu\text{m}$ (The vertical scale is different from the horizontal scale. Both two inlets have $20 \mu\text{m}$ width.).

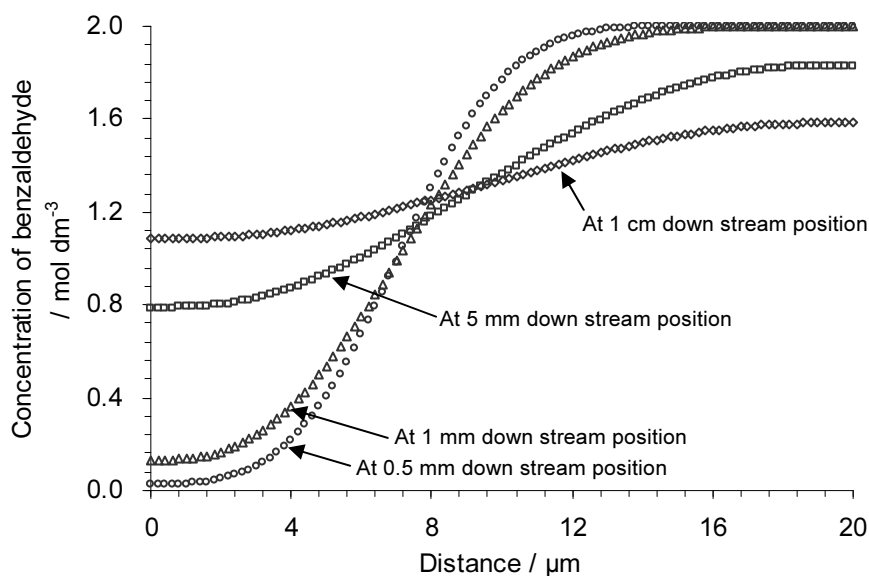


Figure 4-22. Distribution plots for **2a** concentration at specific positions of the microreactor channel corresponding to the CFD simulation of Figure 4-21. D_{BA} was set as $1.32 \times 10^{-7} \text{ cm}^2 \text{ s}^{-1}$. X axis shows the distance from the cathode surface.

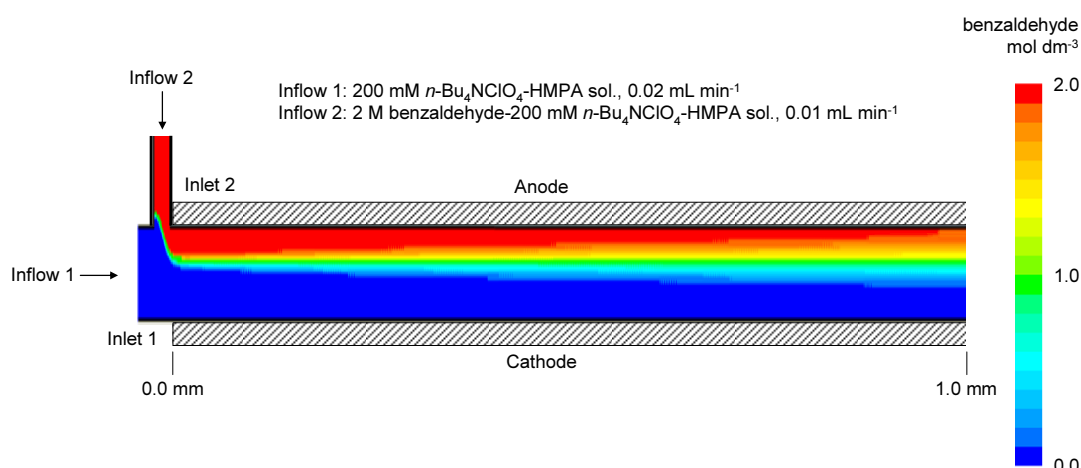


Figure 4-23. Schematic visualization of the CFD simulation result for benzaldehyde diffusion in the microreactor channel from inlets to 1.0 mm down stream position. D_{BA} was set as $1.32 \times 10^{-7} \text{ cm}^2 \text{ s}^{-1}$. The flow rate of Inflow 1 was fixed at 0.02 mL min^{-1} , and that of Inflow 2 was fixed at 0.01 mL min^{-1} . The electrode distance was set as $20 \mu\text{m}$ (The vertical scale is different from the horizontal scale for visualization. Both two inlets have $20 \mu\text{m}$ width.).

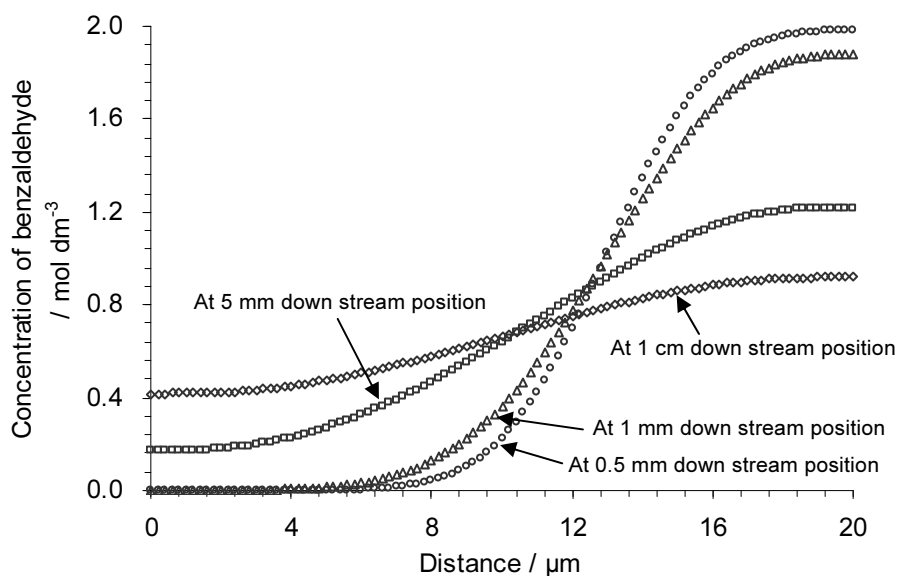


Figure 4-24. Distribution plots for **2a** concentration at specific positions of the microreactor channel corresponding to the CFD simulation of Figure 4-23. D_{BA} was set as $1.32 \times 10^{-7} \text{ cm}^2 \text{ s}^{-1}$. X axis shows the distance from the cathode surface.

4-3-5 Necessity of the liquid-liquid parallel laminar flow mode for the product selectivity control

Next, the necessity of the liquid-liquid parallel laminar flow mode was investigated experimentally. In this cross-coupling reaction, the key step for product selectivity determination is the initial cathodic reduction. If the cathodically generated intermediate can be transferred to the outlet of the electrochemical microreactor without its decomposition or its conversion to undesired byproducts, a flow mode (Figure 4-25(b)), in which an electrolytic solution containing another substrate is introduced at the outlet of the electrochemical microreactor, would be also useful for the effective control of product selectivity. In practice, however, the desired cross-coupling reaction was not proceeded at all. This is ascribed to the fact that the stability of the reactive intermediate generated at the cathode was insufficient to transfer it to the outlet of the reactor without decomposition or side-reactions. In contrast, in the liquid-liquid parallel laminar flow mode, the reactive intermediate can be effectively trapped by another substrate before they are lost (Figure 4-25(a)). Hence, it can be stated that the liquid-liquid parallel laminar flow mode is essentially required for an efficient product selectivity control in the cross-coupling reaction.

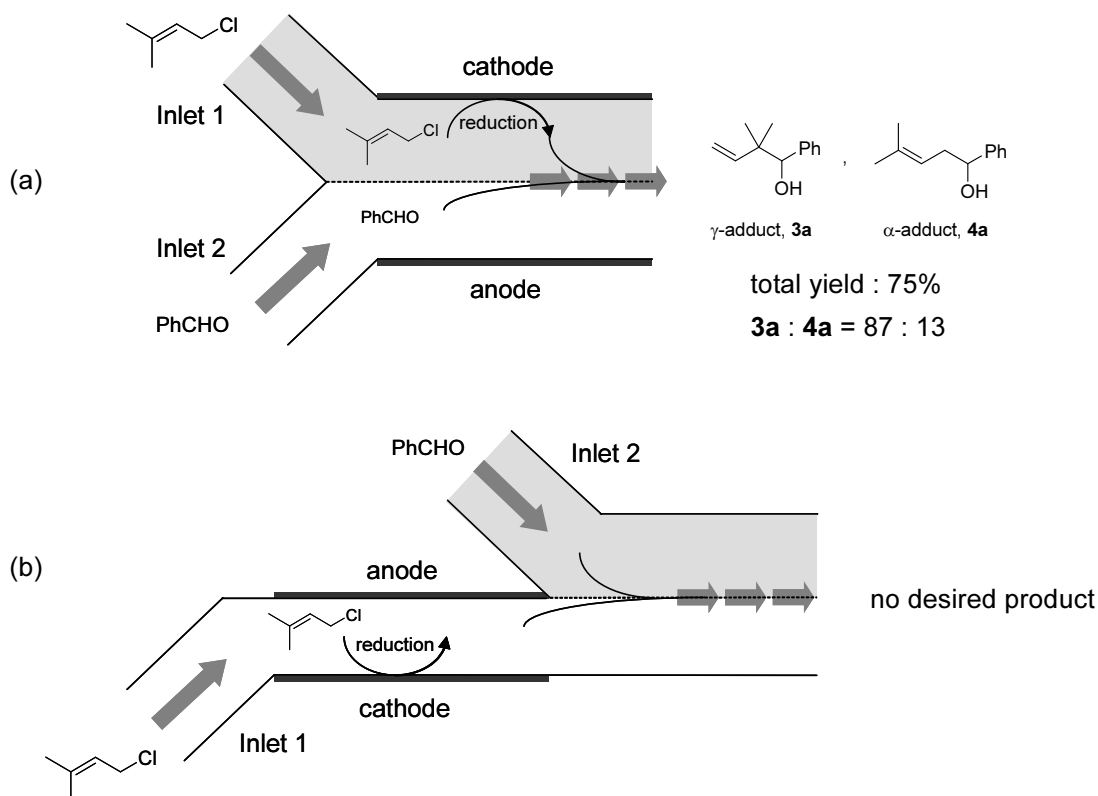


Figure 4-25. Schematic illustration of two kinds of flow modes for the microreactor and their application to the cathodic cross-coupling reaction of 1-chloro-3-methyl-2-butene (**1a**) with benzaldehyde (**2a**) at the Ag cathode. (a) Liquid-liquid parallel laminar flow mode in an electric field. (b) Single laminar flow mode in an electric field. The flow rates of two electrolytic solutions containing **1a** (500 mM) and **2a** (2 M), respectively, were fixed at 0.01 mL min^{-1} each. Current density was 10 mA cm^{-2} . All reactions were performed at 0°C .

4-3-6 Versatility of this system

Finally, the versatility of this microreactor system was investigated by cathodic cross-coupling reactions between **1a** and various aldehydes (**2b-e**). Before the electrolyses using the microreactor, reduction potentials of aldehydes were investigated by cyclic voltammetry recorded at the Pt disk electrode. As results, the reduction peak potentials range from *ca.* -1.76 V to -2.51 V vs. SCE (Figure 4-26). Note that the reduction peak of **1a** was observed at *ca.* -3.02 V at the Pt electrode (Figure 4-5(a)).

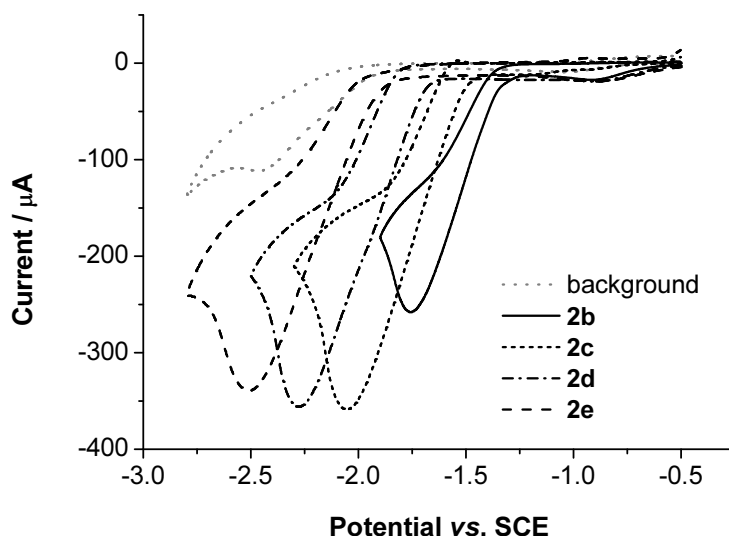
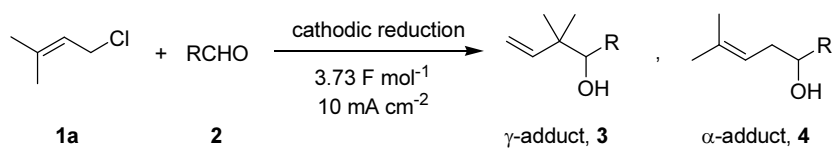


Figure 4-26. Cyclic voltammograms of 50 mM aldehydes (4-(trifluoromethyl)benzaldehyde (**2b**), 2-naphthaldehyde (**2c**), *p*-tolualdehyde (**2d**) and 3-furaldehyde (**2e**)) in HMPA solution containing 200 mM *n*-Bu₄NClO₄ recorded at the Pt disk electrode (3 mm diameter). Scan rate was 100 mV s⁻¹.

Then, cathodic cross-coupling reactions between **1a** and aldehydes (**2b-e**) were carried out using the microreactor with flow mode (a) or flow mode (b) of Figure 4-1. As results, the use of the Pt cathode with flow mode (a) provided the corresponding α -adducts as major products in reasonable yields (Table 4-5, entries 1, 3, 5, and 7). In this flow mode, selectivities were not affected by the reduction potentials of aldehydes. This may be ascribed to the fact that the reduction potentials of aldehydes were lower than that of **1a** enough to reduce aldehydes chemoselectively in any case. On the other hand, the use of the Ag cathode with flow mode (b) afforded the corresponding γ -adducts as major products in good to moderate yields (entries 2, 4, 6, and 8). In this case, selectivities were slightly depended on the reduction potentials of aldehydes. Since the reduction peak of **1a** at the Ag cathode was observed at *ca.* -2.23 V (Figure 4-5(c)), **1a** would be more readily reduced than **2d** or **2e**. Therefore, the reduction

priority would change from aldehydes (**2d** and **2e**) to **1a** in these cases, and consequently, γ -adduct selectivity got better.

From these experiments, it can be concluded that this microreactor system enables chemoselective cathodic reduction and intentional product selectivity control (regioselectivity control) of the cathodic cross-coupling reaction between allylic chloride and a wide range of aldehydes.

Table 4-5. Cathodic carbonyl allylation of various aldehydes using the microreactor.^a

Entry	RCHO ($E_{p,\text{red}}^b$)	Cathode material, flow mode ^c	Products 3, 4	Total yield (%) ^d 3 + 4	Selectivity ^d 3 : 4
1		Pt, flow mode (a)		63	15 : 85
2	2b (-1.76 V)	Ag, flow mode (b)	3b 4b	65	60 : 40
3		Pt, flow mode (a)		59	12 : 88
4	2c (-2.05 V)	Ag, flow mode (b)	3c 4c	54	67 : 33
5		Pt, flow mode (a)		67	10 : 90
6	2d (-2.28 V)	Ag, flow mode (b)	3d 4d	68	74 : 26
7		Pt, flow mode (a)		52	19 : 81
8	2e (-2.51 V)	Ag, flow mode (b)	3e 4e	49	86 : 14

^aExperimental conditions are described in footnote a of Table 4-4. ^bReduction peak potentials were recorded at the Pt disk electrode (Figure 4-26). ^cFlow mode (a) is the flow mode for the selective reduction of aldehyde and flow mode (b) is the flow mode for the selective reduction of **1a**, as shown in Figure 4-1. ^dDetermined by ¹H-NMR analysis using nitromethane as an internal standard.

4-4 Conclusion

Synthetic chemists have always shown a great interest in the control of product selectivity. While many traditional ways for the control of product selectivity were based on chemical factors, recent studies have shown novel types of strategies based on physical factors.

In this chapter, a new strategy for a product selectivity control based on physical factor is described. Intentional chemoselective reduction in a cathodic cross-coupling reaction was successfully carried out by using a liquid-liquid parallel laminar flow mode in a microreactor. The combined use of suitable flow mode and corresponding cathode material enables control of the product selectivity (regioselectivity) in this reaction (γ -adduct/ α -adduct = 8/92 in the case of flow mode (a) with Pt cathode, γ -adduct/ α -adduct = 87/13 in the case of flow mode (b) with Ag cathode in the reaction of 1-chloro-3-methyl-2-butene with benzaldehyde). The necessity of the liquid-liquid parallel laminar flow mode was supported by flow mode experiments. In addition, the formation of liquid-liquid parallel laminar flow in the microreactor was supported by the estimation of substrate diffusion coefficient and CFD simulations. The diffusion coefficient for benzaldehyde in 200 mM *n*-Bu₄NClO₄-HMPA medium was determined as $1.32 \times 10^{-7} \text{ cm}^2 \text{ s}^{-1}$ experimentally, and the flow simulation using this value revealed the formation and stability of the concentration gradient of substrate in the microreactor channel over a specific channel length although the simulation was not completely reflected the results of CV experiments.

This strategy serves as one of the solution for product selectivity control without adding any reactants or catalysts in a electrochemical cross-coupling reaction. It is also worth noting that the present observations open a new aspect of product selectivity control using microreactor systems.

4-5 References

- [1] R. Noyori, T. Ikeda, T. Ohkuma, M. Widhalm, M. Kitamura, H. Takaya, S. Akutagawa, N. Sayo, T. Saito, T. Taketomi, H. Kumabayashi, *J. Am. Chem. Soc.* **1989**, *111*, 9134.
- [2] M. Yoshioka, Y. Sakuma, M. Saito, *J. Org. Chem.* **1999**, *64*, 9247.
- [3] a) K. Hayakawa, M. Yodo, S. Ohsuki, K. Kanematsu, *J. Am. Chem. Soc.* **1984**, *106*, 6735; b) A. Balog, D.P. Curran, *J. Org. Chem.* **1995**, *60*, 337; c) B. Saha, T. Uchida, T. Katsuki, *Tetrahedron: Asymmetry* **2003**, *14*, 823; d) H. Qian, R.A. Widenhoefer, *J. Am. Chem. Soc.* **2003**, *125*, 2056.
- [4] a) K. Matsuda, M. Atobe, T. Nonaka, *Chem. Lett.* **1994**, *9*, 1619; b) M. Atobe, T. Nonaka, *Chem. Lett.* **1995**, *8*, 669; c) M. Atobe, K. Matsuda, T. Nonaka, *Electroanalysis* **1996**, *8*, 784; d) M. Atobe, T. Nonaka, *J. Electroanal. Chem.* **1997**, *425*, 161.
- [5] M. Iannelli, V. Alupei, H. Ritter, *Tetrahedron* **2005**, *61*, 1509.
- [6] a) B.J. Cohen, M.A. Kraus, A. Patchornik, *J. Am. Chem. Soc.* **1977**, *99*, 4165; b) R. Grubbs, C.P. Lau, R. Cukier, C. Brubaker Jr., *J. Am. Chem. Soc.* **1977**, *99*, 4517; c) S.L. Regen, D.P. Lee, *Macromol.* **1977**, *10*, 1418; d) B.J. Cohen, M.A. Kraus, A. Patchornik, *J. Am. Chem. Soc.* **1981**, *103*, 7620.
- [7] T. Tajima, A. Nakajima, *J. Am. Chem. Soc.* **2008**, *130*, 10496.
- [8] S. Suga, A. Nagaki, J. Yoshida, *Chem. Commun.* **2003**, 354.
- [9] a) P. Rys, *Acc. Chem. Res.* **1976**, *9*, 345; b) P. Rys, *Angew. Chem. Int. Ed.* **1977**, *16*, 807.
- [10] S. Suga, D. Yamada, J. Yoshida, *Chem. Lett.* **2010**, *39*, 404.
- [11] For selected reviews and examples of carbonyl allylation, see: a) Y. Yamamoto, N.

- Asao, *Chem. Rev.* **1993**, *93*, 2207; b) Y. Tamaru, in *Perspectives in Organopalladium Chemistry for the XXI Century* (ed. J. Tsuji), Elsevier, Amsterdam, **1999**, p. 215; c) S.E. Denmark, J. Fu, *Chem. Rev.* **2003**, *103*, 2763; d) J.W.J. Kennedy, D.G. Hall, *Angew. Chem. Int. Ed.* **2003**, *42*, 4732; e) M. Kimura, M. Shimizu, K. Shibata, M. Tazoe, Y. Tamaru, *Angew. Chem. Int. Ed.* **2003**, *42*, 3392; f) G. Zanoni, S. Gladiali, A. Marchetti, P. Piccinini, I. Tredici, G. Vidari, *Angew. Chem. Int. Ed.* **2004**, *43*, 846; g) I. Marek, G. Sklute, *Chem. Commun.* **2007**, 1683; h) L.F. Tietze, T. Kinzel, C.C. Brazel, *Acc. Chem. Res.* **2009**, *42*, 367; i) J.E. Bower, I.S. Kim, R.L. Patman, M.J. Krische, *Angew. Chem. Int. Ed.* **2009**, *48*, 34; j) Y. Lu, I.S. Kim, A. Hassan, V. Del, J. David, M.J. Krische, *Angew. Chem. Int. Ed.* **2009**, *48*, 5018.
- [12] M.M. Baizer, J.L. Chruma, *J. Org. Chem.* **1972**, *37*, 1951.
- [13] a) S. Satoh, H. Suginome, M. Tokuda, *Bull. Chem. Soc. Jpn.* **1981**, *54*, 3456; b) M. Tokuda, S. Satoh, H. Suginome, *J. Org. Chem.* **1989**, *54*, 5608.
- [14] a) *Microreactors* (eds. W. Ehrfeld, V. Hessel, H. Löwe), Wiley-VCH, Weinheim, **2000**; b) D. Horii, T. Fuchigami, M. Atobe, *J. Am. Chem. Soc.* **2007**, *129*, 11692; c) D. Horii, F. Amemiya, T. Fuchigami, M. Atobe, *Chem.-Eur. J.* **2008**, *14*, 10382.
- [15] H.S. Schrekker, M.W.G. de Bolster, R.V.A. Orru, L.A. Wessjohann, *J. Org. Chem.* **2002**, *67*, 1975.
- [16] H.-S. Cheng, T.-P. Loh, *J. Am. Chem. Soc.* **2003**, *125*, 4990.
- [17] H.-M. Chang, C.-H. Cheng, *Org. Lett.* **2000**, *22*, 3439.
- [18] Y. Kusuyama, *Bull. Chem. Soc. Jpn.* **1998**, *71*, 685.
- [19] a) S. Rondinini, P.R. Mussini, P. Mutini, G. Sello, *Electrochim. Acta* **2001**, *46*,

- 3245; b) J. Simonet, *J. Electroanal. Chem.* **2005**, 583, 34; c) C. Bellomunno, D. Bonanomi, L. Falciola, M. Longhi, P.R. Musini, L.M. Doubova, G.D. Silvestro, *Electrochim. Acta* **2005**, 50, 2331; d) A.A. Isse, S. Gotardello, C. Maccato, A. Gennaro, *Electrochem. Commun.* **2006**, 8, 1707.
- [20] a) W.R. Fawcett, J.S. Jaworski, *J. Phys. Chem.* **1983**, 87, 2972; b) M. Hoon, W.R. Fawcett, *J. Phys. Chem. A*, **1997**, 101, 3726.
- [21] G.J. Janz, R.P.T. Tomkins, in *Nonaqueous Electrolytes Handbook*, Academic Press, Now York, **1972**, Vol. I, p. 5.
- [22] A.M. Bond, E.A. McLennan, R.S. Stojanovic, F.G. Thomas, *Anal. Chem.* **1987**, 59, 2853.
- [23] a) P.A.Z. Suarez, S. Einloft, J.E.L. Dullius, R.F. de Souza, J. Dupont, *J. Chim. Phys.* **1998**, 95, 1626; b) V.M. Hultgren, A.W.A. Mariotti, A.M. Bond, A.G. Wedd, *Anal. Chem.* **2002**, 74, 3151.
- [24] U. Schröder, J.D. Wadhawan, R.G. Compton, F. Marken, P.A.Z. Suarez, C.S. Consorti, R.F. de Souza, J. Dupont, *New J. Chem.* **2000**, 24, 1009.
- [25] a) C.R. Wilke, P. Chang, *AIChE J. 1* **1955**, 264; b) J.C. Giddings, *Dynamics of Chromatography, Part I, Principles and Theory*, Marcel Dekker, New York, **1965**;
c) R.C. Reid, J.M. Prausnitz, T.K. Sherwood, *The Properties of Gases and Liquids* (3rd Edition), McGraw-Hill, New York, **1977**, p. 567; d) R.E. Treybal, *Mass-transfer Operations*, McGraw-Hill, New York, **1980**; e) D.M. Ruthven, *Principles of Adsorption & Adsorption Processes*, John Wiley and Sons, New York, **1984**; f) M. Suzuki, *Adsorption Engineering*, Kodansha/Elsevier, Tokyo/Amsterdam, **1990**; g) G. Guiochon, S. Golshan-Shirazi, A.M. Katti,

- Fundamentals of Preparative and Nonlinear Chromatography*, Academic Press, Boston, **1994**; h) R.B. Bird, W.E. Stewart, E.N. Lightfoot, *Transport Phenomena*, John Wiley & Sons, New York, **2002**.
- [26] R.C. Reid, J.M. Prausnitz, T.K. Sherwood, *The Properties of Gases and Liquids* (3rd Edition), McGraw-Hill, New York, **1977**, p. 57.
- [27] a) K. Gast, G. Damaschun, R. Misselwitz, D. Zirwer, *Eur. Biophys. J.* **1992**, *21*, 357; G. Damaschun, H. Damaschun, K. Gast, D. Zirwer, *J. Mol. Biol.* **1999**, *291*, 715.
- [28] a) M. Liu, J.K. Nicholson, J.A. Parkinson, J.C. Lindon, *Anal. Chem.* **1997**, *69*, 1504; b) K.F. Morris, B.J. Cutak, A.M. Dixon, C.K. Larive, *Anal. Chem.* **1999**, *71*, 5315.
- [29] K. Pappaert, J. Biesemans, D. Clicq, S. Vankrunkelsven, G. Desmet, *Lab Chip* **2005**, *5*, 1104.

Chapter 5

Summary

Today, microreactor technology is opening up new possibilities for organic synthesis. The many advantages and benefits of this emerging technology are now beyond doubt. However, the microreactor technology has still not been applied for electroorganic synthesis widely.

With this in mind, this thesis has been demonstrated the practical applications of an electrochemical microreactor to electroorganic synthesis in order to establish an integrated system for cleaner and characteristic organic synthesis. The proposed novel systems can be carried out only by using the electrochemical microreactor, which cannot be performed by conventional batch type reactors.

This thesis consists of five chapters. The introduction, advantages, and applications of microreactor technology, and outline of this thesis are described in Chapter 1. The research results are described in details from Chapter 2 to Chapter 4, and summarized as follows.

In Chapter 2, a novel microreactor system for paired electrosynthesis without intentionally added supporting electrolyte was developed. The mechanisms of self-supported systems in each solvent (protic and aprotic solvent) were proposed in the introduction section, respectively. A general design for the self-supported system in aprotic solvent was also discussed. Then, a self-supported paired electrochemical reaction composed of organic chloride reduction/alcohol oxidation combination was successfully carried out to give the corresponding products in good to moderate yields. In this case, cathodically generated chloride ions and anodically generated protons should act as charge carriers, and the cell voltage during the electrolysis was significantly decreased. These experimental results strongly support the proposed mechanisms and design methodology for constructing a self-supported microreactor system.

In Chapter 3, a $[S/\pm e^-/I/\mp e^-/P]$ type electrochemical conversion of benzylamine to dibenzylamine using a microreactor has been successfully demonstrated as an analogue of photocatalytic redox combined reaction. The extremely narrow electrode distance of the microreactor enables to proceed this sequential redox reaction. In contrast, this reaction system could not be achieved by using a conventional batch type reactor. The re-production of *N*-benzylidenebenzylamine by over-oxidation of dibenzylamine inhibited the smooth formation of dibenzylamine in this system, however, this undesired side-reaction would be repressed by specific design of the microreactor and further optimization of the system.

In Chapter 4, a new method for product selectivity control by using a liquid-liquid parallel laminar flow in a microreactor has been successfully demonstrated. The combined use of suitable flow mode in the microreactor and corresponding cathode material enables chemoselective cathodic reduction to control the product regioselectivity in cathodic carbonyl allylation. The necessity of the liquid-liquid parallel laminar flow mode was supported by flow mode experiments. In addition, the substrate diffusion behavior in the microreactor channel was predicted by the estimation of substrate diffusion coefficient and CFD simulations. The flow simulations revealed that the clear concentration gradient of the substrate was formed in the microreactor channel over a specific channel length.

Although proposed electrochemical microreactor systems in this thesis are still in their infancy, it is expected that this study will make significant contributions not only to microreactor technology but also to electroorganic chemistry. Since promising results would be obtained by the integrated use of microreactor technology with electroorganic synthesis, it is hoped that further studies of electrochemical microreactor will be conducted.

List of Publications

For Thesis

- [1] F. Amemiya, D. Horii, T. Fuchigami, M. Atobe, Self-Supported Paired Electrosynthesis Using a Microflow Reactor Without Intentionally Added Electrolyte, *J. Electrochem. Soc.* **2008**, *155*, E162.
- [2] F. Amemiya, K. Fuse, T. Fuchigami, M. Atobe, Chemoselective reaction system using a two inlet micro-flow reactor: application to carbonyl allylation, *Chem. Commun.* **2010**, *46*, 2730. (This article has been selected for inclusion in *Highlights in Chemical Science* of RSC publishing: *Highlights in Chemical Science*, April 2010, Volume 7, Issue 4, p. 4.)
- [3] F. Amemiya, H. Matsumoto, K. Fuse, T. Kashiwagi, C. Kuroda, T. Fuchigami, M. Atobe, Product selectivity control induced by using liquid-liquid parallel laminar flow in a microreactor, *submitted*.
- [4] F. Amemiya, T. Fuchigami, M. Atobe, Electrochemical conversion of primary amine to secondary amine using a microreactor: Analogous system of photocatalytic redox combined synthesis, *submitted*.

For Others

- [5] N. Saino, F. Amemiya, E. Tanabe, K. Kase, S. Okamoto, A Highly Practical Instant Catalyst for Cyclotrimerization of Alkynes to Substituted Benzenes, *Org. Lett.* **2006**, *8*, 1439.
- [6] D. Horii, F. Amemiya, T. Fuchigami, M. Atobe, A Novel Electrosynthetic System for Anodic Substitution Reactions by Using Parallel Laminar Flow in a Microflow Reactor, *Chem. Eur. J.* **2008**, *14*, 10382.

- [7] M. Atobe, S. Ikari, K. Nakabayashi, F. Amemiya, T. Fuchigami, Electrochemical Reaction of Water-Insoluble Organic Droplets in Aqueous Electrolytes Using Acoustic Emulsification, *Langmuir* **2010**, *26*, 9111.
- [8] J.D. Watkins, F. Amemiya, M. Atobe, P.C. Bulman-Page, F. Marken, Liquid | liquid biphasic electrochemistry in ultra-turrax dispersed acetonitrile | aqueous electrolyte systems, *Electrochim. Acta* **2010**, *55*, 8808.
- [9] K. Nakabayashi, F. Amemiya, T. Fuchigami, K. Machida, S. Takeda, K. Tamamitsu, M. Atobe, Highly Clear and Transparent Nanoemulsion Preparation under Surfactant-Free Conditions Using Tandem Acoustic Emulsification, *submitted*.
- [10] T. Kashiwagi, F. Amemiya, T. Fuchigami, M. Atobe, Multi-step reactions of quinones using electrochemical microreactor, *to be submitted*.

Acknowledgements

I would like to express my deepest gratitude to my supervisor, Prof. Dr. Mahito Atobe, for his guidance, suggestions, and encouragement throughout my research, and for his invaluable helps for my academic life during this five years. The lessons he gave me has sunk deep into my heart.

I would also give my sincere thanks to Prof. Dr. Toshio Fuchigami for his beneficial instructions and suggestions on my research, and for a lot of helps.

Special thanks are given to Dr. Shinsuke Inagi, the Assistant Prof. of our research group, for his great suggestions and very kind helps.

I would express my special thanks to Associate Prof. Dr. Hideyuki Matsumoto for his kind cooperation and valuable suggestions for the CFD simulations in Chapter 4.

I wish to express my thanks to Dr. Toshiki Tajima, the Assistant Prof. of Shibaura Institute of Technology, for valuable discussions. It is worth mentioned that Dr. Daisuke Horii gave a lot of helps in my research. Many thanks are also given to past and present members of our research group for their kind cooperation.

I would also express my sincere thanks to Prof. Dr. Frank Marken at the University of Bath, UK, for his kind support, hospitality, and valuable suggestions during my stay in Bath.

This work was financially supported in part by a Grant-in-Aid for JSPS Fellows from the Japanese Ministry of Education, Culture, Sports, Science and Technology. I also thank Tokyo Institute of Technology Global-COE Program for financial support for my research and for my study at the University of Bath, UK.

Finally, I would like to express my sincere thanks to my parents, my brother and sister, other family members, and my fiancée, Yuri Uchiyama, for their always understanding, a great deal of warm supports, and encouragement. I would like to dedicate this thesis to them.

December 27, 2010


Fumihiko Amemiya